The Nanocaterpillar's Random Walk: Diffusion With Ligand-Receptor Contacts

Sophie Marbach,[1,2] Jeana Aojie Zheng,[3] and Miranda Holmes-Cerfon[1]

[1] *Courant Institute of Mathematical Sciences, New York University, NY, 10012, U.S.A.*
[2] *CNRS, Sorbonne Université, Physicochimie des Electrolytes et Nanosystèmes Interfaciaux, F-75005 Paris, France* *
[3] *Department of Physics, New York University, NY, 10012, U.S.A.*

Particles with ligand-receptor contacts bind and unbind fluctuating "legs" to surfaces, whose fluctuations cause the particle to diffuse. Quantifying the diffusion of such "nanoscale caterpillars" is a challenge, since binding events often occur on very short time and length scales. Here we derive an analytical formula, validated by simulations, for the long time translational diffusion coefficient of an overdamped nanocaterpillar, under a range of modeling assumptions. We demonstrate that the effective diffusion coefficient, which depends on the microscopic parameters governing the legs, can be orders of magnitude smaller than the background diffusion coefficient. Furthermore it varies rapidly with temperature, and reproduces the striking variations seen in existing data and our own measurements of the diffusion of DNA-coated colloids. Our model gives insight into the mechanism of motion, and allows us to ask: when does a nanocaterpillar prefer to move by *sliding*, where one leg is always linked to the surface, and when does it prefer to move by *hopping*, which requires all legs to unbind simultaneously? We compare a range of systems (viruses, molecular motors, white blood cells, protein cargos in the nuclear pore complex, bacteria such as Escherichia coli, and DNA-coated colloids) and present guidelines to control the mode of motion for materials design.

Particles with ligand-receptor contacts – or *nanocaterpillars* – harvest binding and unbinding dynamics of their fluctuating *legs* at the nanoscale to move, target, stick, or assemble into large structures [1–4]. Nanocaterpillars are found across multiple scales, spanning a great variety of systems in biology and biomimetic assays – see Fig. 1-A. To name but a few, microscale white blood cells with protein linkers stick and roll on blood vessel walls until they reach a healing target [5–7]. Microscale droplets with protein linkers are used to study cellular-like adhesion [8–10]. Microscale to nanoscale colloids coated with complementary deoxyribonucleic acid (DNA) strands self-assemble into macroscopic crystals [4, 11, 12] with novel optical or selectivity properties [13–16]. Nanoscale viruses transiently adhere with spike proteins to the respiratory mucus to find vulnerable host cells [1, 17–19]. At even smaller scales, protein cargos bind to receptors in the nuclear pore complex for selective transport to a cell's nucleus [20, 21].

For all these systems to function, a nanocaterpillar must *move* relative to the surface to which its legs are attracted. An important question therefore is to characterize *how* it moves, over scales much larger than individual legs. Since legs constantly bind and unbind to the surface, imparting force each time they do so, the particle's macroscopic mobility depends on the microscopic details of its legs. For example, leg flexibility and bond lifetimes control the average mobility of the particle [19, 23, 24], and differences in both parameters can be harvested to detect infected cells [25–27] or prevent viral infections [28]. As another example, leg density affects how DNA-coated colloids nucleate and grow into crystals [29, 30] and governs the long-range alignment of crystals [31–33]. Overall, microscopic details underlie a variety of large-scale modes of motion, such as hopping [3, 17, 34, 35], cohesive motion including rolling and crawling [17, 36], and also transient or firm arrest [3, 5, 37], resulting in large differences in macroscopic mobility.

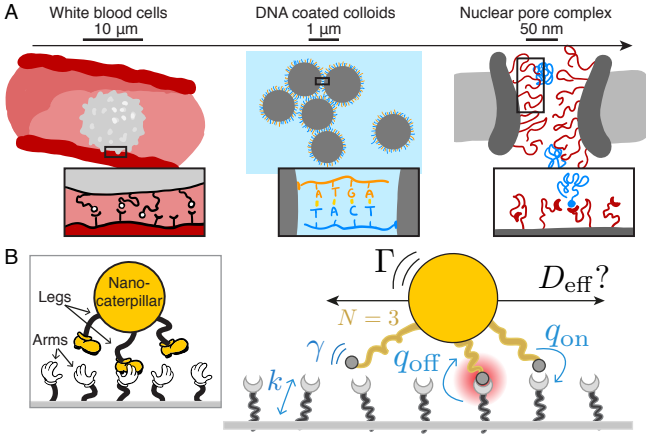

FIG. 1. **Overview of nanocaterpillars.** (A) Multivalent ligand-receptor systems span the micro to nanoscales. White blood cells stick to vessel walls through selectin mediated bonds (inspired from Ref. 7); DNA-coated colloids self-assemble through hybridization of complementary DNA strands; Protein cargos translocate through the polymer mesh of the nuclear pore complex (inspired from Ref. 22). (B) Ligand-receptor systems are modeled here with an arbitrary number of legs N (ligands) and/or arms (receptors). The stochastic model includes binding and unbinding rates q_{on} and q_{off}, spring constant k, and leg friction γ (all fast, in blue); and the bare friction coefficient Γ of the nanocaterpillar (slow, in black). We seek the long-time effective longitudinal diffusion coefficient D_{eff}.

Investigating how microscopic binding details lead to

* sophie@marbach.fr

macroscopic mobility is challenging, as it requires probing time and length scales that can often be quite different [19, 38] – legs can be much smaller than the nanocaterpillar they are attached to, while leg dynamics can be orders of magnitude faster than the timescales of macroscopic motion. Furthermore, many systems have a valency of thousands of leg contacts [31, 38, 39], too many degrees of freedom to resolve experimentally or computationally [22, 40]. To make progress, numerical and analytical models often rely on simplified assumptions, *e.g.* excluding stochastic relaxation of the legs [41, 42], limiting the analysis to a small number of legs [41, 43, 44], or assuming small perturbations [22]. Such models have given insight into a variety of phenomena, such as how specific parameters could favor rolling over sliding [7, 41, 43, 45, 46] or how specific mechanisms could increase overall mobility (with coupling effects such as binding dynamics depending on bond number [47–49] or when numerous adhesive sites are available for a single ligand [22, 50, 51]). Nevertheless, such modeling assumptions are not always justified; for example stochasticity plays a critical role for mobility, facilitating rolling [37], targeted arrest [40], or other walking modes [52]. Furthermore, such models can also not reproduce the order of magnitude decrease of diffusion of DNA-coated colloids [31, 39]. Hence, a systematic derivation of macroscopic mobility from microscopic details that is valid under a broad range of parameters is needed.

In this paper we derive an analytical expression for the effective mobility of a nanocaterpillar in an overdamped system, by systematically coarse-graining over the microscopic details of its legs. Starting from a model that includes the detailed spatial fluctuations of the legs, we use homogenization techniques [22, 53, 54] to average over these fluctuations. We obtain an analytical expression for the effective long-time translational diffusion coefficient of the particle, $D_{\text{eff}}(N, \Gamma, \gamma, k, q_{\text{off}}, q_{\text{on}})$, as a function of the microscopic parameters governing the legs (Eq. (15); see also Fig. 1-B and Sec. I.) The expression depends in a non-trivial way on the friction coefficients of the individual components of the system (legs and particle), with the frictions either adding up arithmetically (like springs in parallel) or harmonically (like springs in series) according to the mechanistic details. We validate our analytical calculations with numerical simulations, which show the expression is accurate over a wide range of parameter values.

Our model gives insight into the mechanism of nanocaterpillar motion, as it allows us to distinguish between two long term modes of motion: *sliding*, where at least one bond is always attached to the surface, and *hopping*, where the particle detaches completely, moves in free space and reattaches. These regimes are controlled by physical properties of the legs, such as stiffness and adhesive strength, allowing us to investigate existing biological and biomimetic systems in a so-called Ashby chart for nanocaterpillars (Sec. II). We identify how critical design parameters (such as the coating density for DNA-coated colloids) controls the preferential mode of motion and reconcile disparate experimental observations on similar systems [31, 39].

Importantly, the effective diffusion can sometimes be orders of magnitude smaller than the background diffusion coefficient, showing the critical effect of the legs on the particle's mobility. This analytical prediction of a dramatically decreased diffusivity is borne out with experimental measurements of the diffusion of DNA-coated colloids, both from existing data [31, 39] and additionally measured in this study. Our model agrees with the data within experimental accuracy over a range of temperatures and for different DNA coating densities on the colloids (Sec. II).

Finally, we derive the effective diffusion coefficient for several variations of the model with varying assumptions, and show that our model incorporates these assumptions as special limits [22, 54], but is accurate over a broader range of parameters and system designs (Sec. III). In particular, previous approaches can not describe the observed orders of magnitude decrease in diffusion [22]. Overall, our results lay the ground to tune mobility features in artificial designs, and provide methodological tools to study more complex motion mediated through ligand-receptors, including rolling or self-avoiding walks due to active cutting of bonds.

I. DERIVING AN ANALYTICAL FORMULA FOR THE EFFECTIVE DIFFUSION COEFFICIENT

In Sections I A-I C we illustrate our homogenization technique pedagogically by considering a 1-legged caterpillar. Our main result for the effective diffusion coefficient of an N-legged caterpillar, Eq. (15), is presented in Section I D.

A. 1-legged caterpillar: constitutive equations

We begin with the simplest possible model: a nanocaterpillar with a single leg (Fig. 2). The leg is permanently fixed to the caterpillar while its other end is mobile, and can attach anywhere on the binding surface. We consider for now a one-dimensional model, where leg fluctuations and particle motion occur on a line, longitudinal to the surface.

The dynamics of the particle position $x(t)$ and leg length $l(t)$ occur over nano to microscales, mostly in dense fluids such as water. In this context, dynamics are well captured by overdamped Langevin equations [55], where inertia plays a negligible role. This is in contrast to previous modeling efforts which used the Langevin equation (with inertia) [54], a point we return to in Sec. III, where we show that the two approaches can give predictions that are orders of magnitude different in certain parameter regimes.

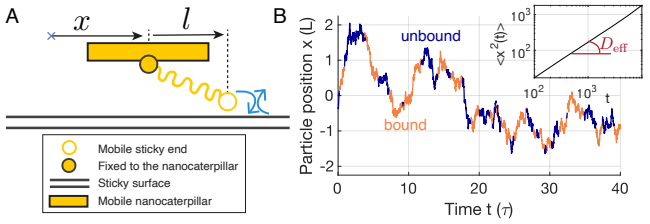

FIG. 2. **1-legged nanocaterpillar model.** (A) The longitudinal extension of the single leg (l) is monitored and feeds back into the longitudinal position (x) of the particle. (B) Simulation trace of the position of a 1-legged particle with time. (inset) The effective long time diffusion D_{eff} is half the slope of the mean squared displacement over long times.

When the legs are unbound they evolve as

$$\frac{dl}{dt} = -\frac{k}{\gamma}(l(t) - l_0) + \sqrt{\frac{2k_BT}{\gamma}}\eta_l(t)\,. \tag{1}$$

Here k is a spring constant describing the recoil force of the leg material, γ is its friction coefficient, l_0 its rest length, k_B is Boltzmann's constant, T is temperature and η_l is a Gaussian white noise satisfying $\overline{\eta_l(t)} = 0$ and $\overline{\eta_l(t)\eta_l(t')} = \delta(t-t')$ where $\bar{\cdot}$ is the average over realizations of the noise. In most systems we consider, legs are made of polymers or proteins, where small leg deformations around equilibrium are well captured by a constant spring constant k [56–58].

The particle's position x when the leg is unbound obeys

$$\frac{dx}{dt} = \sqrt{\frac{2k_BT}{\Gamma}}\eta_x(t) \tag{2}$$

where Γ is the friction coefficient of the particle and $\eta_x(t)$ is a Gaussian white noise uncorrelated with $\eta_l(t)$. The diffusion coefficient for the unbound particle is $D_0 = \frac{k_BT}{\Gamma}$.

We consider for now that the surface is uniformly coated with receptors. The leg can thus bind at any location on the surface with a constant binding rate q_{on} and constant unbinding rate q_{off}. Detailed balance requires $\frac{q_{\text{on}}}{q_{\text{off}}} = \frac{\pi_b}{\pi_u}$ where $\pi_{b/u}$ is the equilibrium probability of the system to be bound or unbound. Typically $\frac{\pi_b}{\pi_u} = e^{-\beta\Delta G}$, where $\beta^{-1} = k_BT$ and $\Delta G < 0$ is the free energy change when the leg binds to the surface [38, 59].

We now seek to describe motion of the system when the leg is bound. In this case, variables are constrained as $x(t) + l(t) - x_{\text{r}} = 0$ where x_{r} is the location of the receptor where the leg tip is attached, which is constant until the leg detaches and reattaches to another location. The stochastic dynamics Eqns. (1) and (2) must be projected [32, 60] onto the constraint surface, see Appendix A. We obtain

$$\frac{dx}{dt} = -\frac{dl}{dt} = \frac{k}{\Gamma+\gamma}(l(t) - l_0) + \sqrt{\frac{2k_BT}{\Gamma+\gamma}}\eta(t) \tag{3}$$

where $\eta(t)$ is a Gaussian white noise. Here we see that the projected dynamics have a natural expression where the effective friction in the bound state is the arithmetic sum of the friction coefficients in the unbound states, $\Gamma + \gamma$. Note that this projection is a crucial step that is often ignored in such derivations [22, 32, 54], and modifies the dynamics in non trivial ways especially with a large number of legs.

The dynamics are now specified through the set of Eqns. (1)-(3), together with the binding and unbinding dynamics. To see what happens over long times, we simulate trajectories for 1 leg – see Fig. 2-B (and simulation details in Appendix B). Over long times, the particle's mean-squared displacement grows linearly with time, and we may extract an effective long time diffusion coefficient D_{eff} – see inset of Fig. 2-B.

B. Homogenization to coarse-grain the fast dynamics

The computational cost of simulating Eqns. (1)-(3) is high, since small time steps are required to resolve the fast relaxation and binding events. We therefore seek an analytical method to coarse-grain over these fast timescales. To apply this method we identify a non-dimensional separation of scales, which is novel compared to other approaches [22, 51, 54] and will allow us to find a result valid over a broad range of parameters. We use homogenization theory to average over the fast scales, eventually obtaining an effective diffusion equation, Eq. (10), with effective diffusivity (Eq. (11)) and related effective friction (Eq. (12)), which is one of the main results of this paper for the special case of a 1-legged caterpillar. A reader interested in the results and physical implications may skip to Section I C.

1. *Set up: partial differential equations to be coarse-grained*

The set of stochastic Eqns. (1)-(3) defines a Markov process that is conveniently studied via the Fokker-Planck equation and its adjoint, the Kolmogorov backward equation [53, 61]. Let $p(x,l,t) = (p_u(x,l,t), p_b(x,l,t))^T$ be the probability density function of finding the system at time t and positions x, l in the unbound or bound states. We obtain from Eqns. (1)-(3) the Fokker-Plank equation

$$\partial_t p = \mathcal{L}^\star p\,, \tag{4}$$

with $\mathcal{L}^\star = \mathcal{V}^\star + \mathcal{Q}^\star$ where

$$\mathcal{V}^\star = \mathrm{diag}\begin{pmatrix} \partial_l\left(\frac{k}{\gamma}(l-l_0) + \frac{k_BT}{\gamma}\partial_l\right) + \frac{k_BT}{\Gamma}\partial_{xx} \\ (\partial_l - \partial_x)\left(\frac{k}{\Gamma+\gamma}(l-l_0) + \frac{k_BT}{\Gamma+\gamma}(\partial_l - \partial_x)\right)\end{pmatrix},$$

$$\mathcal{Q}^\star = \begin{pmatrix} -q_{\mathrm{on}} & q_{\mathrm{off}} \\ q_{\mathrm{on}} & -q_{\mathrm{off}}\end{pmatrix},$$

with an appropriate initial condition. Additionally we require the flux in either state to vanish at infinity, to conserve total probability. The stationary solution of Eq. (4) is $\pi = \frac{e^{-\beta k(l-l_0)^2/2}}{Z}(q_{\mathrm{off}}, q_{\mathrm{on}})^T$ where Z is a normalization constant. This is therefore the equilibrium probability density of the system; it satisfies detailed balance.

While probability densities have an intuitive physical meaning, in the following it will be easier – and mathematically better posed – to consider the adjoint of the Fokker-Planck equation and the corresponding dual functions. These are functions $f(x,l,t) = \int p(x',l',t|x,l)g(x',l')dl'dx'$ that give the expectation of any scalar function $g(x(t),l(t))$, given an initial condition $x(0) = x, l(0) = l$. Once we know how such functions f evolve, we may calculate any statistic g of our stochastic process. Writing $f(x,l,t) = (f_u(x,l,t), f_b(x,l,t))^T$, we have that f satisfies the Kolmogorov backward equation [61]

$$\partial_t f = \mathcal{L}f\,, \quad f(x,l,0) = g(x,l)\,. \tag{5}$$

Here $\mathcal{L}$ is the adjoint operator of $\mathcal{L}^\star$, defined by the operator that satisfies $\langle f, \mathcal{L}^\star p\rangle = \langle \mathcal{L}f, p\rangle$ for any probability density p and statistic f, where $\langle f,p\rangle = \iint (f_u p_u + f_b p_b)dldx$ is the inner product.

2. Non-dimensionalization and assumptions on scales.

We now seek to coarse-grain the fast dynamics, by applying homogenization techniques to the backward equation, Eq. (5). To start, we non-dimensionalize the equation using

$$x \to L_x\tilde{x},\ l - l_0 \to L\tilde{l},\ t \to \tau\tilde{t},$$

where $L = \sqrt{k_BT/k}$ is the reference length of the leg fluctuations, L_x is the scale for the long-time average motion of x, and τ is the timescale associated with this average motion. The latter two scales are not determined *a priori* by any intrinsic scales in the system, but rather are chosen large enough that averaging will be appropriate over such scales; hence we choose $L_x = L/\epsilon$ where $\epsilon \ll 1$ is a small non-dimensional number. We are interested in long time scales corresponding to the diffusion of the particle, hence we expect $\tau = L_x^2/D_0$, which corresponds to $\tau = \frac{1}{\epsilon^2}\frac{\Gamma}{k}$. Importantly, and in contrast with other works [22, 51], here ϵ does not measure the value of physical parameters, but rather, it measures the large observation time scale over which the coarse-grained model is valid. Such long observation times are quite likely in experiments, as typical binding rates and leg dynamics occur at most over 1 ms − 1 s while observation (or other biophysical processes such as internalisation for viruses [17]) happens over the course of 10 min at least [38]. This non-dimensionalization step is crucial as it will allow us to find order of magnitude changes in the diffusion coefficient according to the physical parameters, something that was not captured by previous perturbative approaches [22, 51].

We now assume that the observation time scale is long enough, such that binding and unbinding events, as well as relaxation dynamics, will both occur on comparably short time scales. We can therefore write $\tilde{q}_i = q_i\Gamma/k = O_\epsilon(1)$ and $\gamma/\Gamma = O_\epsilon(1)$. In Sec. III we will see that taking different limits for these physical parameters (such as $\gamma/\Gamma \ll 1$) yields the same result as applying these limits to the final result. Our choices of scalings are therefore quite general and can be easily adapted to more detailed systems.

Using non-dimensional variables (and dropping the $\tilde{\cdot}$ for simplicity) we obtain from the backward equation Eq. (5) a separation in orders of ϵ as

$$\partial_t f = \mathcal{L}f = \left(\frac{1}{\epsilon^2}\mathcal{L}_0 + \frac{1}{\epsilon}\mathcal{L}_1 + \mathcal{L}_2\right)f \tag{6}$$

where

$$\mathcal{L}_0 = \begin{pmatrix} -q_{\mathrm{on}} + \frac{\Gamma}{\gamma}(-l\partial_l + \partial_{ll}) & q_{\mathrm{on}} \\ q_{\mathrm{off}} & -q_{\mathrm{off}} + \frac{\Gamma}{\Gamma+\gamma}(-l\partial_l + \partial_{ll})\end{pmatrix},$$

$$\mathcal{L}_1 = \mathrm{diag}\left(0, \frac{\Gamma}{\Gamma+\gamma}\left(l\partial_x - 2\partial_{lx}\right)\right),$$

$$\mathcal{L}_2 = \mathrm{diag}\left(\partial_{xx}, \frac{\Gamma}{\Gamma+\gamma}\partial_{xx}\right).$$

3. Homogenization method.

We seek a solution to Eq. (6) of the form $f = f_0 + \epsilon f_1 + \epsilon^2 f_2 + ...$ We obtain a hierarchy of equations at different orders in ϵ:

$$O_\epsilon\left(\tfrac{1}{\epsilon^2}\right): \quad \mathcal{L}_0 f_0 = 0, \tag{7}$$

$$O_\epsilon\left(\tfrac{1}{\epsilon}\right): \quad \mathcal{L}_0 f_1 = -\mathcal{L}_1 f_0, \tag{8}$$

$$O_\epsilon(1): \quad \mathcal{L}_0 f_2 = \partial_t f_0 - \mathcal{L}_1 f_1 - \mathcal{L}_2 f_0, \tag{9}$$

$$\vdots \qquad\qquad \vdots$$

and we solve these iteratively for f at each order in ϵ. At lowest order we obtain from Eq. (7) and the vanishing flux at boundaries, $f_0 = a(x,t)\begin{pmatrix}1\\1\end{pmatrix}$, where $a(x,t)$ is an

unknown function of the slow variable x, whose dynamics we seek to determine. The associated equilibrium distribution at lowest order, $\mathcal{L}_0^\star \pi_0 = 0$ is simply the full one $\pi_0 = \pi$.

At the next order, one can check that

$$f_1 = \begin{pmatrix} \gamma q_{\rm on} \\ \\ \Gamma + \gamma q_{\rm on} \end{pmatrix} \frac{l \partial_x a}{\Gamma(1+q_{\rm off}) + \gamma(q_{\rm on}+q_{\rm off})}$$

is a particular integral of Eq. (8), and is the unique solution since we impose that f_1 does not contain terms in the nullspace of $\mathcal{L}_0$.

Finally Eq. (9) possesses a solution if and only if it satisfies the Fredholm alternative [53]

$$\langle (\partial_t f_0 - \mathcal{L}_1 f_1 - \mathcal{L}_2 f_0), \pi_0 \rangle = 0.$$

Standard algebra yields an effective long time diffusion equation for a (in dimensional variables)

$$\partial_t a = D_{\rm eff} \partial_{xx} a, \tag{10}$$

where

$$D_{\rm eff} = \frac{k_B T}{\Gamma_{\rm eff}}, \tag{11}$$

with

$$\begin{aligned} &\frac{1}{\Gamma_{\rm eff}} = \frac{p_0}{\Gamma_0} + \frac{p_1}{\Gamma_1}, \quad \text{with } \Gamma_0 = \Gamma, \ \Gamma_1 = \Gamma + \gamma_{\rm eff} \\ &\text{and } \gamma_{\rm eff} = \gamma + k\left(\frac{1}{q_{\rm off}} + \frac{\gamma}{k}\frac{q_{\rm on}}{q_{\rm off}}\right). \end{aligned} \tag{12}$$

In the above expressions, $p_0 = \frac{q_{\rm off}}{q_{\rm off}+q_{\rm on}}$ is the equilibrium probability to have no bond, and $p_1 = 1 - p_0$ the equilibrium probability to have one bond. $\Gamma_0 = \Gamma$ is the friction in the unbound state and Γ_1 is the effective friction contributing to the bound state.

Eq. (10), which is the backward equation for the particle+leg over long times, is one of the main results of this paper, in the case of a 1-legged caterpillar. It is the backward equation for a particle that evolves as

$$\frac{dx}{dt} = \sqrt{2D_{\rm eff}}\eta_x(t). \tag{13}$$

That is, the particle diffuses, with effective diffusion coefficient $D_{\rm eff}$ and effective friction $\Gamma_{\rm eff}$. The effective diffusivity and friction have the usual interpretation. In particular, if a potential $\mathcal{U}(x)$ were added to the particle Eqns. (2) and (3), one would recover in Eq. (13), following the same coarse-graining procedure, a term $-\frac{1}{\Gamma_{\rm eff}}\partial_x \mathcal{U}$.

In Fig. 3 we compare the analytical result obtained in Eq. (12) (gray line) to numerical simulations of the full stochastic Eqns. (1)-(3) (gray dots). We show the results for a number of system parameters and find perfect agreement over several orders of magnitude of physical parameters. We also predict order of magnitude changes in the diffusion coefficient as the microscopic parameters change.

C. Microscopic parameters determine long term diffusion

How shall we interpret the expressions for the effective diffusivity Eq. (11) and the effective friction Eq. (12)? The effective diffusivity is a weighted sum of the diffusivity in each state, $D_{\rm eff} = p_0 D_0 + p_1 D_1$ where the weights correspond to the probability to be in either state, and $D_i = k_B T/\Gamma_i$. The effective friction, on the other hand, is a harmonic weighted sum of the friction coefficients. That the diffusivity averages arithmetically is to be expected, since the mean squared displacement is an extensive quantity in a system with multiple states. Over a time t we can write

$$\begin{aligned} \overline{x^2(t)} &= 2D_{\rm eff} t = 2D_0 p_0 t + 2D_1 p_1 t \\ &= 2D_0 t_0 + 2D_1 t_1 = \overline{x^2(t)}|_0 + \overline{x^2(t)}|_1, \end{aligned}$$

where t_0 and t_1 refer to the time spent in either state. The novelty here is that the diffusivity in the bound state,

$$D_1 = k_B T(\Gamma + \gamma_{\rm eff})^{-1} \neq k_B T(\Gamma + \gamma)^{-1},$$

is obtained not just from the friction in the bound state, see Eq. (12), but is modified by spring resistance during binding events by an additional term $\gamma_{\rm eff} - \gamma$.

We can interpret this additional term by writing it as

$$\gamma_{\rm eff} - \gamma = k\tau_{\rm eff}, \quad \text{where } \tau_{\rm eff} = \tau_{\rm b} + \tau_{\rm u}^{\rm relax}$$

is the typical time over which the leg's spring resistance acts, with $\tau_{\rm b} = 1/q_{\rm off}$ representing the average bound time, and $\tau_{\rm u}^{\rm relax} = \frac{\gamma}{k}\frac{q_{\rm on}}{q_{\rm off}} = \frac{\gamma}{k}\frac{\tau_{\rm b}}{\tau_{\rm u}}$ representing the bare relaxation time γ/k increased by the ratio of average bound time to average unbound time. This is coherent as the leg fluctuations may only relax in the unbound state. The interpretation of $\tau_{\rm eff}$ is comparable to that in Ref. 54 although the results of Ref. 54 were obtained from underdamped dynamics.

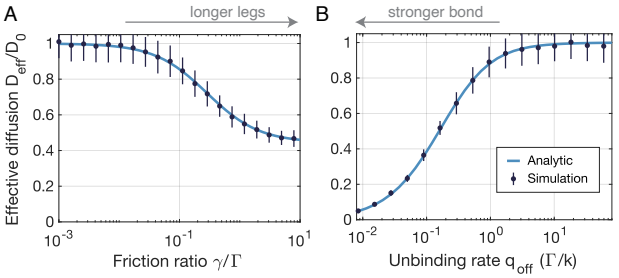

FIG. 3. **Effective diffusion $D_{\rm eff}$ of a 1-legged particle.** Simulation and analytical result Eq. (12) for a 1D system with 1 leg, with respect to (A) friction ratio γ/Γ and (B) unbinding rate $q_{\rm off}$. (A) and (B) share the same y-axis. The other numerical parameters are $q_{\rm on}\Gamma/k = 1.0$, and for (A) $q_{\rm off}\Gamma/k = 0.8$ while for (B) $\gamma/\Gamma = 0.1$. Error bars represent one standard deviation for 100 independent runs.

Fig. 3 shows how the effective diffusion coefficient depends on microscopic parameters such as the leg friction

and binding rates. As the leg friction γ increases, the effective diffusion of the particle decreases (Fig. 3-A). When the leg friction γ is large compared to all other contributions to friction, diffusion in the bound state is frozen $D_1 = 0$, and the effective diffusion corresponds only to mobility in the unbound state $D_{\text{eff}} = p_0 D_0$ ($p_0 = 0.8/1.8 \simeq 0.44$ in Fig. 3-A). As leg friction is typically proportional to the size of the legs, it is thus expected that the bigger the legs, the slower the particle. As the unbinding rate q_{off} decreases, D_{eff} decreases to arbitrarily small values (Fig. 3-B). This slow down is due to spring recoil forces acting over longer times, eventually freezing the particle in a given location. Note that similar qualitative dependencies of the diffusion coefficient on the unbinding rate ($D_{\text{eff}} \sim k_B T q_{\text{off}}/k$) were noted in a numerical model of multivalent transport on discrete sites [44], in a scaling law investigation of sticky reptation in polymers [62], and experimentally in Influenza A viruses [19].

As a test of modeling choice, the analytical expression may also be plotted against numerical simulations of the non-dimensional equations with any value of ϵ. We find perfect agreement up to $\epsilon \lesssim 10$ (Supplementary Fig. S1), regardless of the choice of physical parameters. This highlights that the natural choice $\epsilon = L/L_x$ for coarse-graining purposes, corresponding to bound leg length scales versus unbound particle long range motion, is especially well suited for these types of problems. In the following ϵ is not incorporated in numerical simulations.

D. Diffusion of N-legged caterpillar spans orders of magnitude

We extend our framework to probe nanocaterpillar dynamics with an arbitrary number of legs N (see Fig. 4-A). Eq. (1) is repeated for each unbound leg, and each leg binds to the surface with rates $q_{\text{on}}, q_{\text{off}}$ independently. Eq. (2) gives the particle dynamics when no legs are bound. When n legs are bound, indexed by $i = 1, \ldots, n$, the dynamics of the particle and bound legs are constrained as (Supplementary 1.2)

$$\frac{dx}{dt} = -\frac{dl_i}{dt} = \frac{k}{\Gamma + n\gamma} \sum_{i=1}^{n} (l_i - l_0) + \sqrt{\frac{2k_B T}{\Gamma + n\gamma}}\eta. \quad (14)$$

Note here that the projection step yields a friction coefficient scaling linearly with the number of bonds n, and hence is not a perturbative effect [22]. The set of stochastic equations is now fully determined and can be simulated for any N, see Fig. 4-B.

Similarly as in Sec. I B, coarse-graining predicts a long time effective diffusion with N legs as (Supplementary 1.2)

$$D_{\text{eff}}^{N\,\text{legs}} = \frac{k_B T}{\Gamma_{\text{eff}}^{N\,\text{legs}}} = k_B T \sum_{n=0}^{N} \frac{p_n}{\Gamma_n} \quad (15)$$

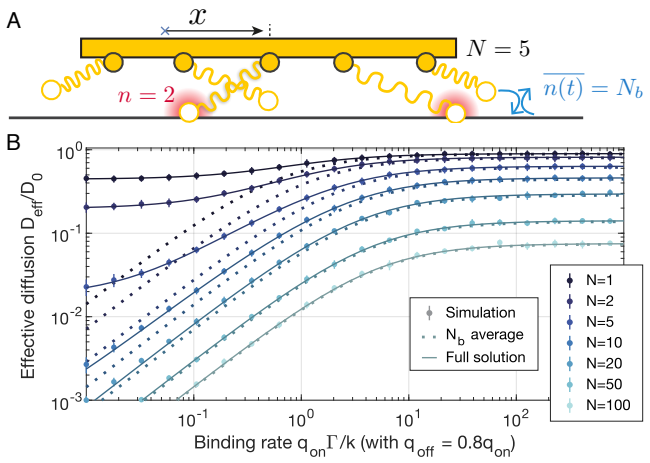

FIG. 4. **N-legged nanocaterpillar model.** (A) The longitudinal extension of N legs are monitored (here $N = 5$) with binding and unbinding. The number of bonds $n(t)$ changes in time, here $n(t) = 2$. The average number of bonds $\overline{n(t)} = N_b$ depends on the binding and unbinding rates. (B) Simulations and analytical results of the effective diffusion coefficient for N-legs according to the binding rate $q_{\text{on}}\Gamma/k$. "N_b average" corresponds to Eq. (16) and "full solution" to Eq. (15). The other numerical parameters are $\gamma/\Gamma = 0.1$ and $q_{\text{off}} = 0.8 q_{\text{on}}$.

where $p_n = \binom{N}{n} \frac{q_{\text{off}}^{N-n} q_{\text{on}}^{n}}{(q_{\text{off}}+q_{\text{on}})^N}$ is the equilibrium probability to have n bonds and Γ_n is the friction coefficient in a state with n bonds. The frictions $\{\Gamma_n\}$ solve a linear system of equations that does not have a simple analytical solution (see Eqns. (S1.20-22)), but can be solved using numerical linear algebra for given parameters as reported in Supplementary 1.2.

Eq. (15) is one of the main results of this paper. It predicts the long-term diffusion coefficient of a nanocaterpillar, as a non-trivial function of the microscopic parameters of the legs. We compare the numerically solved Eq. (15) (full lines) to numerical stochastic simulations with N legs (dots) in Fig. 4-B and find excellent agreement.

The coefficients Γ_n contributing to each bound state can be further investigated to yield an analytical approximation for $\Gamma_{\text{eff}}^{N\,\text{legs}}$. When a large number of legs N is involved in the process, the dominant term in the sum of Eq. (15) corresponds to the average number of bonds $N_b = \sum_{n=0}^{N} n p_n = \frac{q_{\text{on}}}{q_{\text{off}}+q_{\text{on}}} N$. Furthermore, one expects that the coefficients vary weakly around $n = N_b$, simplifying the linear system for the $\{\Gamma_n\}$, yielding

$$\frac{1}{\Gamma_{\text{eff}}^{N\,\text{legs}}} \underset{N\gg 1}{\simeq} \frac{1}{\Gamma_{N_b}} = \frac{1}{\Gamma + N_b \gamma_{\text{eff}}}. \quad (16)$$

The right hand side of Eq. (16) is valid regardless of parameter values (Fig. S3) and provides a good approximation for $\Gamma_{\text{eff}}^{N\,\text{legs}}$ for large values of N (Fig. S2). For example, close agreement with Eq. (15) is obtained as early as $N = 20$, while good qualitative agreement is obtained for $N = 5$ (see Fig. 4-B, dotted line). Eq. (16)

shows that the effective friction with N legs decays linearly with the *average* number of bonds N_b. For systems with a large number of legs (and hence potentially a large average number of bonds) [31, 38, 39], we therefore expect a strong diffusion decrease, covering potentially several orders of magnitude, due to enhanced friction with the surface.

II. DO NANOCATERPILLARS HOP OR SLIDE?

Our model and analytical formula Eq. (15) are useful not only for quantitatively predicting the diffusion coefficients of existing nanocaterpillar systems, but also to obtain insight into the *mechanism* by which particles diffuse. Different experiments with DNA-coated colloids made puzzling and seemingly contradictory observations, whereby similar systems appear to diffuse in different ways. For example, some DNA-coated colloids appear to diffuse through a succession of uncohesive moves, namely hops above the surface [39], while others move cohesively along the surface [31]. The difference between cohesive and uncohesive modes of motion has been noted in a variety of other systems, ranging from virus mobility on surfaces [17, 19] to sticky polymer reptation [62]. Yet the parameters that characterize and quantify these different modes of motion remain to be elucidated. Our model gives insight into this question – do nanocaterpillars prefer to diffuse by "sliding" along the surface, or by "hopping" along it (see Fig. 5-A)?

A. What are hopping and sliding?

We start by quantifying the diffusion associated with either hopping or sliding. The mean squared displacement of a particle whose diffusion coefficient is determined from Eq. (15) can be split into two contributions, as

$$\begin{aligned}\langle x^2\rangle = 2D_{\rm eff}t &= 2p_0\frac{k_BT}{\Gamma_0}t + 2\sum_{n=1}^{N} p_n\frac{k_BT}{\Gamma_n}t \\ &\equiv 2D_{\rm hop}t + 2D_{\rm slide}t.\end{aligned}$$

We identify (a) a *hopping* mode (in accordance with Refs. 34 and 39) where the particle detaches *all bonds* with the surface and moves in free space (see Fig. 5-A), until it forms another bond. In this hopping mode

$$D_{\rm hop} = p_0\frac{k_BT}{\Gamma} = \left(\frac{q_{\rm off}}{q_{\rm off}+q_{\rm on}}\right)^N\frac{k_BT}{\Gamma}. \qquad (17)$$

We also isolate (b) a *sliding* mode (see Fig. 5-A) where the particle keeps at least one bond with the surface, a form of walking with no preferred direction,

$$D_{\rm slide} = \sum_{n=1}^{N}\frac{p_n}{\Gamma_n} \simeq \frac{k_BT}{\Gamma_{N_b}} = \frac{k_BT}{\Gamma + N\frac{q_{\rm on}}{q_{\rm off}+q_{\rm on}}\gamma_{\rm eff}}. \qquad (18)$$

The total mean-squared displacement can be broken up into the sum of the mean-squared displacement when hopping, and the mean-squared displacement when sliding, as $\langle x^2\rangle = 2D_{\rm hop}t + 2D_{\rm slide}t = \langle x^2\rangle_{\rm hop} + \langle x^2\rangle_{\rm slide}$.

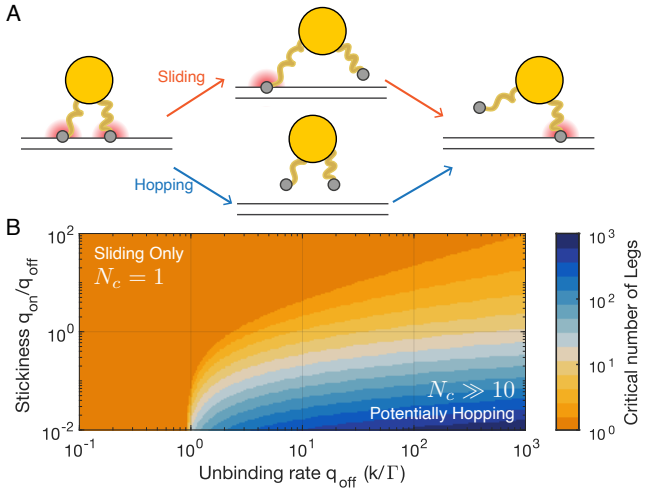

FIG. 5. **Nanocaterpillar diffusion modes with N legs.** (A) Typical modes of motion with N bonds: the nanocaterpillar may either slide (at least one bond remains attached to the surface) or hop (all bonds detach for the particle to move). (B) Critical number of legs N_c required for sliding to be more effective than hopping as a function of stickiness $q_{\rm on}/q_{\rm off}$ and unbinding rate.

An important observation is that $D_{\rm slide}$ decays with the number of legs roughly as $1/N$, while $D_{\rm hop}$ decays exponentially with N, *i.e.* much faster. As soon as a few legs are involved, we may therefore expect that *sliding* dominates *hopping*. This interpretation is natural, since when a system has just a few legs ($N \simeq 1-2$), the odds that the legs all *detach at once* are quite high, therefore favoring hopping. In contrast, in a system with a large number of legs, the odds that all legs *simultaneously* detach are simply too small, and the system walks randomly, remaining close to the surface. In a sense, nanocaterpillars truly are caterpillars walking with nanoscale legs. The scaling quantifying both modes of motion is another essential analytical result of our work.

In general, the critical number of legs $N_c(q_{\rm on}, q_{\rm off}, k, \gamma, \Gamma)$ required to favor sliding ($N \geq N_c$) over hopping ($N \leq N_c$) satisfies

$$\frac{\langle x^2\rangle_{\rm hop}}{\langle x^2\rangle_{\rm slide}} = \frac{D_{\rm hop}}{D_{\rm slide}} = \left(\frac{q_{\rm off}}{q_{\rm off}+q_{\rm on}}\right)^{N_c}\left(1 + N_c\frac{q_{\rm on}}{q_{\rm off}+q_{\rm on}}\frac{\gamma_{\rm eff}}{\Gamma}\right) = 1. \qquad (19)$$

The critical number of legs is controlled by the ratio $q_{\rm on}/q_{\rm off}$, termed henceforth *stickiness*, and by the magnitude of the effective friction in the bound states $\gamma_{\rm eff}$, itself dominated in most systems by the unbinding rate $q_{\rm off}$. We can therefore investigate N_c as a function of stickiness $q_{\rm on}/q_{\rm off}$ and unbinding rate $q_{\rm off}$ (Fig. 5-B). Overall, a system with say $N = 10$ legs is typically dominated by sliding motion. Yet hopping may still occur *e.g.* with

large unbinding rate $q_{\rm off}$. In fact $q_{\rm off}$ increases the friction $\gamma_{\rm eff}$ in the bound states and reduces $D_{\rm slide}$. The number of legs is thus a critical parameter for nanocaterpillar diffusion: controlling both the magnitude of the diffusion decrease and the mode of motion.

B. Distinguishing the diversity of biophysical nanocaterpillars

Whether a nanocaterpillar slides or hops, as predicted by Eq. (19), depends on numerous system parameters. Existing biological and biomimetic systems cover a broad range of parameters that we now explore, to ask which systems prefer to move by sliding and which by hopping, within the framework of our model.

Our model relies on 6 physical parameters $k, \gamma, q_{\rm off}, q_{\rm on}, \Gamma, N$ that can be estimated from the literature for many systems : viruses, molecular motors, white blood cells, protein cargos in the nuclear pore complex, bacteria such as Escherichia coli, and DNA-coated colloids (Supplementary 3). Typically, stickiness values are similar across systems with $q_{\rm on}/q_{\rm off} \sim 0.05 - 0.8 \geq 1$ – when the system is not thermally manipulated as will be explored in Sec. II C. Therefore we consider $q_{\rm on}/q_{\rm off} \simeq 0.1$. Additionally, as legs are generally small compared to particles, $\gamma/\Gamma \simeq 10^{-3} - 10^{-1}$ and therefore the dominant factor in $\gamma_{\rm eff}/\Gamma$ is usually controlled by spring recoil force and unbinding times, as $k/\Gamma q_{\rm off}$. We find $k/\Gamma q_{\rm off} \simeq 10^{-2} - 10^{8}$ in the range of systems studied, confirming that this is a critical factor to discriminate nanocaterpillars. Additionally, as systems have a varied number of legs N, we define an effective relaxation rate

$$\frac{k^{(N)}}{\Gamma} = \frac{k}{\Gamma} N \frac{q_{\rm on}}{q_{\rm off}+q_{\rm on}} \left[\left(\frac{q_{\rm off}+q_{\rm on}}{q_{\rm off}} \right)^{N} - 1 \right]^{-1}$$

that will allow us to predict either sliding or hopping.

We sort systems in a so-to-speak *Ashby* chart, according to the effective relaxation rate $k^{(N)}/\Gamma$ and unbinding rate $q_{\rm off}$ (Fig. 6). This chart summarizes parameter ranges for different systems, and predicts which systems move by sliding and which move by hopping, within the assumptions of our model. If $k^{(N)}/\Gamma q_{\rm off} \leq 1$, according to Eq. (19), sliding (orange region) is favored over hopping (blue region). While other modes of motion could occur for such complex systems, our aim here is to observe these systems in the "projected" sub-space where only sliding and hopping is considered. Interestingly, we find that different groups of systems emerge according to this classification, that we review below.

1. *Sticky hoppers*

We predict that viruses, white blood cells, and molecular motors cannot slide. These systems show very long bond lifetimes, with $\tau_{\rm off} = q_{\rm off}^{-1} \simeq 1 - 100$ s. This is characteristic of strong bonds, for which the interaction energy $|\Delta G| \gg k_B T$. Since for the protein ligands in these systems, $k \simeq 10^{-4}$ N/m and $\Gamma \simeq 10^{-9}$ N.s/m for 1μm particles, we expect $k/\Gamma \simeq 10^{5} \gg q_{\rm off}$ and $\gamma_{\rm eff} \gg \Gamma$. Therefore such systems simply can not slide. Sliding is even more disfavored for coronaviruses (Sars CoV 1 and 2), since the legs are made of very rigid proteins, with $k \simeq 0.5$ N/m [63, 64]. Hopping is therefore a probable mode of motion for these systems.

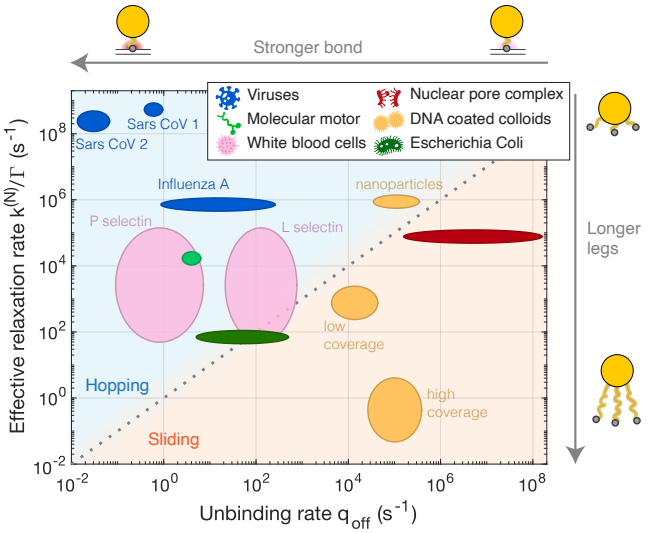

FIG. 6. **Sorting biophysical systems.** Expected regimes of sliding or hopping according to the effective relaxation rate $k^{(N)}/\Gamma$ and unbinding rate $q_{\rm off}$. The gray line corresponds to $k^{(N)}/\Gamma = q_{\rm off}$ and separates the sliding and the hopping regions. Circles represent the range of values found in the literature for parameters of each system. Systems are color coded according to their category in the legend. When multiple systems belong to a category, details are indicated next to the circles. Low and high coverage DNA-coated colloids refer to 1 μm size colloids and nanoparticles to 15 nm size.

These predictions are qualitatively consistent with experimental measurements. The diffusion coefficient of an influenza A virus on protein-coated surfaces was measured as $D_0/D_{\rm eff} \simeq 4 - 190$ [17, 19]. Estimating the typical number of available legs $N \simeq 10$ [65, 66] and the bound probability $q_{\rm on}/(q_{\rm on}+q_{\rm off}) = 20\%$ [66] yields $D_0/D_{\rm hop} = [q_{\rm off}/(q_{\rm on}+q_{\rm off})]^N \simeq 10$, in the range of measured values. Our model predicts that hopping is therefore more probable than sliding for influenza A, at least when considering its translational motion under passive binding and unbinding. This is consistent with Ref. 17, which observed infrequent yet very long spatial steps, termed *gliding* moves. We note that the influenza A virus has also been observed to move via cohesive short spatial steps, that have been attributed to rolling motion [5, 17, 19, 41], which may be due in this context to active bond cleaving [17, 19, 41] that is beyond the scope of passive binding as presented here.

Turning to DNA-coated colloids, while the binding ki-

netics are roughly independent of colloid size, the effective relaxation rate can vary strongly. Nanometre-sized DNA-coated colloids (yellow nanoparticles) have fast relaxation rates as they are small (and therefore Γ is smaller), and are thus sticky hoppers. In contrast, micronscale colloids have slower relaxation rates $k^{(N)}/\Gamma$, all the more as usually a great number of bonds $N \simeq 100$ are involved in the binding process, and thus are prone to slide. We will turn in more detail to DNA-coated colloids in Sec. II C.

2. *Slippery sliders*

Reciprocally, we predict that systems with weak adhesion (equivalent to short bond lifetimes, *i.e.* large q_{off}) may move by sliding. Such systems include proteins translocating through the nuclear pore complex, or white blood cells adhering through L-selectin linkers, which are notably weaker than P-selectin [23]. Sliding may also be accessible to systems with short effective relaxation rate, for which the sticky friction mediated by k/Γ is low. This corresponds to large particles with long legs, as is the case for Escherichia Coli [57] (dark green). DNA-coated colloids with high DNA coverage are prone to slide due to their large number of legs.

C. DNA-coated colloids hop *and* slide, with order of magnitude decrease in their diffusion coefficient

We now turn to probe in more detail the predicted modes of motion and strong decrease in diffusion of DNA-coated colloids by comparing our model's predictions with experimental measurements of DNA-coated colloids. DNA-coated colloids provide a well-controlled model system for testing our analytical results, especially their dependence on N, since the number of DNA legs involved in the sticking process may be easily tuned by changing the temperature [38]. Our aim here is not to build a detailed model to describe all the possible modes of motion of DNA-coated colloids. Rather, we seek potential key parameters that control the magnitude of the diffusion and the mode of motion. To do so, we test whether the predicted strong decrease is coherent with experimental observations over a range of temperatures and for three different experimental designs.

1. *Model parameters can be directly established from experimental data.*

We predict the diffusion coefficients D_{eff} (and D_{slide} and D_{hop}) for three different experimental systems, by determining the parameters involved in Eq. (15) from the literature or from independent measurements, with no fitting parameters (apart from calibrating to the melting temperature, as discussed below). The diffusion coefficients for DNA-coated colloids on flat DNA-coated surfaces have been measured in two different experimental systems reported in the literature [31, 39]. These studies report only very few data points around the melting temperature where motion is diffusive, since in these experimental systems diffusive motion is only observed in a narrow range of temperatures, so the studies focused mainly on the low temperature regime where motion is subdiffusive. We complemented the scarce existing data by performing our own experiments, using recently-developed fabrication [38] and acquisition techniques [31, 39], and we observe diffusive motion over a wider range of temperatures (Supplementary 2). For each of the three experimental datasets, we map reported experimental parameters to the parameters of the model, and detail our process below.

Some parameters are easily estimated using standard results, see Table A2. The friction coefficient Γ is taken as the hindered lateral hydrodynamic friction near a wall [67]; γ and k correspond to hydrodynamic friction and spring resistance of the polymer linker (that links the surface and the complementary DNA strand) and are directly established from polymer dynamics [56]. The binding rate q_{on} depends on the exact – known – DNA sequence used for the complementary stickers and the density of coated DNA strands on surfaces [70].

Other parameters, such as N and N_b (or equivalently N and the ratio $q_{\text{on}}/q_{\text{off}}$) require more extensive modeling of the detailed leg-arm interactions to be evaluated. Recently Refs. 38 and 59 have shown how to establish N and N_b with no fitting parameters, taking as input parameters the DNA sequence used, the coating densities, and the properties of the DNA linker (see Fig. S5), and we employ the method we have developed in Ref. 38.

Finally, since measurements include colloid vertical motion beyond the binding range[71], we further include vertical motion and hence particle buoyancy through a 2×1D model. Such vertical motion is generally slow and only affects the effective probabilities p_n, not the friction coefficients Γ_n. Motion in two lateral dimensions can be straightforwardly extended from our 1D model (see Supplementary 2 for more details).

All parameters are thus readily expressed from detailed experimental system design. The diffusion coefficient D_{eff} is decreased by orders of magnitude at low temperatures. It progressively increases to its "bare" value – corresponding to non-sticky DNA – at high temperatures, with a sharp transition. This sharp transition from the bound to unbound state occurs at a melting temperature T_m specific to each experimental design. The predicted T_m is always close to the experimentally measured T_m (less than 1°C difference) with no fitting parameters.

Nonetheless, intrinsic variations remain in experimental parameters. In particular, different *e.g.* humidity conditions can affect the coating process and exact coating density obtained, and hence the experimental T_m, over about 2°C. To investigate data over the relevant short temperature range where diffusion can be mea-

TABLE A1. Method used to calculate model parameters for the DNA-coated colloids studied experimentally in this work. Parameter values are reported only at the melting temperature T_m. Their dependence on temperature is indicated in the "Comments and References" column.

Parameter	Formula used	Value at T_m	Comments and References
Γ	$\Gamma = 2 \times 6\pi\eta(T)R$	1.6×10^{-8} N.s/m	hydrodynamic friction near a surface [67]; colloid radius $R = 500$ nm; $\eta(T)$ water viscosity with temperature.
γ	$\gamma = 6\pi\eta(T)h$	1.8×10^{-10} N.s/m	with brush height $h \simeq 22$ nm, calculated with Milner-Witten-Cates theory [68], and accounting for increased brush density due to Pluronic F127 (see Ref. 38).
k	$k = 3k_BT/2L\ell$	0.16 mN/m	spring constant for polymers [56]; extended brush length $L \simeq 84$ nm (6500 g/mol PEO + 20 single stranded DNA (ssDNA) bases); persistence length $\ell = 0.5$ nm (average of PEO + ssDNA at 140 mM salt concentration [69])
q_{on}	$q_{\text{on}} = k_{\text{on}}\bar{\sigma}/h\mathcal{N}_A$	4 kHz	where $k_{\text{on}} = 1.6 \times 10^6$ M^{-1}.s^{-1} from Ref. 70, using the exact sequence as in our experiments; $\bar{\sigma} = \sqrt{\sigma\sigma_g}$ where $\sigma = 1/(3.27 \text{ nm})^2$ is the particle coating density and $\sigma_g = 1/(10.8 \text{ nm})^2$ is the glass substrate coating density; Avogadro's number $\mathcal{N}_A$; Independent of T.
q_{off}	$q_{\text{off}} = q_{\text{on}} \frac{N(T)-N_b(T)}{N_b(T)}$	18 kHz	N_b average number of bound legs and N total number of legs available for binding in the interaction region; Dependent on T.

sured, one option could be to fit *e.g.* the value of the coating density on colloids, to obtain the exact experimental T_m – effectively fitting the location of the sharp transition. Instead, we choose to align all data (theoretical or experimental) with respect to its own melting point T_m (predicted or measured). This has the advantage of avoiding fitting and allowing us to easily compare similar experimental systems with slightly different T_m (Supplementary 2).

2. *The coating density controls the mode of motion and the magnitude of the diffusion coefficient decrease.*

The number of legs implied in the sticking process N changes significantly with temperature. At low temperatures $N \gtrsim 100$; the colloids are strongly bound. With increasing temperatures N decreases until the particles are completely unbound and $N = 0$ (see Fig. S5), with a sharp transition at the melting temperature T_m. Importantly, the number of legs is the parameter that changes the most with temperature and controls therefore the magnitude of the long time diffusion D_{eff}.

The three experimental systems differ mainly in the DNA coating density, which implicitly controls the number of legs N involved in the binding process. For densely coated colloids (Fig. 7, A and B), we find excellent agreement between our model calculation for D_{eff} and experimental data, predicting a fast diffusion decrease over 2 orders of magnitude in barely a few temperature degrees. Further, we predict that sliding, or some form of cohesive motion with the surface, is the dominant mode of motion below the melting temperature T_m. In fact the high number of available legs, $N \simeq 100$, due to high coverage, prevents hopping below the melting temperature and colloids primarily slide, consistent with the observed cohesive motion [31]. Hopping emerges as a favorable mode above the melting point, where the average number of available and bound legs significantly decreases due to particle lift-off from the surface. This prediction is consistent with our qualitative observations above the melting point: particles perform long moves over short time intervals, accompanied by more frequent and longer excursions far from the surface. The transition between motion modes occurs for about $N = 40$ legs in contact (Fig. S5).

For DNA-coated colloids with low coverage densities, as in Ref. 39 (Fig. 7 C), our model predicts a diffusion coefficient that is far too large. Yet, D_{hop} is in remarkable agreement with experimental data. In fact, D_{eff} contains sliding motion yet the spacing between legs in Ref. 39 is too large and geometrically prevents sliding. Hence only hopping, or uncohesive motion with the surface, is possible. In fact, for such systems only hopping is observed, resulting in a much stronger slow down of diffusion with decreasing temperature [39]. The DNA coating density therefore appears to be a significant factor in determining how DNA-coated colloids move, allowing it to vary from sliding to hopping.

3. *Other possible modes of motion.*

There are other ways that DNA-coated colloids could move in specific experimental regimes, that could be probed with the analytical tools set forth here, yet

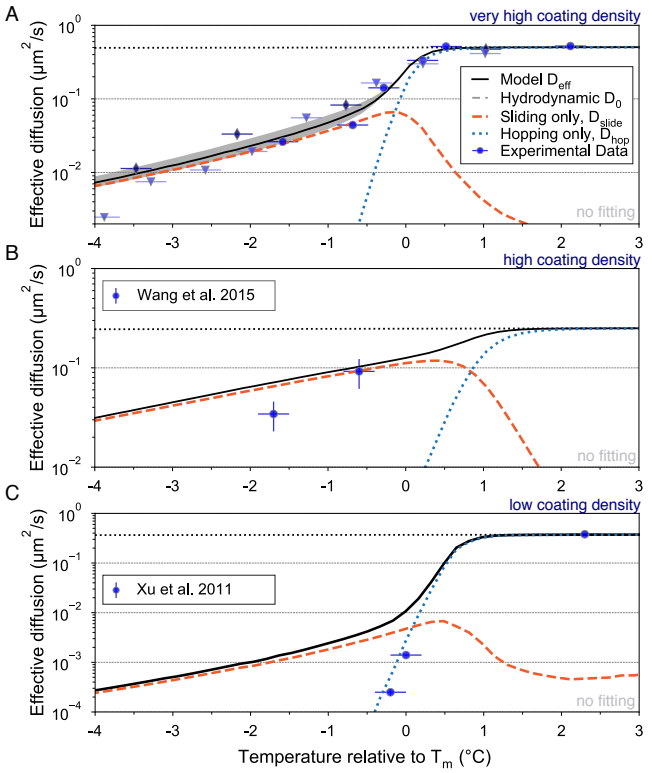

FIG. 7. **Diffusion coefficients of DNA-coated colloids.** Comparison between experimentally measured diffusion coefficients of DNA-coated colloids on DNA-coated surfaces and analytical predictions of D_{eff}, D_{slide}, and D_{hop} (Eqns. (15), (18) and (17)). The DNA-coated colloids have (A) highly dense coatings (1 DNA per 10 nm^2, Supplementary 2) (B) dense coatings (1 DNA per 27 nm^2) from Ref. 31 and (C) sparse coatings (1 DNA per 144 nm^2) from Ref. 39. In (A) the gray region corresponds to uncertainties on the coating density of the substrate, and the different symbols correspond to repeated experiments repeated. The hydrodynamic diffusion $D_0 = k_B T/12\pi\eta R$ corresponds to lateral diffusion near a flat rigid wall, where R is the radius of the colloid and η the solution viscosity. Horizontal error bars correspond to uncertainties on imposed temperature and vertical error bars correspond to uncertainties in determining the diffusion coefficient from data (Supplementary 2).

that we have not yet explored. At lower temperatures, particles don't diffuse, they rather subdiffuse [31, 39], potentially due to inhomogeneities in the coated surfaces [31, 39, 42]. Such spatial dependencies are not accounted for in our model but could be studied through spatially dependent attachment rates $q_{\text{on}}(x)$ or leg number $N(x)$.

Particles may also move by rolling instead of by sliding [31], a motion that could also be investigated with homogenization techniques. Rolling may have a higher mobility at some temperatures [33, 54], since the strands closest to the contact point on the surface do not resist rolling, for geometrical reasons. Yet when a large number of bonds are implied in the binding process, numerous bonds are actually far from the contact point and hence resist rolling. It is possible that rolling is thus favorable only over a small range of temperatures.

Although our model lacks these more complex ingredients and geometries, it is in surprisingly good agreement with our experimental measurements. This suggests we have identified some critical parameters controlling the observed effective diffusion, precisely the coating density and working temperature as they set the number of legs N. Even in a more complex model, containing *e.g.* inhomogeneous coating density, or rotational degrees of freedom, we therefore expect these parameters to play an important role in mobility.

D. Design rules for sliding versus hopping

Herewith we can draw simple design rules for sliding or hopping. Numerous, long wobbly legs with weak adhesive bonds are well adapted for sliding. Short and stiff legs with strong adhesive bonds facilitate hopping. DNA-coated colloids offer various design features to control their mobility: for example, larger particle size, higher DNA coverage, and lower temperature all favor sliding. Further control can be achieved by tuning the microscopic features of the legs, such as their spring constants k, for example by choosing the length of the ligand leg [38]. However, such control is especially hard to achieve experimentally *without* changing other experimental features at the same time. For example, current coating processes generally result in less dense coatings for longer legs [38].

Overall, these design rules allow one to tune artificial systems to control their mobility. This could have consequences in particular in the field of self-assembly of artificial structures, where facilitated cohesive motion is believed to be essential for long-range alignment [31–33].

III. COARSE-GRAINING UNDER DIFFERENT MODELS AND ASSUMPTIONS

In the physical and biological systems we explored, the range of physical parameters was quite broad, suggesting that other scaling ansätze might be appropriate to study long term dynamics. We review alternative approximations and modeling assumptions and compare them to the predictions of the model presented in Section I. We find that our model is the most general, encapsulating perturbative results obtained with other approximations, and that it is naturally modified to account for additional features (such as arms as well as legs). To make the argument simpler, we mainly focus on a 1-legged caterpillar; the comparisons should be similar for a multi-legged caterpillar. Detailed coarse-graining steps are reported in Supplementary 4. All results are summarized in Table A2 (displayed in the Appendix) and compared in Fig. 8.

A. Dynamics with inertia

One may include particle inertia with a small yet finite mass $m \neq 0$, by starting with the underdamped Langevin equations for the particle (rather than the overdamped as we have done) – see Ref. 54. To understand the scales associated with mass, one can compare the correlation time of the particle's velocity when spring recoil forces are at play, $\tau_v \simeq \frac{m(L_x/\tau)}{Lk}$, to the time scale of observation τ [54]. Coarse-grained dynamics require $\frac{\tau_v}{\tau} = \frac{mL_x}{Lk\tau^2} = O(\epsilon)$, which is apparently coherent with a small mass.

Coarse-graining steps (Supplementary 4.1) lead to an effective friction

$$\Gamma^m_{\text{eff}} = p_0\Gamma_0 + p_1\Gamma_1. \tag{20}$$

Notice that the effective friction is the *arithmetic* sum of the frictions in each state – not the *harmonic* sum obtained in Eq. (12) [72]. Eq. (20) is equivalent to Eq. (12) in the limit where the friction correction is small, $\gamma_{\text{eff}} \ll \Gamma$ – see Fig. 8-B (yellow).

However, differences arise beyond this regime. For stiff legs ($\gamma/\Gamma \gg 1$, $k/q_{\text{off}}\Gamma \gg 1$) one finds $\Gamma^m_{\text{eff}} \sim 0$ while $\Gamma_{\text{eff}} \sim \Gamma$. This stark difference has an intuitive explanation: the particle may not move when it is attached with the stiff leg, but it can still move when it is unbound, and therefore the effective friction should remain finite. This is true *unless* the particle has significant inertia and therefore does not have the time to accelerate within the unbound periods. In fact, in the non-dimensionalization we implicitely assumed that $m/\Gamma = \epsilon Lk\tau^2/\Gamma L_x = \Gamma/k\epsilon^2$, such that the inertial relaxation time was in fact assumed to be large compared to the time scale of velocity fluctuations.

This drives the general question of how to account for inertia in such systems, and whether inertia plays a role in the macroscopic diffusion of nanocaterpillars. We will address this question thoroughly in another paper [73], in which we reconcile Eq. (20) and Eq. (12).

B. Choice of time-scale hierarchy

There are other choices for the ordering of time scales. We review these below: we describe their experimental relevance, then briefly examine the effective friction under these different approximations and compare it to our main result Eq. (12).

1. *Fast leg dynamics compared to particle dynamics*

One common approximation is to assume rapid leg dynamics compared to particle dynamics, with $\epsilon = \gamma/\Gamma$ [51]. Such an approximation is consistent with numerous experiments, as legs are typically short, hence fast because of Stokes relation, compared to the large particles investigated (such as white blood cells [7] or DNA-coated colloids [74]).

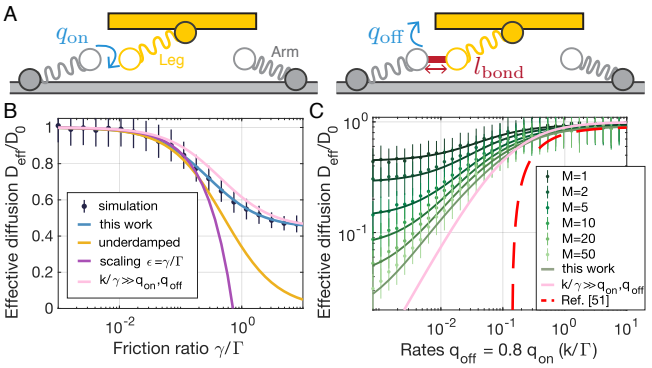

FIG. 8. **Comparing with other coarse-grained models and assumptions.** (A) Schematic for arm and leg dynamics considered in this work. (B) Effective diffusion with respect to friction ratio γ/Γ: calculated with Eq. (12) ("This work"), Eq. (20) ("underdamped"), Eq. (21) ("scaling $\epsilon = \gamma/\Gamma$") and Eq. (22) ("$k/\gamma \gg q_{\text{on}}, q_{\text{off}}$"). (C) Effective diffusion with respect to binding and unbinding rates (keeping $q_{\text{on}}/q_{\text{off}}$ constant), for a particle with 1 leg facing $M = 1-50$ arms: calculated with Eq. (25) ("This work") and Eq. (22) ("$k/\gamma \gg q_{\text{on}}, q_{\text{off}}$"), taking $p_0 = 0$ and $p_1 = 1$ to match the limits in $M \to \infty$. Ref. 51 corresponds both to $k/\gamma \gg q_{\text{on}}, q_{\text{off}}$ and $\gamma/\Gamma = \epsilon$ and was plotted for consistency. For (A) and (B), shared numerical parameters are $q_{\text{on}}\Gamma/k = 1.0$, $q_{\text{off}}\Gamma/k = 0.8$ and $\gamma/\Gamma = 0.1$.

With this assumption one typically relaxes the restriction on lengthscales, as $L \sim L_x$. The observation timescale is $\tau = L^2/D_0 = \Gamma/k$ and binding and unbinding are taken to be fast compared to this time scale, $q_{\text{on}} \sim q_{\text{off}} \sim 1/\tau\epsilon$. One obtains (Supplementary 4.2.1)

$$\frac{1}{\Gamma^{\epsilon=\gamma/\Gamma}_{\text{eff}}} = \frac{p_0}{\Gamma} + \frac{p_1}{\Gamma}\left(1 - \frac{\gamma_{\text{eff}}}{\Gamma}\right). \tag{21}$$

Eq. (21) results in a small correction to the effective friction, of order ϵ. It is equivalent to Eq. (12) in the limit where $\gamma_{\text{eff}} \ll \Gamma$ is small. The assumption $\epsilon = \gamma/\Gamma$ appears thus quite restrictive as it implicitly also requires to observe the system at long time scales compared to the other time scales in the system. Furthermore, contrary to Eq. (12) where the small parameter ϵ disappears, here $1/\Gamma^{\epsilon=\gamma/\Gamma}_{\text{eff}}$ is a first order expansion in $\epsilon \sim \gamma_{\text{eff}}/\Gamma$. We present Eq. (21) against Eq. (12) in Fig. 8-B (purple vs black) and find that Eq. (21) is indeed only valid for small values of γ/Γ. Our choice of scaling $\epsilon = L/L_x$ can thus account for a broad range of bare friction values. Additionally, such an approach can only account for small perturbations to the background mobility, while we find perturbations over several orders of magnitude.

2. *Fast leg dynamics compared to binding dynamics*

Another approximation assumes fast leg relaxation dynamics compared to binding dynamics, $k/\gamma \gg q_{\text{on}}, q_{\text{off}}$ (and both are fast compared to particle dynamics). In

this case leg lengths are sampled from their equilibrium distribution when they bind, corresponding to a "pre-averaging" approximation. Leg lengths are not tracked when they are unbound, allowing to speed up simulations [22, 33, 51, 75]. This limit is relevant to describe stiff legs, *e.g.* rigid polymers such as double stranded DNA – see Table S1.

Coarse-graining gives (Supplementary 4.2.2)

$$\frac{1}{\Gamma_{\text{eff}}^{\text{k}/\gamma\gg\text{q}}} = \frac{p_0}{\Gamma} + \frac{p_1}{\Gamma+\gamma+\frac{k}{q_{\text{off}}}}. \tag{22}$$

The pre-averaged result Eq. (22) is comparable to Eq. (12), yet misses the relaxation term involving $\tau_{\text{u}}^{\text{relax}}$ in γ_{eff}. This confirms that $\tau_{\text{u}}^{\text{relax}}$ originates from unbound relaxation dynamics. This difference results in some differences in D_{eff}, depending on the microscopic parameters (Fig. 8-B). Additionally, the pre-averaged limit may be viewed as the limit regime for a nanocaterpillar with a large number of legs, say $N \gg 1$, where on average 1 or 0 leg is bound to the surface, $N_b \lesssim 1$. This typically requires $q_{\text{on}} \ll q_{\text{off}} \ll k/\gamma$, and indeed Eq. (15) converges to the pre-averaged result in that limit (Supplementary Fig S4).

The validity of pre-averaging is limited to the domain $q_{\text{on}}, q_{\text{off}} \ll k/\gamma$. In systems such as DNA-coated colloids, binding rates q_{on} and q_{off} may be manipulated over orders of magnitude [76], by choosing the DNA sequence or by adjusting temperature, potentially accessing $q_{\text{on}} \gg q_{\text{off}} \gg k/\gamma$ at low temperatures. In this regime, Eq. (12) predicts that the nanocaterpillar is frozen in the bound state, while pre-averaged dynamics still predict a non zero mobility. In these situations pre-averaged dynamics are therefore not suitable. We show later however that introducing numerous arms – more generally a lot of binding partners – can extend the validity range of pre-averaging.

3. Fast binding dynamics compared to leg dynamics

Finally, one can consider fast binding dynamics compared to leg dynamics, $q_{\text{on}}, q_{\text{off}} \gg k/\gamma$. Although this limit is not often considered in simulations, it is relevant for dense arrangements of receptor sites [74]. In fact as the binding rate q_{on} scales linearly with the concentration of receptors, it can increase by orders of magnitude for a leg potentially in contact with a dense array of arms – see Table S1.

Coarse-graining yields (Supplementary 4.2.3)

$$\frac{1}{\Gamma_{\text{eff}}^{q\,\text{fast}}} = \frac{p_0}{\Gamma} + \frac{p_1}{\Gamma+\gamma+k\left(\frac{\gamma}{k}\frac{q_{\text{on}}}{q_{\text{off}}}\right)} \tag{23}$$

which is exactly what is expected in the limit $q_{\text{on}}, q_{\text{off}} \gg k/\gamma$ in Eq. (12). Again, this highlights the physical mechanisms yielding the different contributions in γ_{eff}. Here the average bound time of the leg is small, $\tau_{\text{b}} \ll \gamma/k$, and therefore does not contribute to γ_{eff}.

C. Arms and/or legs

The diversity of nanocaterpillars resides also in their geometry: some particles have legs that attach to a surface [77], some have no legs (or infinitesimally small legs), with binding sites directly on the particle that attach to outstretched receptors on the surface that we refer to as arms [22, 51] (1 arm case in Table A2) and some have both outstretched legs connecting to outstretched arms [33] (arms and legs in Table A2).

1. Arms or legs

A particle with a leg or a bare particle attaching to an arm (1-legged and 1-armed respectively, see Table A2) have nearly equivalent effective dynamics. The only difference resides in the interpretation of Γ in the unbound leg dynamics Eq. (2) – see Supplementary 4.3.1. For the 1-legged case, if the leg's center of mass corresponds to the point grafted to the particle, the unbound friction coefficient is simply increased by the leg as $\Gamma \to \Gamma + \gamma$, where Γ is the bare particle friction coefficient and γ the leg's. If the leg's center of mass is offset from the grafting point on the surface, minor modifications have to be made to Eq. (2) yet lead to very similar dynamics overall. For the 1-armed case, we simply have the unbound friction coefficient Γ to be the bare friction coefficient of the particle. This justifies our approach in Sec. I, where we ignore the details of the leg or arm location and simply treat them as mathematically equivalent.

2. Arm and leg

A 1-legged particle attaching to 1 arm has slightly more interesting dynamics. To investigate this case, we simplify the problem and consider that the leg can bind to the arm regardless of their relative location, with a rigid rod of length l_{bond} that bridges the gap between the sticky points (see Fig. 8-A). In the bound state the constraint is thus $x + l_{\text{leg}} - l_{\text{arm}} = l_{\text{bond}}$. The relative distance l_{bond} is unimportant and can be assumed to be zero, and therefore this model effectively creates an arm with the correct length each time the leg binds.

Although the model is simplistic, it is realistic in the presence of a dense periodic array of arms and allows us to compare the mechanical properties of this geometry compared to a single leg or arm. We find using similar coarse-graining techniques (Supplementary 4.3.2)

$$\frac{1}{\Gamma_{\text{eff}}^{leg+arm}} = \frac{p_0}{\Gamma} + \frac{p_1}{\Gamma+\gamma_{\text{eff},1}(1,1)} \text{ where } \gamma_{\text{eff},1}(1,1) = \frac{\gamma_{\text{eff}}}{2}. \tag{24}$$

The added friction in the bound state is only half that with a single leg or a single arm: friction is distributed harmonically, like the effective spring constant of two

springs in series [78]. Slightly improved mobility is therefore achieved with both an arm and a leg, while the qualitative behavior of the original model is preserved.

3. Leg facing numerous arms

We now consider a leg that can bind to *multiple* arms at the same time. As in the previous section, the M arms do not have particular locations but rather appear with the correct lengths when needed. In that case, the binding rate depends on the number of bound legs. For a given leg, the effective binding rate is $(M-n)q_{\rm on}$, where n is the current number of bound legs, such that $M-n$ corresponds to the number of available binding sites. The effective unbinding rate of each leg remains $q_{\rm off}$. Following the formalism of arm and leg dynamics detailed above (Supplementary 4.3.3) one finds that with M arms,

$$\frac{1}{\Gamma_{\rm eff}^{leg+M\,arms}} = \frac{p_{M,0}}{\Gamma} + \frac{p_{M,1}}{\Gamma+\gamma_{\rm eff,1}(M,1)} \qquad (25)$$

where $p_{M,0} = q_{\rm off}/(q_{\rm off}+Mq_{\rm on})$ and $p_{M,1} = 1-p_{M,0}$ are the probabilities to have 0 or 1 bond. The added friction $\gamma_{\rm eff,1}$ is a harmonic average when M is large

$$\frac{1}{\gamma_{\rm eff,1}(M,1)} \underset{M\gg 1}{\simeq} \frac{1}{\gamma_{\rm eff,M,1}} + \frac{1}{\gamma_{\rm eff,1,1}}, \qquad (26)$$

with $\gamma_{\rm eff,M,1} = k\left(\frac{1}{q_{\rm off}} + \frac{\gamma}{k}\frac{(M-1)q_{\rm on}+q_{\rm off}}{q_{\rm off}}\right)$ the effective friction due to the leg $\gamma_{\rm eff,1,1} = k\left(\frac{1}{q_{\rm off}}+\frac{\gamma}{k}\right)$ due to arms. We see that the factors implying the unbound relaxation time $\tau_{\rm u}^{\rm relax}$ are modified in each case. We give the following interpretation: the average unbound time for the leg is $\tau_{\rm u} = 1/(M-1)q_{\rm on}$, due to $M-1$ other available arms to bind to. For the arms, $\tau_{\rm u} = \infty$ as there are no other legs to bind to once the only leg is bound. The harmonic average in Eq. (26) highlights again that the leg-arm configuration is mathematically similar to the effective force of springs in series.

In the limit of a large number of arms M, the leg is always bound to the surface ($p_1 = 1$) and the correction to the bound state friction converges to

$$\gamma_{\rm eff,1}(M,1) \xrightarrow[M\to\infty]{} \gamma_{\rm eff,1}(1,1) = \gamma + \frac{k}{q_{\rm off}}, \qquad (27)$$

which is the correction to the effective friction for the pre-averaged result, Eq (22).

This limit is surprising. Sec I, Eq. (12) showed that for a leg binding to a uniformly sticky surface, in the limit where the leg is always bound ($p_1 = 1$), the nanocaterpillar is frozen and $D_{\rm eff} = 0$. When the leg is bound to a great many arms this is no longer the case: we recover the diffusion coefficient associated with pre-averaging. We interpret this discrepancy as follows. With many arms binding to a leg, the particle may still move, even in a parameter regime where the leg is always bound. In fact, the leg rapidly swaps between different arms, which have different random lengths and hence apply different random forces, causing the particle's position to fluctuate. Indeed, in Eq. (27) it is apparent that the remaining friction is due to arms and not to the leg. Swapping the particle upside down, this is equivalent to a particle with a large number M of legs binding to a uniformly sticky surface, but where on average only 0 or 1 leg is bound to the surface at a time. Therefore, this limit is equivalent to the pre-averaged result: each time a new arm is bound it is sampled from its equilibrium distribution – as so many arms are within reach.

Simulations with M arms are presented in Fig. 8-C with analytical solutions Eq. (25) (green colors). They indeed converge to the pre-averaged result (pink). For consistency, we also record the result of Ref. 51 (Eq. (2.48)) that corresponds to pre-averaging *and* assumes $\epsilon = \gamma/\Gamma$. It is plotted in Fig. 8-C (red) and agrees with our result only over a limited range of parameters, corresponding to the validity range of Ref. 51.

4. Numerous legs facing numerous arms

N legs binding to M arms induce a long time effective friction that encapsulates the previous result for M arms and that for N legs in Sec. I D (Supplementary 4.3.4). Eq. (15) still holds with adapted bond probabilities p_n, and $\gamma_{\rm eff}$ in Eq. (16) is the harmonic average between arm and leg contributions, $(\gamma_{\rm eff,n}(M,N))^{-1} = \gamma_{\rm eff,M,n}^{-1} + \gamma_{\rm eff,N,n}^{-1}$.

Overall, spanning different limits shows that our methodology to investigate long time dynamics is robust, as it accounts for a broad range of physical parameters and a variety of geometries. It also justifies the use of "pre-averaging" approximations (sampling leg lengths from equilibrium distributions upon binding) to accelerate simulations in specific situations. It also highlights that taking limits of various parameters is subtle, and care must be taken when doing so as the limits do not commute in general.

CONCLUSION

When a particle is coated with ligands that bind and unbind stochastically to receptors on a surface, the ligands impart a random force to the particle each time they bind, causing the particle to undergo a random walk on long timescales. We constructed a model for the coupled dynamics of such a nanocaterpillar and its leg-like ligands, and derived an analytical expression for the nanocaterpillar's long-term effective diffusion coefficient as a function of the microscopic leg parameters. Our simulations showed this expression is valid over a broad range of parameters. Our expression predicts a dramatic decrease in the diffusion coefficient, by several orders of

magnitude, as temperature decreases by a few degrees, a prediction that is borne out in our experimental measurements.

Our model allows us to distinguish between two modes of motion, sliding and hopping, and to identify parameters that govern which mode of motion is preferred, across a wide range of biophysical systems. Typically, systems with a large number of legs will slide, since the mean-squared displacement due to hopping decreases exponentially with the number of bound legs. Hopping is favored for systems with short, stiff legs, and/or strong bonds. Regardless of the mode of motion, the fast binding and relaxation dynamics at the microscale result in an overall slow diffusion of the nanocaterpillar, sometimes many times smaller than the background hydrodynamic diffusion.

We derived the effective diffusivity for a range of other models and scaling assumptions, which allowed us to tease out *e.g.* the effect of having arms (flexible receptors) as well as legs, having significantly more arms than legs or *vice versa*, having significant inertia, *etc.* In particular, we explored the validity range of specific approximations used to accelerate simulations, such as that upon binding, leg lengths are sampled from their equilibrium distributions [22, 33, 51]. We showed this approximation is valid for fast leg dynamics $\gamma/k \ll q_{\rm on}, q_{\rm off}$ in 1D, or when binding to a great number of binding partners, such as many arms, $M \gg 1$, yet its validity should be reassessed in more complex geometries.

There are numerous ways to build upon our model to address additional complexities within the same coarse-graining framework. An important step would be to incorporate particle rotational degrees of freedom, and to ask how rolling compares to hopping and sliding. Rolling has been predicted to lead to a low effective friction in systems with stiff legs, because it doesn't require stretching legs at the contact point [33, 54]. While rolling has been modeled in special situations, none of these account for the full stochastic nature of the motion, nor do they systematically derive a coarse-grained equation from microscopic parameters [41]. A systematic derivation of a rolling diffusion coefficient would involve a few additional mathematical subtleties beyond those that occur here, such as including binding rates with spatial dependencies to account for the variable separation between surfaces [79, 80], but we may nevertheless expect similar parameters (such as spring relaxation times and unbinding rates) to discriminate between rolling and other modes of motion.

Going further, other effects that could be studied include the details of binding kinetics, *e.g.* non-exponential kinetics in DNA hybridization [81–83], which could also impact the long time response [42]; mobility of the leg roots, corresponding to fluidity of the bilayer [10, 84]; and out-of-equilibrium effects, such as white blood cells streaming in blood flow [5, 80], active stepping of molecular motors [49, 85, 86], or proteins that actively cleave bonds on influenza A [17, 36]. Accounting for such effects would require adapting bond dynamics to include increased bond rigidity or bond lifetime in flow [3, 87–91]; binding kinetics coupled to the number of bonds [47, 49]; or memory effects associated with dead zones created by cleaved bonds [26, 36, 52]. Importantly, such improvements require carefully adapting binding rates to preserve detailed balance and physical constraints [32, 79].

Furthermore, detailed hydrodynamic effects may be important to describe certain kinds of nanocaterpillar dynamics. We have accounted for hydrodynamics via the bare friction coefficients (Γ, γ), but these coefficients themselves are coarse-grained, and in reality depend on the distance of a nanocaterpillar to a surface [67] and are coupled to the details of the polymer leg mesh. Indeed, elasticity of the polymer mesh could modify the particle's mobility near the interface, as was predicted for elastic membranes [92, 93]. A more detailed description of the hydrodynamic flow near a nanocaterpillar could help shed light on other systems where mobility through fluid is mediated by slender legs, such as for the Vampire amoeba [94].

Beyond its biophysical details, nanocaterpillar motion resonates with other fields where mobility is determined through adhesive contacts. For example, solid state sliding friction is created by bonds breaking between atoms. Close neighbor interactions between bonds, originating from mechanical interactions, can result in dramatic avalanches of bond breaking that change the sliding motion [95, 96]. Similar correlations between nearby bonds could be at play in some nanocaterpillars. For example, in white blood cells, membrane tension mediates bond-bond interactions [47, 48]. It is therefore interesting to speculate whether avalanches of bond unbinding could also occur for nanocaterpillar systems. Overall, the mathematical framework of coarse-graining is well suited to explore how microscopic features determine macroscopic modes of motion for nanocaterpillars and could facilitate predictive capacity for materials design and biophysical systems.

AUTHOR CONTRIBUTIONS

S.M. derived the mathematical framework, and solved it in all cases; acquired biological data for the Ashby chart; designed and analyzed the numerical simulations; found predictions for the diffusion of DNA-coated colloids. J.A.Z. synthesized DNA-coated colloids, conducted the experiments, and analyzed the experimental data to find diffusion coefficients. M.H.C. supervised the project. S.M. and M.H.C. wrote the paper.

CONFLICTS OF INTEREST

There are no conflicts to declare.

ACKNOWLEDGEMENTS

The authors are grateful for fruitful discussions with Fan Cui, Aleksandar Donev, Christopher E. Miles, and David J. Pine. S.M. acknowledges funding from the MolecularControl project, European Union's Horizon 2020 research and innovation programme under the Marie Skłodowska-Curie grant award number 839225. All authors were supported in part by the MRSEC Program of the National Science Foundation under Award Number DMR-1420073. M.H.-C. was partially supported by the US Department of Energy under Award No. DE-SC0012296, and acknowledges support from the Alfred P. Sloan Foundation.

APPENDIX

Appendix A: Projection of the dynamics in the bound state

To project the stochastic dynamics Eqns. (1) and (2) in the bound case we use a formalism (and notations) similar to Ref. 32; see also [60, 97]. This projection consists in using stiff springs to impose each constraint, and considering the limit where the spring constants go to infinity. The resulting projected equations can be obtained by directly pursuing the steps below (without redoing the reasoning with stiff springs).

We start from stochastic equations in the (x, l) space and seek to project them on the constraint manifold, defined by the constraint $q(x, l) = x + l - x_{\rm r} = 0$. The constraint matrix is therefore

$$C = (\nabla q)^T = \begin{pmatrix} 1 & 1 \end{pmatrix}. \tag{28}$$

We obtain the projector

$$P = I - C^T(CC^T)^{-1}C = \frac{1}{2}\begin{pmatrix} 1 & -1 \\ -1 & 1 \end{pmatrix}. \tag{29}$$

Initially the dynamics of $X = (x, l)^T$ may be written as

$$\frac{dX}{dt} = -\tilde{\Gamma}^{-1}\nabla\mathcal{U}(X) + \sqrt{2k_BT\tilde{\Gamma}^{-1}}\eta_{xl}(t) \tag{30}$$

where the potential $\mathcal{U}(X) = kl^2/2$, the noise $\eta_{xl} = (\eta_x, \eta_l)^T$ and the friction matrix is

$$\tilde{\Gamma} = \begin{pmatrix} \Gamma & 0 \\ 0 & \gamma \end{pmatrix}. \tag{31}$$

The projected friction and its Moore-Penrose pseudo-inverse are

$$\Gamma_P = P\tilde{\Gamma}P = \tfrac{\Gamma+\gamma}{4}\begin{pmatrix} 1 & -1 \\ -1 & 1 \end{pmatrix}, \tag{32}$$

$$\Gamma_P^\dagger = \tfrac{1}{\Gamma+\gamma}\begin{pmatrix} 1 & -1 \\ -1 & 1 \end{pmatrix} \tag{33}$$

with a square root

$$\sigma_P = \sqrt{\Gamma_P^\dagger} = \frac{1}{\sqrt{\Gamma+\gamma}}\begin{pmatrix} 1 & 0 \\ -1 & 0 \end{pmatrix}. \tag{34}$$

We obtain the projected dynamics

$$\frac{dX}{dt} = -\Gamma_P^\dagger\nabla\mathcal{U}(X) + \sqrt{2k_BT\Gamma_P^\dagger}\eta_{xl}(t) \tag{35}$$

where additional terms are needed if C is not constant over the constraint manifold [60, 97]. One can check that this exactly yields the bound dynamics Eq. (3), with $\eta = \eta_x$ (this decomposition of the noise is not unique but this does not impact the dynamics in a weak sense).

Appendix B: Numerical simulations

Stochastic simulations of particle and leg dynamics are conducted using a custom made Fortran 90 routine. Fast random number generation is performed according to a Mersenne twister algorithm. Normally distributed random numbers are used for particle displacement while uniformly distributed random numbers are used to determine binding events. Equations are simulated in their non-dimensional form. The step dt was chosen to be much small than all other time scales of the system. Typically $dt = \frac{1}{100}\min\left(\frac{q_{\rm on}\Gamma}{k}, \frac{q_{\rm on}\Gamma}{k}, \frac{\gamma}{\Gamma}\right)$. The system is simulated for $N_T = 10^8$ time steps, and the simulation is repeated over $N_{\rm runs} = 100$ independent runs (with renewed random number seed).

To simulate binding and unbinding events, for each leg, at each time step, we choose a random number R uniformly distributed between 0 and 1 and then:

- if the leg is bound, and if $R > q_{\rm off}dt$ then the leg becomes unbound. Otherwise it remains bound.
- if the leg is unbound, and if $R > q_{\rm on}dt$ then the leg becomes bound. Otherwise it remains unbound.

This simulation routine approximates well the exponential binding dynamics expected from the continuous equations since $dt \ll q_{\rm off}^{-1}, q_{\rm on}^{-1}$. To simulate all other stochastic equations we use a standard Euler-Maruyama discretization.

TABLE A2. Summary of different models and their effective long time friction. The 1-leg case corresponds to a system where the leg's center of mass is fixed on the particle. Apart from the 1-leg case, we ignore differences between Γ and $\tilde{\Gamma}$ to simplify notations.

Model	Sketch	Result
Main geometries		
1-arm	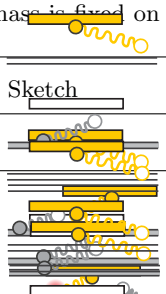	$\frac{1}{\Gamma_{\rm eff}} = \frac{p_0}{\Gamma_0} + \frac{p_1}{\Gamma_1}$, $\Gamma_0 = \Gamma$, $\Gamma_1 = \Gamma + \gamma_{\rm eff}$, $\gamma_{\rm eff} = k\left(\frac{1}{q_{\rm off}} + \frac{\gamma}{k}\frac{q_{\rm on}}{q_{\rm off}}\right)$
1-leg	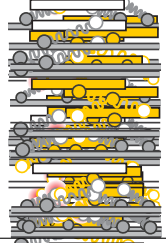	$\frac{1}{\Gamma_{\rm eff}} = \frac{p_0}{\Gamma_0} + \frac{p_1}{\Gamma_1}$, $\Gamma_0 = \tilde{\Gamma}$, $\Gamma_1 = \tilde{\Gamma} + \gamma_{\rm eff}$, $\tilde{\Gamma} = \Gamma + \gamma$
N-legs	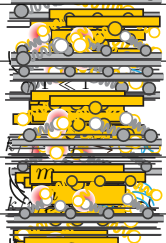	$\frac{1}{\Gamma_{\rm eff}} = \sum_{n=0}^{N} \frac{p_n}{\Gamma_n}$, $p_n = \binom{N}{n}\frac{q_{\rm off}^{N-n} q_{\rm on}^{n}}{(q_{\rm off}+q_{\rm on})^N}$, $\Gamma_n \underset{N\gg 1}{\simeq} \Gamma + n\gamma_{\rm eff}$
Inertial dynamics		
1-leg, inertia	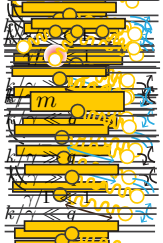	$\Gamma_{\rm eff} = p_0\Gamma_0 + p_1\Gamma_1$, $\Gamma_0 = \Gamma$, $\Gamma_1 = \Gamma + \gamma_{\rm eff}$
Limit regimes		
Small legs	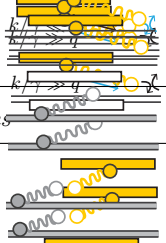	$\frac{1}{\Gamma_{\rm eff}} = \frac{p_0}{\Gamma} + \frac{p_1}{\Gamma}\left(1 - \frac{\gamma_{\rm eff}}{\Gamma}\right)$
Fast legs	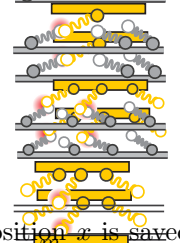	$\frac{1}{\Gamma_{\rm eff}} = \frac{p_0}{\Gamma_0} + \frac{p_1}{\Gamma_1}$, $\Gamma_0 = \Gamma$, $\Gamma_1 = \gamma + \frac{k}{q_{\rm off}}$
Fast binding		$\frac{1}{\Gamma_{\rm eff}} = \frac{p_0}{\Gamma_0} + \frac{p_1}{\Gamma_1}$, $\Gamma_0 = \Gamma$, $\Gamma_1 = \gamma + k\left(\frac{\gamma}{k}\frac{q_{\rm on}}{q_{\rm off}}\right)$
Extended geometries		
1-arm, 1-leg	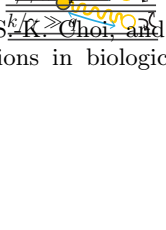	$\frac{1}{\Gamma_{\rm eff}} = \frac{p_0}{\Gamma_0} + \frac{p_1}{\Gamma_1}$, $\Gamma_0 = \Gamma$, $\Gamma_1 = \Gamma + \frac{1}{2}\gamma_{\rm eff}$
M-arms, N-legs		$\begin{cases} \frac{1}{\Gamma_{\rm eff}} = \sum_{n=0}^{N} \frac{p_n}{\Gamma_n}, \Gamma_n = \Gamma + n\gamma_{\rm eff,n}(M,N), \\ (\gamma_{\rm eff,n}(M,N))^{-1} \simeq (\gamma_{\rm eff,M,n})^{-1} + (\gamma_{\rm eff,N,n})^{-1}, \gamma_{\rm eff,P,n} = \gamma + k\left(\frac{1}{q_{\rm off}} + \frac{\gamma}{k}\frac{(P-n)q_{\rm on}}{q_{\rm off}}\right) \end{cases}$

The particle position x is saved every 10^4 time steps, and the mean squared displacement $< (x(t+t_0) - x(t_0))^2 >_{t_0}$ (averaged over initial times t_0) is computed up to $N_T/100 = 10^6$ time steps. The effective diffusion coefficient for each run $D_{\rm eff,i}$ is obtained from the analytical least square regression of $< (x(t+t_0) - x(t_0))^2 >_{t_0}$ with time. The average value over the runs $D_{\rm eff} = \frac{1}{N_{\rm runs}}\sum_i D_{\rm eff,i}$ is retained as the effective long time diffusion coefficient. The standard deviation of $D_{\rm eff,i}$ allows to draw error bars in all simulation plots.

[1] M. Mammen, S.-K. Choi, and G. M. Whitesides, Polyvalent interactions in biological systems: implications for design and use of multivalent ligands and inhibitors,

Angewandte Chemie International Edition **37**, 2754 (1998).
[2] P. C. Bressloff and J. M. Newby, Stochastic models of intracellular transport, Reviews of Modern Physics **85**, 135 (2013).
[3] D. A. Hammer, Adhesive dynamics, Journal of biomechanical engineering **136**, 021006 (2014).
[4] W. B. Rogers, W. M. Shih, and V. N. Manoharan, Using dna to program the self-assembly of colloidal nanoparticles and microparticles, Nature Reviews Materials **1**, 1 (2016).
[5] R. Alon and S. Feigelson, From rolling to arrest on blood vessels: leukocyte tap dancing on endothelial integrin ligands and chemokines at sub-second contacts, in *Seminars in immunology*, Vol. 14 (Elsevier, 2002) pp. 93–104.
[6] K. Ley, C. Laudanna, M. I. Cybulsky, and S. Nourshargh, Getting to the site of inflammation: the leukocyte adhesion cascade updated, Nature Reviews Immunology **7**, 678 (2007).
[7] C. Korn and U. Schwarz, Dynamic states of cells adhering in shear flow: from slipping to rolling, Physical review E **77**, 041904 (2008).
[8] Y. Zhang, A. McMullen, L.-L. Pontani, X. He, R. Sha, N. C. Seeman, J. Brujic, and P. M. Chaikin, Sequential self-assembly of dna functionalized droplets, Nature communications **8**, 1 (2017).
[9] L.-L. Pontani, I. Jorjadze, and J. Brujic, Cis and trans cooperativity of e-cadherin mediates adhesion in biomimetic lipid droplets, Biophysical journal **110**, 391 (2016).
[10] S. Merminod, J. R. Edison, H. Fang, M. F. Hagan, and W. B. Rogers, Avidity and surface mobility in multivalent ligand-receptor binding, Nanoscale (2021).
[11] R. J. Macfarlane, B. Lee, M. R. Jones, N. Harris, G. C. Schatz, and C. A. Mirkin, Nanoparticle superlattice engineering with dna, science **334**, 204 (2011).
[12] D. J. Lewis, L. Z. Zornberg, D. J. Carter, and R. J. Macfarlane, Single-crystal winterbottom constructions of nanoparticle superlattices, Nature materials **19**, 719 (2020).
[13] J.-G. Park, S.-H. Kim, S. Magkiriadou, T. M. Choi, Y.-S. Kim, and V. N. Manoharan, Full-spectrum photonic pigments with non-iridescent structural colors through colloidal assembly, Angewandte Chemie International Edition **53**, 2899 (2014).
[14] M. He, J. P. Gales, É. Ducrot, Z. Gong, G.-R. Yi, S. Sacanna, and D. J. Pine, Colloidal diamond, Nature **585**, 524 (2020).
[15] R. Merindol, N. Martin, T. Beneyton, J.-C. Baret, and S. Ravaine, Fast and ample light controlled actuation of monodisperse all-dna microgels, Advanced Functional Materials **31**, 2010396 (2021).
[16] C. R. Bilchak, M. Jhalaria, Y. Huang, Z. Abbas, J. Midya, F. M. Benedetti, D. Parisi, W. Egger, M. Dickmann, M. Minelli, *et al.*, Tuning selectivities in gas separation membranes based on polymer-grafted nanoparticles, ACS nano **14**, 17174 (2020).
[17] T. Sakai, S. I. Nishimura, T. Naito, and M. Saito, Influenza a virus hemagglutinin and neuraminidase act as novel motile machinery, Scientific reports **7**, 1 (2017).
[18] T. Sakai, H. Takagi, Y. Muraki, and M. Saito, Unique directional motility of influenza c virus controlled by its filamentous morphology and short-range motions, Journal of virology **92**, e01522 (2018).
[19] M. Müller, D. Lauster, H. H. Wildenauer, A. Herrmann, and S. Block, Mobility-based quantification of multivalent virus-receptor interactions: New insights into influenza a virus binding mode, Nano letters **19**, 1875 (2019).
[20] T. D. Allen, J. Cronshaw, S. Bagley, E. Kiseleva, and M. W. Goldberg, The nuclear pore complex: mediator of translocation between nucleus and cytoplasm, Journal of cell science **113**, 1651 (2000).
[21] I. V. Aramburu and E. A. Lemke, Floppy but not sloppy: Interaction mechanism of fg-nucleoporins and nuclear transport receptors, in *Seminars in cell & developmental biology*, Vol. 68 (Elsevier, 2017) pp. 34–41.
[22] B. Fogelson and J. P. Keener, Enhanced nucleocytoplasmic transport due to competition for elastic binding sites, Biophysical journal **115**, 108 (2018).
[23] R. Alon, S. Chen, K. D. Puri, E. B. Finger, and T. A. Springer, The kinetics of l-selectin tethers and the mechanics of selectin-mediated rolling, The Journal of cell biology **138**, 1169 (1997).
[24] R. Shrivastava, A. Rai, M. Salapaka, and S. Sivaramakrishnan, Stiffness of cargo–motor linkage tunes myosin vi motility and response to load, Biochemistry **58**, 4721 (2019).
[25] A. K. Dasanna and U. S. Schwarz, Adhesion-based sorting of blood cells: an adhesive dynamics simulation study, Soft matter **14**, 9061 (2018).
[26] K. Yehl, A. Mugler, S. Vivek, Y. Liu, Y. Zhang, M. Fan, E. R. Weeks, and K. Salaita, High-speed dna-based rolling motors powered by rnase h, Nature nanotechnology **11**, 184 (2016).
[27] R. Karnik, S. Hong, H. Zhang, Y. Mei, D. G. Anderson, J. M. Karp, and R. Langer, Nanomechanical control of cell rolling in two dimensions through surface patterning of receptors, Nano letters **8**, 1153 (2008).
[28] Y.-Y. Wang, A. Kannan, K. L. Nunn, M. A. Murphy, D. B. Subramani, T. Moench, R. Cone, and S. K. Lai, Igg in cervicovaginal mucus traps hsv and prevents vaginal herpes infections, Mucosal immunology **7**, 1036 (2014).
[29] A. Hensley, W. M. Jacobs, and W. B. Rogers, Classical nucleation and growth of dna-programmed colloidal crystallization, arXiv preprint arXiv:2105.14631 (2021).
[30] D. J. Lewis, P. A. Gabrys, and R. J. Macfarlane, Dna-directed non-langmuir deposition of programmable atom equivalents, Langmuir **34**, 14842 (2018).
[31] Y. Wang, Y. Wang, X. Zheng, É. Ducrot, J. S. Yodh, M. Weck, and D. J. Pine, Crystallization of dna-coated colloids, Nature communications **6**, 1 (2015).
[32] M. Holmes-Cerfon, Stochastic disks that roll, Physical Review E **94**, 052112 (2016).
[33] P. K. Jana and B. M. Mognetti, Translational and rotational dynamics of colloidal particles interacting through reacting linkers, Physical Review E **100**, 060601 (2019).
[34] C. Loverdo, O. Benichou, R. Voituriez, A. Biebricher, I. Bonnet, and P. Desbiolles, Quantifying hopping and jumping in facilitated diffusion of dna-binding proteins, Physical review letters **102**, 188101 (2009).
[35] P. E. Hamming, N. J. Overeem, and J. Huskens, Influenza as a molecular walker, Chemical science **11**, 27 (2019).
[36] M. D. Vahey and D. A. Fletcher, Influenza a virus surface proteins are organized to help penetrate host mucus, Elife **8**, e43764 (2019).

[37] K. Ramesh, R. Thaokar, J. R. Prakash, and R. Prabhakar, Significance of thermal fluctuations and hydrodynamic interactions in receptor-ligand-mediated adhesive dynamics of a spherical particle in wall-bound shear flow, Physical Review E **91**, 022302 (2015).

[38] F. Cui, S. Marbach, J. Zheng, M. Holmes-Cerfon, and D. S. Pine, Comprehensive view of nanoscale interactions between dna-coated colloids, to appear (2021).

[39] Q. Xu, L. Feng, R. Sha, N. Seeman, and P. Chaikin, Subdiffusion of a sticky particle on a surface, Physical review letters **106**, 228102 (2011).

[40] C. Etchegaray and N. Meunier, A stochastic model for cell adhesion to the vascular wall, Journal of mathematical biology **79**, 1665 (2019).

[41] F. Ziebert and I. M. Kulić, How influenza's spike motor works, Physical Review Letters **126**, 218101 (2021).

[42] N. A. Licata and A. V. Tkachenko, Colloids with key-lock interactions: Nonexponential relaxation, aging, and anomalous diffusion, Physical Review E **76**, 041405 (2007).

[43] S. Bose, S. K. Das, J. M. Karp, and R. Karnik, A semi-analytical model to study the effect of cortical tension on cell rolling, Biophysical journal **99**, 3870 (2010).

[44] A. Kowalewski, N. R. Forde, and C. S. Korosec, Multivalent diffusive transport, The Journal of Physical Chemistry B (2021).

[45] K. E. Caputo and D. A. Hammer, Effect of microvillus deformability on leukocyte adhesion explored using adhesive dynamics simulations, Biophysical journal **89**, 187 (2005).

[46] B. Grec, B. Maury, N. Meunier, and L. Navoret, A 1d model of leukocyte adhesion coupling bond dynamics with blood velocity, Journal of theoretical biology **452**, 35 (2018).

[47] S. Klumpp and R. Lipowsky, Cooperative cargo transport by several molecular motors, Proceedings of the National Academy of Sciences **102**, 17284 (2005).

[48] S. F. Fenz, T. Bihr, D. Schmidt, R. Merkel, U. Seifert, K. Sengupta, and A.-S. Smith, Membrane fluctuations mediate lateral interaction between cadherin bonds, Nature physics **13**, 906 (2017).

[49] C. E. Miles, S. D. Lawley, and J. P. Keener, Analysis of nonprocessive molecular motor transport using renewal reward theory, SIAM Journal on Applied Mathematics **78**, 2511 (2018).

[50] C. P. Goodrich, M. P. Brenner, and K. Ribbeck, Enhanced diffusion by binding to the crosslinks of a polymer gel, Nature communications **9**, 1 (2018).

[51] B. Fogelson and J. P. Keener, Transport facilitated by rapid binding to elastic tethers, SIAM Journal on Applied Mathematics **79**, 1405 (2019).

[52] C. S. Korosec, L. Jindal, M. Schneider, I. C. de la Barca, M. J. Zuckermann, N. R. Forde, and E. Emberly, Substrate stiffness tunes the dynamics of polyvalent rolling motors, Soft Matter **17**, 1468 (2021).

[53] G. Pavliotis and A. Stuart, *Multiscale methods: averaging and homogenization* (Springer Science & Business Media, 2008).

[54] J. P. Lee-Thorp and M. Holmes-Cerfon, Modeling the relative dynamics of dna-coated colloids, Soft matter **14**, 8147 (2018).

[55] X. Bian, C. Kim, and G. E. Karniadakis, 111 years of brownian motion, Soft Matter **12**, 6331 (2016).

[56] M. Rubinstein, R. H. Colby, *et al.*, *Polymer physics*, Vol. 23 (Oxford university press New York, 2003).

[57] E. Miller, T. Garcia, S. Hultgren, and A. F. Oberhauser, The mechanical properties of e. coli type 1 pili measured by atomic force microscopy techniques, Biophysical journal **91**, 3848 (2006).

[58] R. Y. Lim, N.-P. Huang, J. Köser, J. Deng, K. A. Lau, K. Schwarz-Herion, B. Fahrenkrog, and U. Aebi, Flexible phenylalanine-glycine nucleoporins as entropic barriers to nucleocytoplasmic transport, Proceedings of the National Academy of Sciences **103**, 9512 (2006).

[59] P. Varilly, S. Angioletti-Uberti, B. M. Mognetti, and D. Frenkel, A general theory of dna-mediated and other valence-limited colloidal interactions, The Journal of chemical physics **137**, 094108 (2012).

[60] G. Ciccotti, T. Lelievre, and E. Vanden-Eijnden, Projection of diffusions on submanifolds: Application to mean force computation, Communications on Pure and Applied Mathematics: A Journal Issued by the Courant Institute of Mathematical Sciences **61**, 371 (2008).

[61] C. W. Gardiner *et al.*, *Handbook of stochastic methods*, Vol. 3 (springer Berlin, 1985).

[62] L. Leibler, M. Rubinstein, and R. H. Colby, Dynamics of reversible networks, Macromolecules **24**, 4701 (1991).

[63] W. Cao, C. Dong, S. Kim, D. Hou, W. Tai, L. Du, W. Im, and X. F. Zhang, Biomechanical characterization of sars-cov-2 spike rbd and human ace2 protein-protein interaction, Biophysical journal **120**, 1011 (2021).

[64] M. Ponga, Quantifying the adhesive strength between the sars-cov-2 s-proteins and human receptor and its effect in therapeutics, Scientific reports **10**, 1 (2020).

[65] A. Harris, G. Cardone, D. C. Winkler, J. B. Heymann, M. Brecher, J. M. White, and A. C. Steven, Influenza virus pleiomorphy characterized by cryoelectron tomography, Proceedings of the National Academy of Sciences **103**, 19123 (2006).

[66] V. Reiter-Scherer, J. L. Cuellar-Camacho, S. Bhatia, R. Haag, A. Herrmann, D. Lauster, and J. P. Rabe, Force spectroscopy shows dynamic binding of influenza hemagglutinin and neuraminidase to sialic acid, Biophysical journal **116**, 1037 (2019).

[67] H. Brenner, The slow motion of a sphere through a viscous fluid towards a plane surface, Chemical Engineering Science **16**, 242 (1961).

[68] S. T. Milner, T. A. Witten, and M. E. Cates, Theory of the grafted polymer brush, Macromolecules **21**, 2610 (1988).

[69] H. Chen, S. P. Meisburger, S. A. Pabit, J. L. Sutton, W. W. Webb, and L. Pollack, Ionic strength-dependent persistence lengths of single-stranded RNA and DNA, Proceedings of the National Academy of Sciences **109**, 799 (2012).

[70] J. X. Zhang, J. Z. Fang, W. Duan, L. R. Wu, A. W. Zhang, N. Dalchau, B. Yordanov, R. Petersen, A. Phillips, and D. Y. Zhang, Predicting dna hybridization kinetics from sequence, Nature chemistry **10**, 91 (2018).

[71] The binding range is about 20 nm, but this is not optically removable as the vertical resolution is about 200 nm.

[72] Eq. (20) corresponds to the result derived in Ref. 54, with in addition projected dynamics for the bound state, and base friction of the particle ($\Gamma \neq 0$).

[73] S. Marbach and M. Holmes-Cerfon, Can mass change the diffusion coefficient of dna-coated colloids?, arXiv preprint arXiv:2112.05266 (2021).

[74] J. S. Oh, Y. Wang, D. J. Pine, and G.-R. Yi, High-density peo-b-dna brushes on polymer particles for colloidal superstructures, Chemistry of Materials **27**, 8337 (2015).

[75] C. Fröhner and F. Noé, Reversible interacting-particle reaction dynamics, The Journal of Physical Chemistry B **122**, 11240 (2018).

[76] S. Xu, J. Zhan, B. Man, S. Jiang, W. Yue, S. Gao, C. Guo, H. Liu, Z. Li, J. Wang, *et al.*, Real-time reliable determination of binding kinetics of dna hybridization using a multi-channel graphene biosensor, Nature communications **8**, 1 (2017).

[77] K.-C. Chang, D. F. Tees, and D. A. Hammer, The state diagram for cell adhesion under flow: leukocyte rolling and firm adhesion, Proceedings of the National Academy of Sciences **97**, 11262 (2000).

[78] Note however that attaching springs with different spring constants would not lead to a similar harmonic sum of effective frictions, as the effective friction contains more contributions than those originating from the spring recoil force (analytical results not shown here).

[79] C. Korn and U. Schwarz, Mean first passage times for bond formation for a brownian particle in linear shear flow above a wall, The Journal of chemical physics **126**, 03B605 (2007).

[80] U. S. Schwarz and R. Alon, L-selectin-mediated leukocyte tethering in shear flow is controlled by multiple contacts and cytoskeletal anchorage facilitating fast rebinding events, Proceedings of the National Academy of Sciences **101**, 6940 (2004).

[81] M. I. Wallace, L. Ying, S. Balasubramanian, and D. Klenerman, Non-arrhenius kinetics for the loop closure of a dna hairpin, Proceedings of the National Academy of Sciences **98**, 5584 (2001).

[82] W. B. Rogers, T. Sinno, and J. C. Crocker, Kinetics and non-exponential binding of dna-coated colloids, Soft Matter **9**, 6412 (2013).

[83] K.-T. Wu, L. Feng, R. Sha, R. Dreyfus, A. Y. Grosberg, N. C. Seeman, and P. M. Chaikin, Kinetics of dna-coated sticky particles, Physical Review E **88**, 022304 (2013).

[84] N. Sarpangala and A. Gopinathan, Cargo surface fluidity reduces inter-motor interference, promotes load-sharing and enhances run-lengths in an atp dependent manner, bioRxiv (2021).

[85] S. A. McKinley, A. Athreya, J. Fricks, and P. R. Kramer, Asymptotic analysis of microtubule-based transport by multiple identical molecular motors, Journal of theoretical biology **305**, 54 (2012).

[86] C. S. Peskin and T. C. Elston, The role of protein flexibility in molecular motor function: coupled diffusion in a tilted periodic potential, SIAM Journal on Applied Mathematics **60**, 842 (2000).

[87] G. I. Bell, Models for the specific adhesion of cells to cells, Science **200**, 618 (1978).

[88] P. S. Doyle, B. Ladoux, and J.-L. Viovy, Dynamics of a tethered polymer in shear flow, Physical review letters **84**, 4769 (2000).

[89] S. Chen and T. A. Springer, Selectin receptor–ligand bonds: Formation limited by shear rate and dissociation governed by the bell model, Proceedings of the National Academy of Sciences **98**, 950 (2001).

[90] D. E Leckband, Novel functions and binding mechanisms of carbohydrate-binding proteins determined by force measurements, Current Protein and Peptide Science **12**, 743 (2011).

[91] S. Rakshit and S. Sivasankar, Biomechanics of cell adhesion: how force regulates the lifetime of adhesive bonds at the single molecule level, Physical Chemistry Chemical Physics **16**, 2211 (2014).

[92] A. Daddi-Moussa-Ider, A. Guckenberger, and S. Gekle, Long-lived anomalous thermal diffusion induced by elastic cell membranes on nearby particles, Physical Review E **93**, 012612 (2016).

[93] V. Bertin, Y. Amarouchene, E. Raphael, and T. Salez, Soft-lubrication interactions between a rigid sphere and an elastic wall, arXiv preprint arXiv:2104.00900 (2021).

[94] S. Hess, N. Sausen, and M. Melkonian, Shedding light on vampires: the phylogeny of vampyrellid amoebae revisited, PLoS One **7**, e31165 (2012).

[95] T. W. de Geus, M. Popović, W. Ji, A. Rosso, and M. Wyart, How collective asperity detachments nucleate slip at frictional interfaces, Proceedings of the National Academy of Sciences **116**, 23977 (2019).

[96] W. Ji, T. W. de Geus, E. Agoritsas, and M. Wyart, Geometry of hopping processes and local excitations in glasses, arXiv preprint arXiv:2106.13153 (2021).

[97] M. Holmes-Cerfon, S. J. Gortler, and M. P. Brenner, A geometrical approach to computing free-energy landscapes from short-ranged potentials, Proceedings of the National Academy of Sciences **110**, E5 (2013).

Supplementary information

S. Marbach, J. A. Zheng, M. Holmes-Cerfon

Contents

1 N-legged, one dimensional, caterpillar model

Note that unless specifically mentioned, in the entire supplementary information l is used as a shortcut notation for spring length relative to its rest length $l - l_0$.

1.1 Agreement of simulation and analytical results regardless of the value of ϵ for the 1-legged caterpillar

In Fig. S1 we present agreement between the effective diffusion evaluated using stochastic simulations and evaluated with the analytical formula Eq. (12) of the main paper.

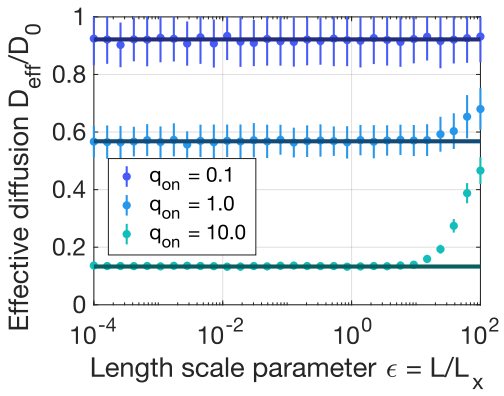

Figure S1: Simulation results for different values of the non-dimensionalizing parameter $\epsilon = L/L_x$ characterizing the difference between the length scale of oscillations of legs L versus the length scale of particle displacement L_x, for the case of a 1-legged caterpillar. Various values of the attachment rate q_{on} are explored (given in non-dimensional units $k/\Gamma\epsilon^2$). The other numerical parameters are $\gamma/\Gamma = 0.1$ and $q_{\text{off}} = 0.8k/\Gamma\epsilon^2$. The lines correspond to the analytical formula Eq. (12) of the main paper.

1.2 N legs facing a uniformly sticky surface

1.2.1 Method on an example: 2 legs facing a sticky surface

To investigate dynamics of caterpillars with multiple legs, we start by illustrating the framework on a 2 leg system.

Projection of the dynamics in the bound state The first step is to write the projected dynamics in the bound state. If there are 2 legs, when only 1 of them is bound, then the dynamics of the unbound leg are completely independent of the bound one and the projected bound equations are the same as those reported in the main paper. When 2 legs are bound however we must project again the dynamics. We therefore have 2 constraints $q_1(x, l_1, l_2) = x + l_1 + x_{r,1} = 0$ and $q_2(x, l_1, l_2) = x + l_2 + x_{r,2} = 0$ where x_r are reference positions when either of the legs first form their bond. The constraint matrix is therefore

$$C = (\nabla q)^T = \begin{pmatrix} 1 & 1 & 0 \\ 1 & 0 & 1 \end{pmatrix}. \tag{S1.1}$$

We then get the projector

$$P = I - C^T(CC^T)^{-1}C = \frac{1}{3}\begin{pmatrix} 1 & -1 & -1 \\ -1 & 1 & 1 \\ -1 & 1 & 1 \end{pmatrix} \tag{S1.2}$$

The friction matrix is in the unbound configuration

$$\tilde{\Gamma} = \begin{pmatrix} \Gamma & 0 & 0 \\ 0 & \gamma & 0 \\ 0 & 0 & \gamma \end{pmatrix} \tag{S1.3}$$

giving a projected friction and its Moore-Penrose pseudo-inverse as

$$\Gamma_P = P\tilde{\Gamma}P \quad = \tfrac{\Gamma+2\gamma}{3}P, \tag{S1.4}$$

$$\Gamma_P^\dagger \quad = \tfrac{1}{\Gamma+2\gamma}3P \tag{S1.5}$$

with a square root

$$\sigma_P = \sqrt{\Gamma_P^\dagger} = \frac{1}{\sqrt{\Gamma+2\gamma}} \begin{pmatrix} 1 & 0 & 0 \\ -1 & 0 & 0 \\ -1 & 0 & 0 \end{pmatrix}. \tag{S1.6}$$

We obtain the projected dynamics

$$\frac{dx}{dt} = -\frac{dl_1}{dt} = -\frac{dl_2}{dt} = \frac{k(l_1+l_2)}{\Gamma+2\gamma} + \sqrt{\frac{2k_BT}{\Gamma+2\gamma}}\eta(t) \tag{S1.7}$$

where $\eta(t)$ is a white Gaussian noise. The friction in the bound state is therefore naturally the sum of the frictions $\Gamma + 2\gamma$.

Generator for the dynamics For 2 legs we can write the full generator (in non-dimensional scales) $\mathcal{L}^{(2)} = \frac{1}{\epsilon^2}\mathcal{L}_0^{(2)} + \frac{1}{\epsilon}\mathcal{L}_1^{(2)} + \mathcal{L}_2^{(2)}$. The generator is now an operator acting on a space of 4 states (#1 has no bond, $\#2-3$ have 1 bond, where the leg 1 is bound in state #2 and reciprocally, and #4 has 2 bonds). The lowest order generator is

$$\mathcal{L}_0^{(2)} = \mathcal{Q}+\mathcal{U}_0 = \begin{pmatrix} -2q_{\text{on}} & q_{\text{on}} & q_{\text{on}} & 0 \\ q_{\text{off}} & -q_{\text{off}}-q_{\text{on}} & 0 & q_{\text{on}} \\ q_{\text{off}} & 0 & -q_{\text{off}}-q_{\text{on}} & q_{\text{on}} \\ 0 & q_{\text{off}} & q_{\text{off}} & 2q_{\text{off}} \end{pmatrix} + \text{diag} \begin{pmatrix} \frac{\Gamma}{\gamma}\left(D_{l_1}+D_{l_2}\right) \\ \frac{\Gamma}{\Gamma+\gamma}D_{l_1} + \frac{\Gamma}{\gamma}D_{l_2} \\ \frac{\Gamma}{\gamma}D_{l_1} + \frac{\Gamma}{\Gamma+\gamma}D_{l_2} \\ \frac{\Gamma}{\Gamma+2\gamma}\left(-(l_1+l_2)(\partial_{l_1}+\partial_{l_2}) + (\partial_{l_1}+\partial_{l_2})^2\right) \end{pmatrix} \tag{S1.8}$$

where $D_{l_i} = -l_i\partial_{l_i} + \partial_{l_i l_i}$ is an operator for the unbound tether i. The next orders are

$$\mathcal{L}_1^{(2)} = \text{diag} \begin{pmatrix} 0 \\ \frac{\Gamma}{\Gamma+\gamma}(l_1\partial_x - 2\partial_{xl_1}) \\ \frac{\Gamma}{\Gamma+\gamma}(l_2\partial_x - 2\partial_{xl_2}) \\ \frac{\Gamma}{\Gamma+2\gamma}((l_1+l_2)\partial_x - 2\partial_{xl_1} - 2\partial_{xl_2}) \end{pmatrix} \text{ and } \mathcal{L}_2^{(2)} = \text{diag} \begin{pmatrix} \partial_{xx} \\ \frac{\Gamma}{\Gamma+\gamma}\partial_{xx} \\ \frac{\Gamma}{\Gamma+\gamma}\partial_{xx} \\ \frac{\Gamma}{\Gamma+2\gamma}\partial_{xx} \end{pmatrix}. \tag{S1.9}$$

The equilibrium distribution is simply

$$\pi \propto \begin{pmatrix} (q_{\text{off}}/q_{\text{on}})^2 \\ q_{\text{off}}/q_{\text{on}} \\ q_{\text{off}}/q_{\text{on}} \\ 1 \end{pmatrix} e^{-l_1^2/2} e^{-l_2^2/2}. \tag{S1.10}$$

Long time solution We now seek a solution as an expansion in ϵ, $f = f_0 + \epsilon f_1 + ...$ In a very similar way as systematically observed in similar derivations we find $f_0 = a(x,t)\begin{pmatrix}1 & 1 & 1 & 1\end{pmatrix}^T$ at lowest order. The associated equilibrium distribution is $\pi_0 = \pi$. At the following order we need to solve $\mathcal{L}_0^{(2)} f_1 = -\mathcal{L}_1^{(2)} f_0$ and we will seek a natural solution (that strongly reflects the symmetry of the problem) as

$$f_1 = \begin{pmatrix} u_0 l_1 + u_0 l_2 \\ b_1 l_1 + u_1 l_2 \\ u_1 l_1 + b_1 l_2 \\ b_2 l_1 + b_2 l_2 \end{pmatrix} \partial_x a \tag{S1.11}$$

where u_n and b_n are constants that solve a linear system of equations (with non zero determinant), and u_n and b_n refer respectively to unbound and bound contributions with n bonds in the system. We do not report the equation system here but will come to it later on. At the next order, to find a solution for f_2 we require the Fredholm alternative, $\langle \partial_t f_0 - \mathcal{L}_2^{(2)} f_0 - \mathcal{L}_1^{(2)} f_1, \pi_0 \rangle = 0$, which gives

$$\left(\frac{q_{\text{off}}^2}{q_{\text{on}}^2} + \frac{2q_{\text{off}}}{q_{\text{on}}} + 1\right)\partial_t a = \frac{q_{\text{off}}^2}{q_{\text{on}}^2}\partial_{xx} a + 2\frac{q_{\text{off}}}{q_{\text{on}}}\frac{\Gamma}{\Gamma+\gamma}(1-b_1)\,\partial_{xx} a + (1-2b_2)\,\partial_{xx} a \tag{S1.12}$$

which can be rewritten as a weighted sum (in dimensional scales)

$$\partial_t a = k_B T \left(\frac{p_0}{\Gamma} + \frac{p_1}{\frac{\Gamma+\gamma}{(1-b_1)}} + \frac{p_2}{\frac{\Gamma+2\gamma}{(1-2b_2)}}\right)\partial_{xx} a \tag{S1.13}$$

where p_k is the probability to have k bonds ($p_0 = q_{\text{off}}^2/Z$, $p_1 = 2q_{\text{off}}q_{\text{on}}/Z$ and $p_2 = q_{\text{on}}^2/Z$ with $p_0 + p_1 + p_2 = 1$). The above expression clearly shows that the effective inverse friction is a weighted sum of inverse friction coefficients

$$\frac{1}{\Gamma_{\text{eff}}^{2\,\text{legs}}} = \sum_{n=0}^{2}\frac{p_n}{\Gamma_n} = \sum_{n=0}^{2}\frac{p_n}{\frac{\Gamma+n\gamma}{(1-nb_n)}}. \tag{S1.14}$$

We will show this expression for all N below. The linear system of equations solved by the u_k and b_k can now be given

$$\begin{aligned}
-2q_{\text{on}}u_0 + q_{\text{on}}b_1 + q_{\text{on}}u_1 - \frac{\Gamma}{\gamma}u_0 &= 0, \text{ (unbound contributions in the 0 bond state)} \\
q_{\text{off}}u_0 - q_{\text{off}}u_1 - q_{\text{on}}u_1 + q_{\text{on}}b_2 - \frac{\Gamma}{\gamma}u_1 &= 0, \text{ (unbound contributions in a 1 bond state)} \\
q_{\text{off}}u_0 - q_{\text{off}}b_1 - q_{\text{on}}b_1 + q_{\text{on}}b_2 - \frac{\Gamma}{\Gamma+\gamma}b_1 &= -\frac{\Gamma}{\Gamma+\gamma}, \text{ (bound contributions in a 1 bond state)} \\
q_{\text{off}}b_1 + q_{\text{off}}u_1 - 2q_{\text{off}}b_2 - 2\frac{\Gamma}{\Gamma+2\gamma}b_2 &= -\frac{\Gamma}{\Gamma+2\gamma}, \text{ (bound contributions in the 2 bonds state).}
\end{aligned} \tag{S1.15}$$

Solving the above linear system yields lengthy expressions for b_k and u_k. One can show however that the effective contributions for the bound states can be expanded as

$$\Gamma_1 = \Gamma + \gamma_{\text{eff}}\left(1 - O(\frac{\gamma_{\text{eff}}}{\Gamma})\right)\ \Gamma_2 = \Gamma + 2\gamma_{\text{eff}}\left(1 + O(\frac{\gamma_{\text{eff}}}{\Gamma})\right) \tag{S1.16}$$

such that we find already some a linear scaling as $\Gamma_n \sim \Gamma + n\gamma_{\text{eff}}$.

1.2.2 N legs

Projection of the dynamics with N legs. The projection formalism naturally extends to N legs. For n bound legs we find that the friction is simply $\Gamma + n\gamma$, such that the projected dynamics are for the first n bound legs

$$\frac{dx}{dt} = -\frac{dl_1}{dt} = ... = -\frac{dl_n}{dt} = \frac{k\sum_{i=1}^{n}(l_i)}{\Gamma + n\gamma} + \sqrt{2\frac{k_B T}{\Gamma + n\gamma}}\eta(t). \tag{S1.17}$$

System of equations for N legs The generator is now an operator acting on 2^N states, and we order these states according to their number of bonds (0 bonds, all 1 bond states, all 2 bonds states, ...). For N legs we can write the full generator (in non-dimensional scales) $\mathcal{L}^{(N)} = \frac{1}{\epsilon^2}\mathcal{L}_0^{(N)} + \frac{1}{\epsilon}\mathcal{L}_1^{(N)} + \mathcal{L}_2^{(N)}$, where all $\mathcal{L}_i^{(N)}$ terms are very similar to the ones introduced for $N = 2$ and can be naturally generalized. Similarly the equilibrium distribution is naturally extended as

$$\pi = e^{-\sum_{i=1}^N l_i^2/2}\left((q_{\text{off}}/q_{\text{on}})^N \quad (q_{\text{off}}/q_{\text{on}})^{N-1} \quad (q_{\text{off}}/q_{\text{on}})^{N-1} \quad .... \quad (q_{\text{off}}/q_{\text{on}})^{N-2} \quad ... \quad 1\right)^T. \tag{S1.18}$$

Long time solution with N legs We now seek a solution as an expansion in ϵ, $f = f_0 + \epsilon f_1 + ...$ In a very similar way as systematically observed in similar derivations we find $f_0 = a(x,t)\left(1 \quad ... \quad 1\right)^T$ at lowest order. The associated equilibrium distribution is $\pi_0 = \pi$. At the following order we need to solve $\mathcal{L}_0^{(N)} f_1 = -\mathcal{L}_1^{(N)} f_0$ and we will seek a natural solution (that strongly reflects the symmetry of the problem) as

$$f_1 = \begin{pmatrix} u_0 l_1 + u_0 l_2 + ... + u_0 l_N \\ b_1 l_1 + u_1 l_2 + ... + u_1 l_N \\ u_1 l_1 + b_1 l_2 + ... + u_1 l_N \\ ... \\ b_2 l_1 + b_2 l_2 + u_2 l_3 ... + u_2 l_N \\ ... \\ b_N l_1 + b_N l_2 + ... + b_N l_N \end{pmatrix} \partial_x a \tag{S1.19}$$

where u_n and b_n refer respectively to unbound and bound contributions with n bonds in the system. We now seek the general system of equations satisfied by u_n and b_n. For a number of bonds n, consider that a given focus tether is unbound, say i. This will therefore allow us to obtain an equation on the unbound contributions of that tether (that in l_i) so primarily on u_n. The tether is relaxing yielding a contribution $-\frac{\Gamma}{\gamma}u_n$. There are n possible bonds to undo leading to a contribution $(-nq_{\text{off}}u_n)$. In any $n-1$ bond configurations starting from our initial configuration, the focus tether will still be unbound (u_{n-1}), such that we get an $(+nq_{\text{off}}u_{n-1})$ contribution. There are $N-n$ bonds to form $(-(N-n)q_{\text{on}}u_n)$. In forming bonds, only 1 choice yields to bind the focus tether $(q_{\text{on}}b_{n+1})$ while the other forming bonds will not be the focus tether $((N-n-1)q_{\text{on}}u_{n+1})$. The right hand side terms (from $\mathcal{L}_1^{(N)}f_0$) corresponding to unbound tethers are 0. This yields the first line of the system of equations Eq. (S1.20) below. If one considers a bound focus tether, similarly one can derive contributions due to binding and unbinding. The bound relaxation terms yield a contribution $(-\frac{n\Gamma}{\Gamma+n\gamma}b_n)$. Additionally, the right hand side terms (coming from $\mathcal{L}_1^{(N)}f_0$) corresponding to the unbound tether is $-\frac{\Gamma}{\Gamma+n\gamma}$. We obtain

$$\begin{cases} nq_{\text{off}}u_{n-1} - nq_{\text{off}}u_n - (N-n)q_{\text{on}}u_n + q_{\text{on}}b_{n+1} + (N-n-1)q_{\text{on}}u_{n+1} - \dfrac{\Gamma}{\gamma}u_n = 0 \\ q_{\text{off}}u_{n-1} + (n-1)q_{\text{off}}b_{n-1} - nq_{\text{off}}b_n - (N-n)q_{\text{on}}b_n + (N-n)q_{\text{on}}b_{n+1} - \dfrac{n\Gamma}{\Gamma+n\gamma}b_n = -\dfrac{\Gamma}{\Gamma+n\gamma}. \end{cases} \tag{S1.20}$$

The system Eq. (S1.20) applies for all $n = 0..N$, taking as boundary equations $u_N = 0$ and $b_0 = 0$. Unfortunately the system does not simplify further but its determinant is non zero, showing that a non trivial solution exists. We will study it further later but for now conclude on the long time solution. At the next order, to find a solution for f_2 we require the Fredholm alternative, $\langle \partial_t f_0 - \mathcal{L}_2^{(N)} f_0 - \mathcal{L}_1^{(N)} f_1, \pi_0 \rangle = 0$, which yields after some algebraic manipulations (back in dimensional scales)

$$\partial_t a = k_B T \left(\frac{p_0}{\Gamma} + \frac{p_1}{\frac{\Gamma+\gamma}{(1-b_1)}} + \frac{p_2}{\frac{\Gamma+2\gamma}{(1-2b_2)}} + ... + \frac{p_N}{\frac{\Gamma+N\gamma}{(1-Nb_N)}} \right) \partial_{xx} a \tag{S1.21}$$

where $p_n = \frac{\binom{N}{n} x^n (1-x)^{N-n}}{Z}$ with $x = q_{\text{on}}/q_{\text{off}}$ is the probability to have n bonds. Writing in full generality

$$\Gamma_n = \frac{\Gamma + n\gamma}{(1 - nb_n)} \tag{S1.22}$$

we indeed recover Eq. (15) of the main manuscript. We also see that the coefficients Γ_n indeed correspond to friction contributions in a state with n bonds as only n and b_n, that corresponds to the bound contributions, intervene.

Resolution when the system is dominated by the average number of bonds We can search for a closed (simpler) system for Eq. (S1.20) where the dominant terms will originate from the average number of bonds $N_b = \sum_{n=0}^{N} np_n = N\frac{q_{\text{on}}}{q_{\text{on}}+q_{\text{off}}}$. We assume that, around this average number, terms do not change much (the derivatives are close to 0), meaning we can approximate $u_{N_b} \simeq u_{N_b-1} \simeq u_{N_b+1} \equiv \bar{u}$, and similarly for $b_{N_b} = \bar{b}$ leading to

$$\begin{cases} -q_{\text{on}}\bar{u} + q_{\text{on}}\bar{b} - \frac{\Gamma}{\gamma}\bar{u} = 0 \\ q_{\text{off}}\bar{u} - q_{\text{off}}\bar{b} - \frac{N_b\Gamma}{\Gamma+N_b\gamma}\bar{b} = -\frac{\Gamma}{\Gamma+N_b\gamma} \end{cases} \tag{S1.23}$$

Solving the system for $\bar{b}$ and $\bar{u}$ yields then the value of the friction coefficient for the average number of bonds (back in dimensional scales)

$$\Gamma_{N_b} = \frac{\Gamma + N_b\gamma}{1 - N_b\bar{b}} = \Gamma + N_b\left(\gamma + \frac{k}{q_{\text{off}}} + \gamma\frac{q_{\text{on}}}{q_{\text{off}}}\right) \tag{S1.24}$$

Eq. (S1
solutio

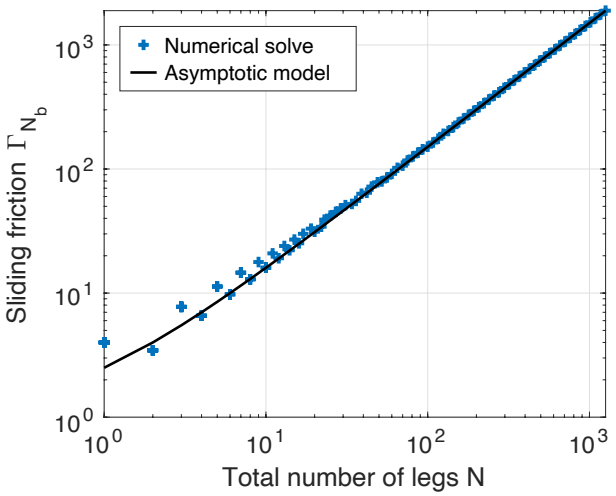

Figure S2: Value of friction coefficient for the average number of bonds as evaluated using Eq. (S1.24) or equivalently Eq. (15) of the main paper ("Asymptotic model") and fully solving the system of equations Eq. (S1.20) and presenting the value Γ_n for the index n closest to N_b ("Numerical solve"). Here the values of other parameters (in dimensional scales) are all set to $1 = \frac{q_{\text{on}}\Gamma}{k} = \frac{q_{\text{off}}\Gamma}{k} = \frac{\gamma}{\Gamma}$.

Empirical solution for an arbitrary number of bonds An interesting question is then to investigate Γ_n, the effective friction contributing to the state with n bonds, in the large N (total number of legs) limit. This requires solving the full system Eq. (S1.20). This system is not easily amenable to analytical calculations, and instead we use it as a benchmark to explore a phenomenological law for Γ_n.

First, it is natural to assume that the correction $\Gamma_n - \Gamma$ typically contains a term $n\gamma$ coming from added friction of the n bonds (as is noted already in the projected dynamics). Then, recall forces are also exerting

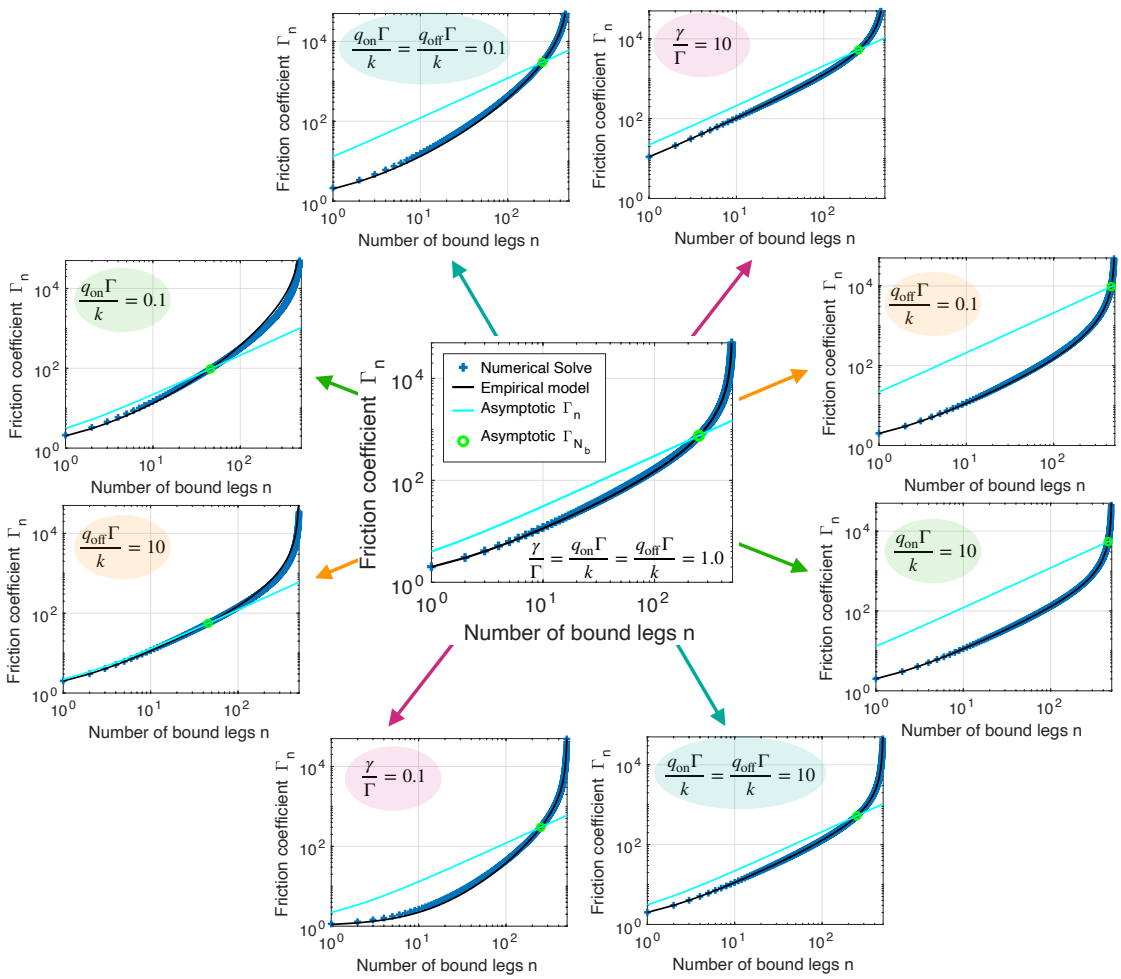

Figure S3: Value of friction coefficients Γ_n for all possible number of bonds (for a maximum of $N = 500$) as evaluated using Eq. (S1.27) ("Empirical model") and fully solving for the system of equations Eq. (S1.20) and presenting the values Γ_n ("Numerical Solve"). Index N_b is highlighted in green in each plot, and calculated from Eq. (16) . The "Asymptotic Γ_n" result corresponds to Eq. (S1.28). Here the values of other parameters (in dimensional scales) are all set to $1 = \frac{q_{on}\Gamma}{k} = \frac{q_{off}\Gamma}{k} = \frac{\gamma}{\Gamma}$ unless another indication is given.

friction. Typically n bonds are exerting friction due to recall forces. Yet for this final contribution to Γ_n, the situation is not the same for n bonds as for N_b bonds. Around $n = N_b$, the probabilities to be in a state with one more bond or one bond less are more or less the same, $p(N_b - 1) \simeq p(N_b) \simeq p(N_b + 1)$. For n bonds, we have in general (for example investigating the probability to undo a bond)

$$\begin{aligned}\frac{p(n)}{p(n-1)} &= \frac{\binom{N}{n} p_0^n (1-p_0)^{N-n}}{\binom{N}{n-1} p_0^{n-1} (1-p_0)^{N-n+1}} \\ &= \frac{\binom{N}{n} p_0^n (1-p_0)^{N-n} p_0}{\binom{N}{n} \frac{n}{N-n+1} p_0^n (1-p_0)^{N-n} (1-p_0)} \\ &= \frac{p_0}{(1-p_0)} \frac{N-n+1}{n} = \frac{N_b}{N-N_b} \frac{N-n+1}{n}\end{aligned} \tag{S1.25}$$

We expect that the typical time over which the spring resistance acts τ_{eff} has to be modified by the propensity

to unbind (coming from the state with n bonds) as $\tau_{\rm eff} \to \tau_{\rm eff} \frac{p(n-1)}{p(n)}$. We obtain, wrapping up all contributions

$$\Gamma_n = \Gamma + n\left(\gamma + k\tau_{\rm eff}\frac{p(n-1)}{p(n)}\right) = \Gamma + n\left(\gamma + k\frac{p(n-1)}{p(n)}\left[\frac{1}{q_{\rm off}} + \frac{\gamma}{k}\frac{q_{\rm on}}{q_{\rm off}}\right]\right). \tag{S1.26}$$

which explicitly writes as

$$\Gamma_n = \Gamma + n\left(\gamma + k\frac{N-N_b}{N-(n-1)}\frac{n}{N_b}\left[\frac{1}{q_{\rm off}} + \frac{\gamma}{k}\frac{q_{\rm on}}{q_{\rm off}}\right]\right) \tag{S1.27}$$

Eq. (S1.27) is compared to the full solution of the linear system in Fig. S3. We find excellent agreement over a broad range of parameters. Notice that also around $n \simeq N_b$ and for $N_b \ll N$ we find the limit behavior

$$\Gamma_n = \Gamma + n\left(\gamma + \left[\frac{k}{q_{\rm off}} + \gamma\frac{q_{\rm on}}{q_{\rm off}}\right]\right) \tag{S1.28}$$

which allows us to recover, as anticipated, the result for $n = N_b$ of Eq. (16) .

2 Comparison to experimental data for diffusion of DNA-coated colloids

2.1 Experimental data for the diffusion of DNA-coated colloids: I. Additional data

2.1.1 Preparation of material

DNA coated polystyrene colloids We synthesize DNA-coated polystyrene (PS) spheres using the swelling/deswelling method reported in Ref. [1]. Polystyrene-b-poly(ethylene oxide) copolymer PS(3800 g/mol)-b-PEO(6500 g/mol) is purchased from Polymer Source Inc, and is first functionalized with azide at the end of the PEO chain [2]. PS-b-PEO-N3 are then attached to the PS particles using the swelling/deswelling method. In the synthesis, 15 μL of 1μm particles (10 w/v, purchased from Thermo Scientific), 125 μL Deionized (DI) water, 160 μL tetrahydrofuran (THF) and 100 μL of PS-b-PEO-N3 are mixed at room temperature. The mixture is placed on a horizontal shaker (1000 rpm) for 1.5 hours to fully swell the PS particles and absorb the PS block of the PS-b-PEO-N3 molecules. Then THF is slowly removed from the solution via evaporation by adding DI water, leaving the hydrophobic PS blocks physically inserted into the particles and the hydrophilic PEO chains extending out into the solution. The particles are washed with DI water three times to remove excess polymers.

Single stranded DNA (ssDNA, 20 bases, purchased from Integrated DNA Technologies) with 5' dibenzocyclooctyne (DBCO) end modification, is clicked to the N3 (at the end of PS-b-PEO-N3) through strain promoted alkyne-azide cycloaddition [1]. PS particles previously coated with the PS-b-PEO-N3 polymer brush are dispersed in 200 μL of 500 mM PBS buffer, at pH 7.4. Then 10 μL of DBCO-DNA (0.1 mM) are added to the suspension. The mixture is left to react for 48 hours on a horizontal shaker (1000 rpm). The final product is washed in DI water three times and stored in 140 mM PBS buffer. The DNA coverage density is measured using flow cytometry and we obtain $\sigma = 1/(3.27\ \text{nm}^2)$. The DNA sequence used on the colloids is 5'-/DBCO/-T_{14}-ACCGCA-3'.

DNA coated glass substrate DNA coated substrates are prepared using the same swelling/deswelling method. First, an ultra thin PS layer is spin-coated to a cleaned 22 mm x 22 mm glass coverslip (purchased from Bioscience Tools). The substrate is then swelled in the same PS-b-PEO-N3 solution in THF for 4 hours. Then THF is slowly removed from the solution via evaporation. DNA clicking is performed in a home made PDMS reaction chamber for 48 hours on a shaking stage, then washed 10 times in DI water to remove extra DNA. The entire sample is sealed in the 140 mM PBS buffer (ph 7.4) with 0.3% w/v pluronic F127 surfactants, using UV glue to avoid any external flow or evaporation of the buffer. The DNA sequence used on the glass substrate is complementary to that on the particles, 5'-/DBCO/-T_{14}-TGCGGT-3'.

2.1.2 Tracking DNA coated colloids

Particle positions measurements To study the diffusion of DNA coated colloids, we track the motion of about 500 particles as they bind and diffuse on the DNA coated substrate – see Fig. S4-A. The sample is mounted on a homemade lab microscope (Nikon Eclipse Ti 60X, 72nm pixel size, depth of focus 560 nm) thermal stage with a temperature controller. Tracer particles fixed on the substrate are used to substract camera drift during the tracking. Displacement measurements are performed by tracking particles over the temperature range 28-62 °C – see Fig. S4-B. At each temperature, particles are tracked over a time range of 20 min at a frame rate of 5 images per second. For the highest temperature reported here, $T = 59.1$ °C, particles diffuse faster and we only track them over 5 min, with 10 images per second. Images are then analyzed using the TrackPy software to obtain individual particle positions with time. Particles that do not move at all even at high temperatures are removed from the analysis. These particles are likely in a low density area where steric repulsion is not sufficient to screen van der Waals attraction, and therefore are "crashed" on the surface.

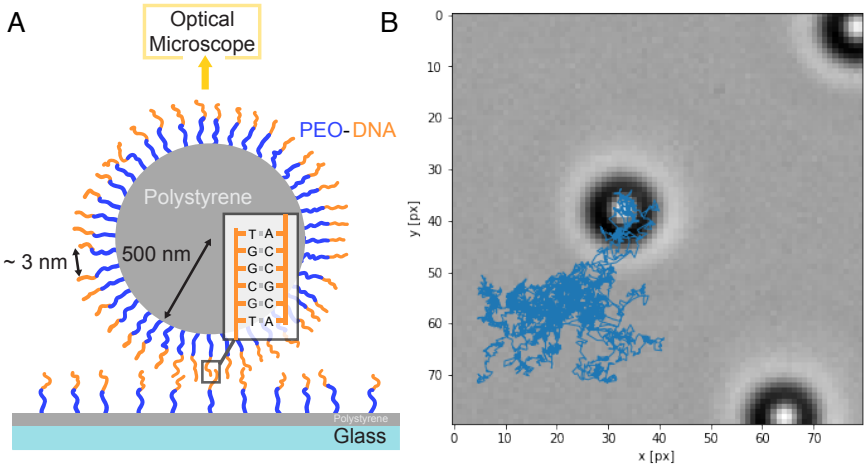

Figure S4: **Experimental setup to measure diffusion of DNA-coated colloids on DNA-coated surfaces.** (A) Schematic of a DNA-coated colloid attaching to a DNA-coated substrate, with the specific DNA sequence used in this study. Diffusion of the colloids is tracked from on-top. (B) Example of a colloid trajectory over an 18 min time frame (in blue) overlaid on the bright-field microscope image corresponding to the colloid's initial position. Here 1 px corresponds to 0.108 μm.

Mean square displacement analysis We fit the ensemble mean-squared displacement to a power law as $< \boldsymbol{x}^2(t) >= 4Dt^{\alpha}$, where $\boldsymbol{x}$ is the position of each particle on the surface plane, using a linear regression in log space to get the diffusion coefficient D and the power on time α. Typically, α decreases from ~ 1 at high temperatures to values < 1 at lower temperatures. Around the melting transition however, there exists a window of a few degrees where the motion is diffusive and we obtained $1.02 > \alpha > 0.94$. On this temperature window we then fix $\alpha = 1$ and the effective diffusivity D_{eff} is obtained by fitting the ensemble-averaged mean-square displacement to the power law $\langle \boldsymbol{x}^2(t) \rangle = 4D_{\text{eff}}t$.

Melting curve To compare different measurements with one another we define a kinetic melting temperature. This temperature T_m corresponds to the temperature for which the measured diffusion coefficient is half that of the high temperature diffusion coefficient (the latter corresponding to the hydrodynamic diffusion coefficient).

Reproducibility and error bars The entire experimental process (synthesis and mean square displacement measurements) are reproduced 3 times and the results are reported with different symbols in Fig. 7A of the main manuscript. Note that the synthesis is performed with slight variations of the coating process (shaking time), yet very similar behavior is obtained – for example the melting temperatures for each of

the samples are within 3°C of each other. Such disparity in melting temperature can occur due to density differences originating while performing the same synthesis and hence we do not report further details here.

As the average for D_{eff} is calculated over a great number of particles, the typical error on D_{eff}, for example due to the fitting procedure, is very small – typically smaller than the size of the points used to represent data and also much smaller than intrinsic disparities from sample to sample due to density fluctuations on the surface coverage during sample preparation. Therefore we do not report any vertical error bars. The exact temperature measured can slightly fluctuate, due to potential drift of the temperature controller, thus it is reasonable to assume a 0.2°C error bar on each experimental data point.

2.2 Experimental data for the diffusion of DNA-coated colloids: II. Existing data

Diffusion of DNA-coated colloids from existing data was obtained from 2 published references [3, 4].

High coating density diffusion coefficients from Ref. [4] Diffusion coefficients from Ref. [4] were obtained by fitting a linear law through extracted mean square displacement data using WebPlotDigitizer [5] – when the diffusion exponent α is greater than ~ 0.8. Mean square displacement data in Ref. [4] represents the projected mean square displacement $\langle \boldsymbol{r}^2 \rangle$ covered on a half-sphere, when the displacement on the half-sphere is observed from on-top. The actual surface covered $\langle \boldsymbol{x}^2 \rangle$ is therefore larger than that measured on the projected area, and we can write $\langle \boldsymbol{x}^2 \rangle = \mathcal{A} \langle \boldsymbol{r}^2 \rangle$ where $\mathcal{A}$ is an area correction number. If the particle covers the entire area typically $\mathcal{A} \simeq 2$ since $2\pi R^2$ is the actual area of the half sphere of radius R, and πR^2 is the projected area. This typically accounts for the fact that the particles does not spend the same amount of time on the sides of the half-sphere and on the top, and that on the sides displacements can be fully orthogonal to the observation projection plane. Additionally, since motion is constrained to the half-sphere, in practice the random walk is constrained and folded back onto the sphere. If it were unconstrained on the sphere we would typically have $4\pi R^2$ of area covered projected on πR^2 so we take $\mathcal{A} = 4$ as an upper bound on $\mathcal{A}$. $\mathcal{A} = 2$ is our lower bound. These bounds allow us to define error bars for the diffusion data of Ref. [4]. Again, considering potential density fluctuations on either surfaces and other experimental uncertainties due to calibration of the temperature controller, it is reasonable to assume a 0.2°C error bar on each experimental data point.

The detailed parameters of the DNA-coated colloids used in Ref. [4] are provided in that reference and we use their specific values to perform analytical predictions for D_{eff}, see details below. The melting temperature in Ref. [4] is defined as the temperature for which the fraction of single particles is 50%, since the particles can self-assemble in arrays. This is a typical thermodynamic quantity hence we use a the thermodynamic definition of melting [6]

$$p_{\text{unbound}}^{Ref.\ [4]} = 1 - \frac{1}{Z} \int_0^{h_c} e^{-\phi(h)/k_B T} dh \tag{S2.1}$$

where $\phi(h)$ is a particle-particle interaction potential, $h_c \simeq 20$ nm is a typical interaction range and Z a normalization constant. We find without any fitting that $T_m^{\text{theo}} = 25.3$°C which is not too far from the experimental melting temperature $T_m = 28.9$°C. The difference is likely due to the slightly different method used to quantify T_m. We align experimental data relative to T_m and theoretical data relative to T_m^{theo}.

Low coating density diffusion coefficients from Ref. [3] Ref. [3] provides the diffusion coefficients for their DNA-coated particles above the melting temperature $T_m = 44.7$°C as $D_{\text{eff}}(47^\circ\ \text{C}) = 0.38\ \mu\text{m}^2/\text{s}$, and at the melting temperature $D_{\text{eff}}(44.7^\circ\ \text{C}) = 1.4 \times 10^{-3}\ \mu\text{m}^2/\text{s}$. Additionally, for the data provided 0.27° C below T_m, the exponent for diffusion is $\alpha \sim 0.8$ and we can estimate the diffusion coefficient from a linear fit to the data. We obtain $D_{\text{eff}}(44.5^\circ\ \text{C}) = \frac{30\ \mu\text{m}^2}{30000\text{s} \times 4} = 0.25 \times 10^{-3}\ \mu\text{m}^2/\text{s}$.

The detailed parameters of the DNA-coated colloids used in Ref. [3] are provided in that reference and we use their respective values to perform analytical predictions for D_{eff}, see details below. The melting temperature in Ref. [3] is defined as the temperature for which the fraction of moving particles is 50%, where " Moving is defined as a displacement larger than 50 nm (1 pixel) between frames (frame rate = 1 Hz)". We

can relate to this moving quantity by defining the unbound probability as

$$p_{\text{unbound}}^{Ref.\ [3]} = 1 - \text{erf}\left(\frac{\Delta x_{\max}}{\sqrt{4D_{\text{eff}}\Delta t_{\max}}}\right) \tag{S2.2}$$

measuring the probability that a step is larger than $\Delta x_{\max} = 50$ nm during a time interval $\Delta t_{\max} = 1$ s where the diffusion coefficient of the particle is D_{eff}. Here we use D_{eff} as predicted by hopping motion only since only hopping is occurring in this sample due to geometrical constraints. We find $T_m^{\text{theo}} = 44.2°\text{C}$ close to the experimental measurement of $T_m = 44.7°\text{C}$. We align experimental data relative to T_m and theoretical data relative to T_m^{theo}. In line with previous analysis we also add 0.2°C error bar on each experimental data point.

2.3 Modeling tools for DNA-coated colloids

2.3.1 Number of legs and average number of bonds

To evaluate D_{eff} from Eq. (15) , we must evaluate the parameters of the 1D nanocaterpillar model. As mentioned in the main manuscript, some parameters, such as N and N_b (or equivalently N and the ratio $q_{\text{on}}/q_{\text{off}}$) require careful modeling of the detailed leg-arm interactions [6] to be estimated.

We thus calculate the detailed DNA-DNA brush interactions, accounting for leg density, leg length and DNA sequence, by evaluating the interaction energy $\phi(h)$ of the DNA-coated colloid with another coated surface at separation distance h. Following Ref. [6], $\phi(h)$ includes repulsive steric interactions [7] and attractive binding interactions, with entropic terms due to loss of degrees of freedom upon binding and competition for binding partners [8].

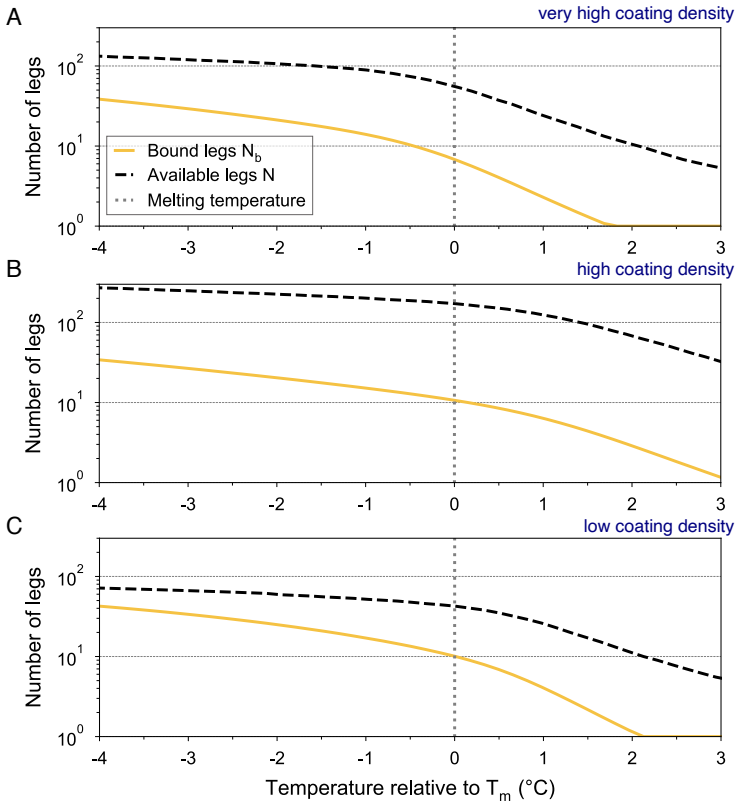

Figure S5: **Number of legs N and average number of bonds N_b involved in the binding process predicted from theory.** N and N_b are evaluated from detailed microscopic interactions for each system corresponding to detailed design parameters of DNA-coated colloids used (A) in this work (B) in Ref. [4] and (C) in Ref. [3].

All parameters are precisely known in the experimental system, but one: the coating density. We can estimate it by looking at the thermodynamic unbound probability obtained from the Boltzmann distribution as $p_u \sim \int_0^{h_c} e^{-\beta\phi(h)} dh$, and comparing it to the similar quantity calculated experimentally. The experimental data shows that the unbound probability transitions around $T_m = 55-58°$ C which corresponds to theoretical curves obtained with a surface density ranging from 1 DNA per (9 nm)^2 to (12 nm)^2. We therefore use 1 DNA per (10.5 nm)^2 as a center value and the extremal values to calculate a fidelity interval for D_{eff} (gray area in Fig. 6A). These obtained values are within the range of expected values [6].

The average number of bonds N_b (gold in Fig. S5) and the number of legs within reach N (dashed black) with respect to temperature are then readily evaluated from the model leading to $\phi(h)$. The number of bonds at the melting temperature is only $N_b(T_m) \simeq 10$ while the number of available legs can be quite high $N(T_m) \simeq 100$. The number of bonds N_b increases strongly with decreasing temperature, from 0 to 40 over the 4°C window, thus potentially accounting for most of the decrease in diffusion.

2.3.2 3D geometry

In general the particle can explore positions not just in one dimension but in 3D. Here we discuss how to take into account this full geometry.

Second lateral dimension The second lateral dimension is – to some extent – a trivial extension of the 1-lateral dimension model derived in the main manuscript. We consider the constitutive equations for the leg and the particle in 2 lateral dimensions (x, y), simplifying here to $\ell_0 = 0$, namely considering that the rest state of the tether lies right above the surface and that deformations are still quadratic in the leg extension. We have

$$\frac{d\boldsymbol{l}}{dt} = -\frac{k}{\gamma}|\boldsymbol{l}|\frac{\boldsymbol{l}}{|\boldsymbol{l}|} + \sqrt{2\frac{k_BT}{\gamma}}\boldsymbol{\eta_l}$$
$$\frac{d\boldsymbol{x}}{dt} = +\sqrt{2\frac{k_BT}{\gamma}}\boldsymbol{\eta_x}.$$

The leg extension $\boldsymbol{l}$ is readily projected on both coordinates:

$$|\boldsymbol{l}|\frac{\boldsymbol{l}}{|\boldsymbol{l}|} = \boldsymbol{l} = l_x\boldsymbol{u}_x + l_y\boldsymbol{u}_y$$

and similarly for the noise operators. We obtain

$$\frac{dl_i}{dt} = -\frac{k}{\gamma}l_i + \sqrt{2\frac{k_BT}{\gamma}}\eta_{l,i}$$
$$\frac{dx_i}{dt} = +\sqrt{2\frac{k_BT}{\gamma}}\eta_{x,i}.$$

where $i = (x, y)$ refers to both lateral dimensions. The equations are fully uncoupled and hence it is not necessary to conduct further calculations to conclude that the effective long time motion should write as

$$\frac{d\boldsymbol{x}}{dt} = +\sqrt{2D_{\text{eff}}}\boldsymbol{\eta_x}.$$

where D_{eff} has the same expression as in the main manuscript.

Vertical dimension The particle may also venture far from the surface, where binding is not possible. To account for this 3D geometry, we use an extension of our main model.

One option to account for such a 2D dependence is to add a vertical degree of freedom say z for the particle, together with spatially dependent rates $q_{\text{on}}(z), q_{\text{off}}(z)$. This is not a trivial modification, especially as there are different ways to set the spatial dependence z of $q_{\text{on}}(z), q_{\text{off}}(z)$ (see for example the variability between Refs. [9, 10, 11]).

Instead we rely on a simplified geometrical approach, that has been shown to accurately reproduce a 2D geometry in another context [12], where we describe the system with 2 × 1D lines. For a 1-legged particle, we consider that the particle can switch between two regions where its dynamics are constrained to 1D:

surface and bulk regions. The particle enters the surface region with rate $Q_{\rm on}$, and then can bind to the surface with rate $q_{\rm on}$. If the particle is *unbound* in the surface region, it may lift off from the surface region to the bulk region with rate $Q_{\rm off}$. $\frac{Q_{\rm on}}{Q_{\rm off}}$ corresponds to the ratio of positions where the receptors are within and beyond reach. In DNA-coated colloid explorations, where particles are considered on top of a sticky surface, the ratio can be small or large depending on the density mismatch between the particle material and the surrounding fluid, that is otherwise described by the particle's gravitational height [3]. For other systems, such as white blood cells that are confined within blood vessels, particles are always close to the wall [13] and hence the ratio is quite large. Approach and lift-off from the surface are slow processes that scale like the diffusive dynamics of the particle and thus we may assume $Q_i\tau \sim O_\epsilon(1)$.

Performing similar coarse-graining steps (see following paragraph), we obtain an effective friction

$$\frac{1}{\Gamma_{\rm eff}^{2\times 1D}} = \frac{p_0^{2\times 1D}}{\Gamma_0} + \frac{p_1^{2\times 1D}}{\Gamma_1} \tag{S2.3}$$

where the probability to be in either states takes into account the added degree of freedom, $p_1^{2\times 1D} = Q_{\rm on}q_{\rm on}/Z$ and $p_0^{2\times 1D} = q_{\rm off}(Q_{\rm on}+Q_{\rm off})/Z$ with Z a normalization constant such that $p_0^{2\times 1D} + p_1^{2\times 1D} = 1$. The added degree of freedom does not change the result of Eq. (12) , simply the mathematical interpretation of the probability factors. Note that this framework has been verified against numerical simulations.

The values of $Q_{\rm on}$ and $Q_{\rm off}$ can be evaluated from the detailed interaction potential $\phi(h)$ of a DNA-coated colloid and the surface. In fact, the probability to be near the surface, in the absence of binding, is measured by

$$\frac{Q_{\rm on}}{Q_{\rm on}+Q_{\rm off}} = \int_0^{h_p} e^{-\beta(\phi(h)-\phi_{\rm bind}(h))}dh/Z \tag{S2.4}$$

where $\phi_{\rm bind}(h)$ measures the contributions to the interaction potential due to binding, $h_p \simeq 20$ nm measures the typical width of attractive interactions (region of space where binding could happen) and Z is a normalizing factor. For our DNA-coated colloids we find $\frac{Q_{\rm on}}{Q_{\rm on}+Q_{\rm off}} \simeq 0.0015$ and that the ratio does not depend much on temperature. It also does not depend significantly on the exact value of h_p for $h_p = 2-40$ nm.

For an N-legged caterpillar, the result generalizes to a change in the probability factors p_n in Eq. (15) for $D_{\rm eff}$. We have $p_0^{2\times 1D} = q_{\rm off}^N(Q_{\rm on}+Q_{\rm off})/Z$ and $p_n^{2\times 1D} = \binom{N}{n} q_{\rm off}^{N-n} q_{\rm on}^n Q_{\rm on}/Z$ such that $Z = Q_{\rm on}(q_{\rm on}+q_{\rm off})^N + Q_{\rm off}q_{\rm off}^N$.

2.3.3 2×1D, 1 legged nanocaterpillar model

In this section we derive the effective 1-legged long term caterpillar dynamics in an effective "2D" geometry by using the 2×1D mapping. The steps are carefully detailed so as to serve as an additional pedagogical explanation of the coarse-graining procedure introduced in the main text.

Constitutive equations of the 2×1D, 1-legged caterpillar model Let $p(x,l,t) = (p_V, p_u, p_b)^T$ be the probability distribution function of finding the system at time t in state x, l far from the surface (V), or close to the surface with a bound (b) or an unbound (u) leg. It obeys the Schmoluchowski equation

$$\partial_t p = \mathcal{L}^\star p \text{ with } \mathcal{L}^\star = \mathcal{Q}^\star + \mathcal{U}^\star \tag{S2.5}$$

where $\mathcal{Q}^\star$ is the matrix of rates to going from one state to another

$$\mathcal{Q}^\star = \begin{pmatrix} -Q_{\rm on} & Q_{\rm off} & 0 \\ Q_{\rm on} & -Q_{\rm off}-q_{\rm on} & q_{\rm off} \\ 0 & q_{\rm on} & -q_{\rm off} \end{pmatrix} \tag{S2.6}$$

and $\mathcal{U}^\star$ contains the dynamics in each state

$$\mathcal{U}^\star = \text{diag}\begin{pmatrix} \partial_l\left(\frac{k}{\gamma}(l-l_0)+\frac{k_BT}{\gamma}\partial_l\right)+\frac{k_BT}{\Gamma}\partial_{xx} \\ \partial_l\left(\frac{k}{\gamma}(l-l_0)+\frac{k_BT}{\gamma}\partial_l\right)+\frac{k_BT}{\Gamma}\partial_{xx} \\ (\partial_l-\partial_x)\left(\frac{k}{\Gamma+\gamma}(l-l_0)+\frac{k_BT}{\Gamma+\gamma}(\partial_l-\partial_x)\right) \end{pmatrix}. \tag{S2.7}$$

Consistently, the equilibrium distribution $\pi = \frac{e^{-\beta k(l-l_0)^2/2}}{Z}\left(\frac{Q^{\text{off}}}{Q^{\text{on}}},\quad 1,\quad \frac{q_{\text{on}}}{q_{\text{off}}}\right)^T$ is indeed a stationary solution of Eq. (S2.5). Note that here Q_{on} and Q_{off} represent respectively the rates at which the particle approaches and leaves the vicinity of the surface, namely the region of space where binding is possible.

Non-dimensionalization Using the non-dimensional notation introduced in the main text allows to separate the Schmoluchowski operator $\mathcal{L}^\star$ in fast and slow operators. In the following, it will be somewhat easier to conduct the reasoning not on $\mathcal{L}^\star$ but on its adjoint $\mathcal{L}$, the generator of the system, defined such that for appropriate functions f, we have $\langle f, \mathcal{L}^\star p\rangle = \langle \mathcal{L} f, p\rangle$, where $\langle f, g\rangle = \iint (f_V g_V + f_u g_u + f_b g_b) dl dx$ is the inner product. We therefore seek a solution f of the dynamics

$$\partial_t f = \mathcal{L} f = \left(\frac{1}{\epsilon^2}\mathcal{L}_0 + \frac{1}{\epsilon}\mathcal{L}_1 + \mathcal{L}_2\right) \tag{S2.8}$$

where

$$\mathcal{L}_0 = \begin{pmatrix} \frac{\Gamma}{\gamma}(-l\partial_l + \partial_{ll}) & 0 & 0 \\ 0 & -q_{\text{on}} + \frac{\Gamma}{\gamma}(-l\partial_l + \partial_{ll}) & q_{\text{on}} \\ 0 & q_{\text{off}} & -q_{\text{off}} + \frac{\Gamma}{\Gamma+\gamma}(-l\partial_l + \partial_{ll}) \end{pmatrix}, \tag{S2.9}$$

$$\mathcal{L}_1 = \text{diag}\left(0, 0, \frac{\Gamma}{\Gamma+\gamma}\left(l\partial_x - 2\partial_{lx}\right)\right) \tag{S2.10}$$

and

$$\mathcal{L}_2 = \begin{pmatrix} -Q_{\text{on}} & Q_{\text{on}} & 0 \\ Q_{\text{off}} & -Q_{\text{off}} & 0 \\ 0 & 0 & 0 \end{pmatrix} + \text{diag}\left(1, 1, \frac{\Gamma}{\Gamma+\gamma}\right)\partial_{xx}. \tag{S2.11}$$

Additionally, f has to satisfy boundary conditions of no flux at infinity

$$\partial_l f(x, l, t)|_{l=\pm\infty} = 0 \tag{S2.12}$$

which correspond to the usual no flux in probability space (where the flux in probability space satisfies $(lp + \partial_l p)\,|_{l=\pm\infty} = 0$). This condition is physical as it imposes conservation of probability. Note that we expect these boundary conditions to be satisfied only at lowest order in ϵ.

Homogenization We seek a solution to Eq. (S2.8) as an expansion in the small parameter ϵ, as $f = f_0 + \epsilon f_1 + \epsilon f_2 + ...$ At lowest order we need to satisfy $\mathcal{L}_0 f_0 = 0$ which yields the general solution

$$f_0 = \begin{pmatrix} a_V(x,t) \\ a_S(x,t) \\ a_S(x,t) \end{pmatrix} + \int_0^l e^{y^2/2} dy \begin{pmatrix} b_V(x,t) \\ b_S(x,t) \\ b_S(x,t) \end{pmatrix} \tag{S2.13}$$

where a_S, a_V, b_S and b_V are all integration "constants" and S and V denote surface and volume terms. With the boundary conditions on f we get $b_S(x,t) = b_V(x,t) = 0$. Note that such boundary conditions also allow the cross product $\langle f_0, \pi\rangle$ to remain finite which will be expected later to use the Fredholm alternative.

The associated equilibrium distribution at lowest order π_0 spans a two dimensional space described by $(\pi_{0,V}(x,t), \pi_{0,S}(x,t))$ such that

$$\pi_0 = \frac{1}{Z}\begin{pmatrix} \pi_{0,V}(x,t) \\ \pi_{0,S}(x,t)) \\ \pi_{0,S}(x,t))\frac{q_{\text{on}}}{q_{\text{off}}} \end{pmatrix} e^{-l^2/2}. \tag{S2.14}$$

We therefore expect that our long time dynamics will consist in a 2×2 matrix describing the joint evolution of surface variables $(a_S(x,t))$ and volume variables $(a_V(x,t))$.

At the next order we need to satisfy $\mathcal{L}_0 f_1 = -\mathcal{L}_1 f_0$. f_1 is the sum of a particular integral and a complementary function (*i.e.* a function in the nullspace of $\mathcal{L}_0$). The complementary function can be taken to be 0 otherwise f_1 would contain terms that are redundant with f_0. One can check that the particular integral to this equation is simply

$$f_1 = \begin{pmatrix} 0 \\ \gamma q_{\text{on}} \\ \Gamma + \gamma q_{\text{on}} \end{pmatrix} \frac{l\partial_x a}{\Gamma(1+q_{\text{off}}) + \gamma(q_{\text{on}} + q_{\text{off}})}. \tag{S2.15}$$

At the following order we need to find a solution to $\mathcal{L}_0 f_2 = \partial_t f_0 - \mathcal{L}_2 f_0 - \mathcal{L}_1 f_1$. This equation has a solution if the right hand side terms of the equal sign satisfy the Fredholm alternative [14], namely

$$\langle \partial_t f_0 - \mathcal{L}_2 f_0 - \mathcal{L}_1 f_1, \pi_0 \rangle = 0. \tag{S2.16}$$

As π_0 spans a 2D space described by $(\pi_{0,V}(x,t), \pi_{0,S}(x,t))$ we can evaluate the Fredholm alternative on an orthogonal basis of this space; specifically here we will investigate the Fredholm alternative on $(1,0)$ then $(0,1)$. On the volume space we have

$$\partial_t a_V = \partial_{xx} a_V - Q_{\text{on}} a_V + Q_{\text{on}} a_S. \tag{S2.17}$$

On the surface space the terms are more lengthy and we split them for readability

$$\langle \partial_t f_0, \pi_0 \rangle = \left(1 + \frac{q_{\text{on}}}{q_{\text{off}}}\right) \partial_t a_S, \tag{S2.18}$$

$$\langle \mathcal{L}_2 f_0, \pi_0 \rangle = -Q_{\text{on}} a_S + Q_{\text{on}} a_V + \partial_{xx} a_S + \frac{q_{\text{on}}}{q_{\text{off}}} \partial_{xx} a \tag{S2.19}$$

and finally

$$\langle \mathcal{L}_1 f_1, \pi_0 \rangle = -\frac{q_{\text{on}}}{q_{\text{off}}} \frac{\Gamma + \gamma q_{\text{on}}}{\Gamma(1+q_{\text{off}}) + \gamma(q_{\text{on}} + q_{\text{off}})} \partial_{xx} a_S. \tag{S2.20}$$

Compiling all contributions on the surface we find

$$\begin{aligned} \partial_t a_S = &-Q_{\text{off}} a_S + Q_{\text{off}} a_V \\ &+ \frac{q_{\text{off}}}{q_{\text{off}} + q_{\text{on}}} \partial_{xx} a_S + \frac{q_{\text{off}}}{q_{\text{off}} + q_{\text{on}}} \frac{\Gamma}{\Gamma + \gamma \frac{1 + q_{\text{off}} + q_{\text{on}}}{q_{\text{off}}}} \partial_{xx} a_S. \end{aligned} \tag{S2.21}$$

Overall we have found effective long time dynamics described by the generator (in dimensional scales)

$$\mathcal{L}_{\text{eff}} = \begin{pmatrix} -Q_{\text{on}} + \frac{k_B T}{\Gamma} \partial_{xx} & Q_{\text{on}} \\ Q_{\text{off}} \frac{q_{\text{off}}}{q_{\text{on}} + q_{\text{off}}} & -Q_{\text{off}} \frac{q_{\text{off}}}{q_{\text{on}} + q_{\text{off}}} + \frac{k_B T}{\Gamma_{\text{eff}}} \partial_{xx} \end{pmatrix}, \text{ such that } \partial_t a = \mathcal{L}_{\text{eff}} a. \tag{S2.22}$$

Here $\Gamma_{\text{eff}}^{-1} = p_0 \Gamma_0^{-1} + p_1 \Gamma_1^{-1}$ with $\Gamma_0 = \Gamma$, $\Gamma_1 = \Gamma + \gamma + k\left(\frac{1}{q_{\text{off}}} + \frac{k}{\gamma} \frac{q_{\text{on}}}{q_{\text{off}}}\right)$, $p_0 = q_{\text{off}}/(q_{\text{off}} + q_{\text{on}})$ is the probability to have no bond near the surface and $p_1 = 1 - p_0$ is the probability to have 1 bond near the surface. Note that the expression of Γ_{eff} is exactly that when focusing only on surface dynamics and discarding effective 2D dynamics (see Eq. (12) of the main paper). This shows that homogenization steps in the embedded 2×1D geometry do not entangle with surface dynamics. To understand the meaning of this effective generator, we go one step further.

Long (long) times We now wish to understand the long time dynamics of the generator $\mathcal{L}_{\text{eff}}$. We search for long (long) time dynamics by using a non-dimensionalization that seeks even longer times as

$$t \to \tilde{t} \frac{\tau}{\epsilon}, \; x \to \tilde{x} L_x \tag{S2.23}$$

where $\tau = L_y^2/D_0 = L_y^2\Gamma/k_BT$ and $L_y/L_x = 1/\sqrt{\epsilon}$ corresponds to the far horizontal scales x is going to explore (compared to the shorter vertical scales). $Q_{\rm on}$ and $Q_{\rm off}$ are typically associated with the time scale that the particle takes to diffuse vertically and therefore $Q_{\rm on}\tau \sim 1$ and likewise $Q_{\rm off}\tau \sim 1$. We obtain the non-dimensional generator

$$\mathcal{L}_{\rm eff} = \frac{1}{\epsilon}\begin{pmatrix} -Q_{\rm on} & Q_{\rm on} \\ Q_{\rm off}\frac{q_{\rm off}}{q_{\rm on}+q_{\rm off}} & -Q_{\rm off}\frac{q_{\rm off}}{q_{\rm on}+q_{\rm off}} \end{pmatrix} + \begin{pmatrix} \partial_{xx} & 0 \\ 0 & \frac{\Gamma}{\Gamma_{\rm eff}}\partial_{xx} \end{pmatrix} = \frac{1}{\epsilon}\mathcal{L}_0 + \mathcal{L}_1 \tag{S2.24}$$

and we search for a solution f of the equation $\partial_t f = \mathcal{L}_{\rm eff} f$ expanded in ϵ as $f = f_0 + \epsilon f_1 + ...$

At lowest order we obtain from $\mathcal{L}_0 f_0 = 0$, $f_0 = a(x,t)\begin{pmatrix}1\\1\end{pmatrix}$, with the associated equilibrium distribution

$$\pi_0 = \frac{1}{Z}\begin{pmatrix} Q_{\rm off}\frac{q_{\rm off}}{q_{\rm on}+q_{\rm off}} \\ Q_{\rm on} \end{pmatrix}. \tag{S2.25}$$

At the next order we need to satisfy the Fredholm alternative, namely $\langle \partial_t f_0 - \mathcal{L}_1 f_0, \pi_0\rangle = 0$ leading to (back in dimensional scales)

$$\partial_t a = \frac{k_BT}{\Gamma_{\rm eff}^{2\times 1{\rm D}}}\partial_{xx} a \tag{S2.26}$$

where

$$\frac{1}{\Gamma_{\rm eff}^{2\times 1{\rm D}}} = \frac{Q_{\rm off}q_{\rm off}}{Q_{\rm off}q_{\rm off} + Q_{\rm on}\left(q_{\rm on}+q_{\rm off}\right)}\frac{1}{\Gamma} + \frac{Q_{\rm on}\left(q_{\rm on}+q_{\rm off}\right)}{Q_{\rm off}q_{\rm off} + Q_{\rm on}\left(q_{\rm on}+q_{\rm off}\right)}\frac{1}{\Gamma_{\rm eff}}. \tag{S2.27}$$

Expanding terms with the expression of $\Gamma_{\rm eff}$ and rearranging we can summarize the result in the explicit form, similarly as in Eq. (12) of the main paper,

$$\boxed{\frac{1}{\Gamma_{\rm eff}^{2\times 1{\rm D}}} = \frac{p_0^{2\times 1D}}{\Gamma_0} + \frac{p_1^{2\times 1D}}{\Gamma_1}} \tag{S2.28}$$

where

$$\boxed{p_0^{2\times 1D} = \frac{(Q_{\rm off}+Q_{\rm on})q_{\rm off}}{Z} \text{ and } p_1^{2\times 1D} = \frac{Q_{\rm on}q_{\rm on}}{Z}} \tag{S2.29}$$

are the probabilities to have respectively 0 and 1 bond, $Z = (Q_{\rm off}+Q_{\rm on})q_{\rm off} + Q_{\rm on}q_{\rm on}$ and $\Gamma_0 = \Gamma$ is the friction in the unbound state and $\Gamma_1 = \Gamma + \gamma + k\left(\frac{1}{q_{\rm off}} + \frac{k}{\gamma}\frac{q_{\rm on}}{q_{\rm off}}\right)$ is that contributing to the bound state. A similar result for an N legged caterpillar, simply adapting the probabilities, is thus used to quantify diffusion of DNA-coated colloids on surfaces.

To recover surface only dynamics, one simply has to take $Q_{\rm on}/Q_{\rm off} \to \infty$ in the above expression. In that case one can easily obtain the surface only effective friction Eq. (12) of the main text.

3 List of parameters for typical biological and artificial systems

Quantity	Range of values	Details
DNA coated colloids - low coverage large colloids		
R	525 nm	Low coverage streptavidin beads of [3]
η	0.0006Pa.s	Viscosity of water at the melting temperature 44 $^\circ C$
a	$10-15$ nm	estimated with for double stranded DNA, 60 nucleotides [15]
k	1×10^{-4} N/m	$k\simeq 3\frac{k_BT}{2Ll_p}$ where $l_p\simeq 3.4$ nm is the typical persistence length corresponding to 10 base pairs in a helix and $L\simeq 60(l_p/10)\simeq 20$ nm [3]
$q_{\rm on}$	2500 $\rm s^{-1}$	from $q_{\rm on}\sim k_{\rm on}\sigma/a\mathcal{N}_{\mathcal{A}}$ with $k_{\rm on}=2.2\times10^6 M^{-1}s^{-1}$ (44.7 $^\circ C$) (value predicted from Ref. [16] for the CCAAGTTATGA sequence used in [3], measurements on sequences with a similar number of bases show slightly lower hybridization rates [17])
$q_{\rm off}$	25000 $\rm s^{-1}$	estimated unbinding rate around the melting temperature with a bound probability of 10% (evaluated using full potential profile estimates following [6]). Expected $q_{\rm off}\simeq q_{\rm on}$ at lower temperatures
σ	$1/(12\,{\rm nm}-18\,{\rm nm})^2$	coating density [3]
D	1.4×10^{-3} $\mu\rm m^2/s$	at the melting temperature [3]
D_0	0.37 $\mu\rm m^2/s$	calculated as $D_0=k_BT/12\pi\eta R$ with $T=44\,^\circ$C (since close to the surface, longitudinal friction is doubled due to hydrodynamic interactions)
D_0/D	270	diffusion decrease factor, calculated with range of above values
N	$40-70$	estimated from $N\simeq 2\pi Rh\sigma$ taking $h\simeq a/3$ the typical penetration length of the layers, and density limited by the surface density, probably in the lower range $\sigma=1/(16\ {\rm nm})^2$
$N(T_m)$	40	number of involved legs at the melting point, using the methodology described in Ref. [6]. Taking symmetric (particle and flat surface) density with $\sigma=1/(17\ {\rm nm})^2$ and the exact DNA sequences and polymer types detailed in Ref. [3]
$D_0/D_{\rm hop}$	$45-800$	calculated with $D_{\rm hop}=D_0q_{\rm off}^N/(q_{\rm off}+q_{\rm on})^N$ with values above.
DNA coated colloids - high coverage large colloids		
R	500 nm	High coverage beads of [6]
η	0.0005Pa.s	Viscosity of water at melting temperatures 50-60 $^\circ C$
a	$13-18$ nm	measured lengths of 6.5 k PEO strands tethered with 20 nucleotides of single stranded DNA [6]
k	2×10^{-4} N/m	$k\simeq 3\frac{k_BT}{2L\ell_p}$ expected spring constant with $\ell_p\simeq 0.5$ nm and $L=80$ nm (mixed brush with PEO and DNA)
$q_{\rm on}$	$1.3-1.9\times10^4$ $\rm s^{-1}$	from $q_{\rm on}\sim k_{\rm on}\sigma/a\mathcal{N}_{\mathcal{A}}$ with $k_{\rm on}=1.6\times10^6 M^{-1}s^{-1}$ (55 $^\circ C$) (value predicted from Ref. [16] for the ACCGCA sequence used in [6])
$q_{\rm off}$	$1.3-1.9\times10^5$ $\rm s^{-1}$	estimated unbinding rate at the melting temperature with a bound probability of 10% (evaluated using full potential profile estimates following [6]). Expected $q_{\rm off}\simeq q_{\rm on}$ at lower temperatures
σ	$1/(3.27\ {\rm nm})^2$	measured coating density [6]
N	$140-190$	estimated from $N\simeq 2\pi Rh\sigma$ taking $h\simeq a/3$ the typical penetration length of the layers, and density limited by the surface density, probably in the lower range $\sigma=1/(10\ {\rm nm})^2$

Table S1: Parameter values for DNA coated colloids (large colloids)

Quantity	Range of values	Details
DNA coated nanoparticles		
R	7.5 nm	Gold nanoparticles of Ref. [18]
η	0.0006Pa.s	Viscosity of water at the melting temperature 44 $^{\circ}C$
a	10 nm	Estimated in Ref. [18]
k	2×10^{-4} N/m	$k \simeq 3\frac{k_B T}{2Ll_p}$ where $l_p \simeq 3.4$ nm is the typical persistence length corresponding to 10 base pairs in a helix and $L \simeq 30(l_p/10) \simeq 10$ nm [18]
$q_{\rm on}$	2×10^4 s^{-1}	from $q_{\rm on} \sim k_{\rm on}\sigma/a\mathcal{N}_{\mathcal{A}}$ with $k_{\rm on} = 1.0 \times 10^6 M^{-1}s^{-1}$ (44 $^{\circ}C$) (value predicted from Ref. [16] for the CGCG sequence used in [18])
$q_{\rm off}$	2×10^5 s^{-1}	estimated unbinding rate around the melting temperature with a bound probability of 10% (evaluated using full potential profile estimates following [6]). Expected $q_{\rm off} \simeq q_{\rm on}$ at lower temperatures
σ	$1/(3$ nm$)^2$	from 80 strands/ 15 nm particle [19]
N	$15 - 20$	estimated from $N \simeq 2\pi R_{\rm eff} h \sigma_{\rm eff}$ taking $h \simeq a/3$ the typical penetration length of the layers, effective radius of coated nanocolloid $R_{\rm eff} = R + h$ and density at the outer layer $\sigma_{\rm eff} = \sigma R^2/R_{\rm eff}^2$

Table S2: Parameter values for DNA coated nanoparticles

Quantity	Range of values	Details
Leukocyte adhesion mediated by P-selectin or L-selectin		
R	4.15 μm	typical cell size [20]
η	0.001Pa.s	typical physiological conditions [21]
a	300 nm	typical microvillus length [22]
k	$4 \times 10^{-5} - 5 \times 10^{-3}$ N/m	typical spring constant of microvilli [22] up to spring constant of the bond itself (excluding microvilli) [23]
N_b	1-2	typical number of contacts [24, 25]
σ	$15 - 30$ μm^{-2}	typical density of ligands [26, 25]
N	$40 - 80$	calculated from $N \simeq 2\pi R h \sigma$ taking $h \simeq a/3$ the typical penetration length of the layers. Coherent with Ref. [27].
P-selectin		
$q_{\rm on}$	$4 - 300$ s^{-1}	from $q_{\rm on} \sim k_{\rm on}\sigma/a\mathcal{N}_{\mathcal{A}}$ with measured binding rates $k_{\rm on} = (4 - 100) \times 10^5$ M^{-1}s^{-1} [23, 28, 25]
$q_{\rm off}$	$0.02 - 1.6$ s^{-1}	measured unbinding rate [23, 28, 21]
L-selectin		
$q_{\rm on}$	$(0.4 - 4) \times 10^4$ s^{-1}	measured binding rates [24]
$q_{\rm off}$	$7 - 250$ s^{-1}	measured unbinding rate [29, 26], shorter lifetime than P-selectin

Table S3: Parameter values for white blood cells

Quantity	Range of values	Details
E. Coli motility mediated by adhesion between FimH adhesin at the tip of pili and glycoproteins on the surface		
R	350 nm and $L = 3$ μm	cylindrical features [30]
η	0.001Pa.s	typical physiological conditions [21]
a	100 nm	pili characteristic size to calculate hydrodynamic resistance, from $\sqrt{2L_c\ell}$, see below [31]
k	0.6 μN/m	typical spring constant as $k_BT/L_c\ell$ where $L_c = 2$ μm is the contour length and $\ell = 3.3$ nm is the persistence length [31]
$q_{\rm on}$	$5 - 125$ s^{-1}	from $q_{\rm on} \sim k_{\rm on}\sigma/a\mathcal{N}_{\mathcal{A}}$ with measured binding rates $k_{\rm on} = 2 - 50 \times 10^5$ M^{-1}s^{-1} [32, 33, 34]
$q_{\rm off}$	$1 - 100$ s^{-1}	measured unbinding rate [32, 33, 34]
σ	$15 - 45$ μm^{-2}	Pili density, calculated from 100-300 pili over the cylinder surface [35]
N	$2 - 7$	calculated from $N \simeq 2rL\sigma$ taking $r \simeq \sqrt{2aR/3}$ the typical half width of the cylinder in contact.

Table S4: Parameter values for Escherichia Coli

Quantity	Range of values	Details
Cargo transport by molecular motors		
R	1 μm	typical cargo size [36]
η	0.001Pa.s	typical physiological conditions [21]
a	25 nm	microtubule diameter [37]
k	$0.2 - 0.5$ mN/m	typical spring constant [37, 38]
$q_{\rm on}$	0.4 s^{-1}	measured individual binding rate [39]
$q_{\rm off}$	4 s^{-1}	measured unbinding rate [40]

Table S5: Parameter values for molecular motors

Quantity	Range of values	Details
Protein cargos in the nuclear pore complex		
R	50 nm	estimated from $D = 4$ μm^2/s for karyopherin-β which is a major transporter in the NPC [41, 42], $R = k_BT/6\pi\eta D$, and using η as below
η	0.001Pa.s	typical physiological conditions [21]
a	$8 - 10$ nm	estimated with worm like chain model in [43]
k	0.06-0.1 mN/m	typical spring constant of the Nucleoporin Nup 153 [43]
$q_{\rm on}$	$3\times10^5 - 3\times10^8$ s^{-1}	from $q_{\rm on} \sim k_{\rm on}\rho$ with $k_{\rm on} = 10^7 - 10^9$ M^{-1}s^{-1} [42]
$q_{\rm off}$	$10^4 - 10^7$ s^{-1}	estimated unbinding rate [42]
ρ	$30 - 250$mM	concentration of Nup in pore [42, 44]

Table S6: Parameter values for nuclear pore transport

Quantity	Range of values	Details
Influenza A		
R	60 nm	average measured diameter [45]
η	0.001Pa.s	typical physiological conditions [21]
a	$12-15$ nm	typical height of Hemagglutinin [46, 45]
k	$1-2$ mN/m	typical spring constant [46, 47]
q_{on}	$0.07-130$ s^{-1}	calculated from $q_{\text{on}} \sim q_{\text{off}}/K_D\sigma/a\mathcal{N}_{\mathcal{A}}$ with $K_D = 2-950$ mM [48, 46]
q_{off}	$0.1-30$ s^{-1}	measured unbinding rate (focused on Hemagglutinin to Sialic Acid) [46, 49, 47, 50]
$x = \frac{q_{\text{on}}}{q_{\text{on}}+q_{\text{off}}}$	0.2	Bound fraction at equilibrium [46]
σ	6800 μm^{-2}	average measured coverage of HA proteins on virus (85% of total (HA + NA)) [45]
D	$0.05-0.5$ μm^2/s	measured on typical lipid bilayers with sialic acid receptors [49], strongly dependent on q_{off} in the same qualitative way as predicted in out theory
D	0.01 μm^2/s	also measured on typical surfaces [50]
D_0	1.9 μm^2/s	calculated as $D_0 = k_BT/12\pi\eta R$ with $T = 37\,^\circ$C (since close to the surface, longitudinal friction is doubled due to hydrodynamic interactions)
D_0/D	$4-190$	diffusion decrease factor, calculated with range of above values
N	$10-13$	calculated from $N \simeq 2\pi Rh\sigma$ taking $h \simeq a/3$ the typical penetration length of the layers.
D_0/D_{hop}	$9-20$	calculated with $D_{\text{hop}} = D_0 q_{\text{off}}^N/(q_{\text{off}}+q_{\text{on}})^N$ with values above.
SARS CoV 2		
R	50 nm	typical virus size [51]
η	0.001Pa.s	typical physiological conditions [21]
a	$6-23$ nm	ligand protein characteristic size [52, 51]
k	$0.1-0.4$ N/m	typical spring constant from simulation results [53] and [54]
q_{on}	$770-1500$ s^{-1}	from $q_{\text{on}} \sim k_{\text{on}}\sigma/a\mathcal{N}_{\mathcal{A}}$ with $k_{\text{on}} = 0.7-1.4\times10^5$ M^{-1}s^{-1} [52, 55]
q_{off}	0.05 s$^{-1}-0.01$ s^{-1}	measured unbinding rate of individual ligand-receptor pairs [53, 52]
N	$1-2$	calculated from $N \simeq 2\pi Rh\sigma$ taking $h \simeq a/3$ the typical penetration length of the layers.
x	0.1-0.2	Bound fraction at equilibrium [52] in AFM experiments
σ	1000 μm^{-2}	density of spike proteins on the surface [51]
SARS CoV 1		
R	50 nm	typical virus size [51]
η	0.001Pa.s	typical physiological conditions [21]
a	$6-23$ nm	ligand protein characteristic size [52, 51]
k	0.6 N/m	typical spring constant from simulation results [53]
q_{on}	$1200-2500$ s^{-1}	from $q_{\text{on}} \sim k_{\text{on}}\sigma/a\mathcal{N}_{\mathcal{A}}$ with $k_{\text{on}} = 0.7-1.4\times10^5$ M^{-1}s^{-1} [52, 55] (similar to Sars CoV 2 [55])
q_{off}	0.6 s^{-1}	measured unbinding rate of individual ligand-receptor pairs [53]
N	$1-4$	calculated from $N \simeq 2\pi Rh\sigma$ taking $h \simeq a/3$ the typical penetration length of the layers.
x	0.1-0.2	Bound fraction at equilibrium is similar to Sars CoV 2 [52, 55]
σ	1600 μm^{-2}	density of spike proteins on the surface [51]

Table S7: Parameter values for viruses

4 Coarse-graining under different models and assumptions

4.1 Coarse-graining with particle inertia

While more details on inertial effects with multivalent receptor contacts will be written in a separate paper [56], here we briefly recapitulate some results of this work to support claims made in the main manuscript.

4.1.1 Equations set up with particle inertia

We consider now that the particle has inertia, described by a mass m. To simplify derivations we can neglect inertial effects from the legs, as in general the legs are much smaller than the particle itself, and hence have much lower mass. Alternatively, in Ref. [56] we will show that one can start with inertia on all components, and take the limit of small mass of the legs relative to particle mass on the final result, and obtain the same result as if the limits were inverted.

We thus write the unbound equations for a particle with a single leg as

$$\begin{cases} \frac{dl}{dt} &= -\frac{k}{\gamma}l + \sqrt{2\frac{k_BT}{\gamma}}\eta_l \\ \frac{dx}{dt} &= v \\ \frac{dv}{dt} &= \frac{1}{m}\left(-\Gamma v + \sqrt{2k_BT\Gamma}\eta_x\right) \end{cases} \tag{S4.1}$$

where m is the mass of the particle and v the velocity of the particle.

When the leg is bound to the surface, it is not necessary to project the dynamics. Writing Newton's second law on the system of the (particle+leg bound to surface) one finds the bound equations

$$\begin{cases} \frac{dl}{dt} &= v \\ \frac{dx}{dt} &= v \\ \frac{dv}{dt} &= \frac{1}{m}\Big[-\Gamma v + \sqrt{2k_BT\Gamma}\eta_x + \left(-\gamma v - kl + \sqrt{2k_BT\gamma}\eta_l\right) \Big] \end{cases}. \tag{S4.2}$$

4.1.2 Possible resolution with particle inertia following Ref. [57]

The generator for the system is

$$\mathcal{L} = \begin{pmatrix} -q_{\rm on} - \frac{k}{\gamma}l\partial_l + \frac{k_BT}{\gamma}\partial_{ll} + v\partial_x - \frac{\Gamma}{m}v\partial_v + \frac{k_BT\Gamma}{m^2}\partial_{vv} & +q_{\rm on} \\ +q_{\rm off} & -q_{\rm off} + v\partial_x + v\partial_l - \frac{k}{m}l\partial_v - \frac{\Gamma+\gamma}{m}v\partial_v + \frac{k_BT(\Gamma+\gamma)}{m^2}\partial_{vv} \end{pmatrix} \tag{S4.3}$$

with a natural stationary distribution (now including a Boltzmann factor corresponding to the kinetic energy of the particle)

$$\pi = \frac{1}{Z}\begin{pmatrix} q_{\rm off}/q_{\rm on} \\ 1 \end{pmatrix} e^{-kl^2/2k_BT} e^{-mv^2/2k_BT}. \tag{S4.4}$$

In addition to non-dimensionalizing space and time we need to non-dimensionalize the velocity. We then take (on top of usual non-dimensional quantities in the paper, reported here for completeness)

$$x \to L_x\tilde{x},\ l \to L\tilde{l},\ t \to \tau\tilde{t}, v \to \tilde{v}L_x/\tau = \tilde{v}\frac{L}{\epsilon}\frac{\epsilon^2 k}{\Gamma}. \tag{S4.5}$$

Mass also needs to be non-dimensionalized. Here we write, following Ref. [57], $m = \tilde{m}Lk\tau^2/L_x$. The dimensionless number $mL_x/(Lk\tau)1/\tau = \tau_v/\tau$ can be interpreted as the ratio of the correlation time of the velocity τ_v to the time scale of observation τ. We require $\tau/\tau_v = \frac{1}{\tilde{m}\epsilon}$ such that we may observe coarse grained

dynamics. Dropping the $\tilde{\cdot}$ notation we find the non-dimensional generator

$$\begin{aligned}\mathcal{L} = \frac{1}{\epsilon^2}\mathcal{L}_0 + \frac{1}{\epsilon}\mathcal{L}_1 + \mathcal{L}_2 =& \frac{1}{\epsilon^2}\begin{pmatrix} -q_{\text{on}} - \frac{\Gamma}{\gamma} l\partial_l + \frac{\Gamma}{\gamma}\partial_{ll} & +q_{\text{on}} \\ +q_{\text{off}} & -q_{\text{off}} \end{pmatrix} + \frac{1}{\epsilon}\begin{pmatrix} 0 & 0 \\ 0 & v\partial_l - \frac{1}{m} l\partial_v \end{pmatrix} \\ &+ \begin{pmatrix} v\partial_x - \frac{1}{m} v\partial_v + \frac{1}{m^2}\partial_{vv} & 0 \\ 0 & v\partial_x - \frac{\Gamma+\gamma}{\Gamma}\frac{1}{m} v\partial_v + \frac{\Gamma+\gamma}{\Gamma}\frac{1}{m^2}\partial_{vv} \end{pmatrix}\end{aligned} \tag{S4.6}$$

We can then set up a similar step by step search of a solution at multiple orders seeking a solution $f = f_0 + \epsilon f_1 + \epsilon f_2 + ...$

At lowest order solving $\mathcal{L}_0 f_0 = 0$ yields simply $f_0 = a(x,t)\begin{pmatrix} 1 \\ 1 \end{pmatrix}$ and the associated equilibrium distribution $\pi_0 = \frac{1}{Z'}\begin{pmatrix} q_{\text{off}}/q_{\text{on}} \\ 1 \end{pmatrix} e^{-l^2/2}$.

At the next order we need to solve $\mathcal{L}_0 f_1 = \frac{l}{m}\partial_v a \begin{pmatrix} 0 \\ 1 \end{pmatrix}$ that is easily shown to yield

$$f_1 = -\frac{1}{1 + \frac{(\gamma+\Gamma)q_{\text{off}}}{\gamma q_{\text{on}} + \Gamma}} \left(\frac{q_{\text{off}}}{q_{\text{on}} + \Gamma/\gamma}\right) \frac{l\partial_v a}{m}. \tag{S4.7}$$

To find a solution at the following order, we need to satisfy the Fredholm alternative $\langle \partial_t f_0 - \mathcal{L}_2 f_0 - \mathcal{L}_1 f_1, \pi_0 \rangle = 0$. Standard algebra yields an equation for the function $a(x,v,t)$ as (back in dimensional scales)

$$\partial_t a = v\partial_x a - \frac{\Gamma^m_{\text{eff}}}{m} v\partial_v a + \frac{k_B T \Gamma^m_{\text{eff}}}{m^2}\partial_{vv} a \tag{S4.8}$$

which corresponds to an inertial motion with friction

$$\boxed{\Gamma^m_{\text{eff}} = \frac{q_{\text{off}}}{q_{\text{on}} + q_{\text{off}}}\Gamma + \frac{q_{\text{on}}}{q_{\text{on}} + q_{\text{off}}}\left(\Gamma + \gamma + k\left(\frac{1}{q_{\text{off}}} + \frac{\gamma}{k}\frac{q_{\text{on}}}{q_{\text{off}}}\right)\right)} \tag{S4.9}$$

which writes with the notations of the main paper

$$\boxed{\Gamma^m_{\text{eff}} = p_0\Gamma_0 + p_1\Gamma_1} \tag{S4.10}$$

which is exactly Eq. (20) of the main paper.

As highlighted in the main paper, there is a notable difference between $\Gamma^m_{\text{eff}} = p_0\Gamma_0 + p_1\Gamma_1$, with inertia, and $\Gamma^{-1}_{\text{eff}} = p_0\Gamma_0^{-1} + p_1\Gamma_1^{-1}$ when inertia is neglected. In particular, the results are not equivalent when unbinding rates are slow such as $q_{\text{off}}\Gamma/k \ll 1$. We will reconcile these results in a separate paper [56].

4.2 Choice of time-scale hierarchy

4.2.1 Averaging with a different choice of scaling $\varepsilon = \gamma/\Gamma$

It is common to assume a different choice of scalings assuming fast unbound tether dynamics. This choice of assumptions can be formulated mathematically as $\gamma/\Gamma = \gamma_r\epsilon^2$, where γ_r is a non-dimensional number of order 1. This typically corresponds to short legs on a large particle, as γ and Γ are expected to scale with leg size and particle size via Stokes law. When doing such a reasoning, it is also common to lighten the assumption on scale separation for x and l and take $L = L_x$ [58]. We keep other non-dimensional scalings. For simplicity we will write $\varepsilon = \epsilon^2$ as no terms in ϵ appear now. We then obtain the non-dimensional

generator as an expansion $\mathcal{L} = \frac{1}{\varepsilon}\mathcal{L}_0 + \mathcal{L}_1 + \varepsilon\mathcal{L}_2 + \varepsilon^2\mathcal{L}_3 + ...$, with the first terms as

$$\mathcal{L} = \frac{1}{\varepsilon}\begin{pmatrix} -q_{\text{on}} - \frac{1}{\gamma_r}l\partial_l + \frac{1}{\gamma_r}\partial_{ll} & q_{\text{on}} \\ q_{\text{off}} & -q_{\text{off}} \end{pmatrix} + \begin{pmatrix} \partial_{xx} & 0 \\ 0 & l(\partial_x - \partial_l) + (\partial_x - \partial_l)^2 \end{pmatrix} + \varepsilon \begin{pmatrix} 0 & 0 \\ 0 & -\gamma_r l(\partial_x - \partial_l) - \gamma_r(\partial_x - \partial_l)^2 \end{pmatrix} + ... \tag{S4.11}$$

Notice above that the non-dimensionalization for the binding rates $q_{\text{on}}, q_{\text{off}}$ is such that it assumes binding and unbinding to be much faster than the long time dynamics searched for.

We look for a solution as $f = f_0 + \varepsilon f_1 + \varepsilon^2 f_2 + ...$ At first order we find easily $f_0 = a(x,t)\begin{pmatrix} 1 \\ 1 \end{pmatrix}$ associated with the equilibrium distribution $\pi_0 \propto \begin{pmatrix} q_{\text{off}}/q_{\text{on}} \\ 1 \end{pmatrix} e^{-l^2/2}$.

At the following order, to find a solution f_1, we require the Fredholm alternative, namely $\langle \partial_t f_0 - \mathcal{L}_1 f_0, \pi_0 \rangle = 0$, yielding

$$\partial_t a - \partial_{xx} a = 0. \tag{S4.12}$$

We can now solve for $\mathcal{L}_0 f_1 = -\mathcal{L}_1 f_0 + \partial_t f_0$ making use of this first order equation on a. The equation to be solved simplifies to $\mathcal{L}_0 f_1 = -\begin{pmatrix} 1 \\ 0 \end{pmatrix} l\partial_x a$. This gives

$$f_1 = \frac{l\partial_x a}{q_{\text{off}}}\begin{pmatrix} \gamma_r q_{\text{on}} \\ 1 + \gamma_r q_{\text{on}} \end{pmatrix}. \tag{S4.13}$$

To solve for f_2 we require the Fredholm alternative at the following order, namely $\langle \partial_t f_0 + \varepsilon\partial_t f_1 - \mathcal{L}_1 f_0 - \varepsilon\mathcal{L}_1 f_1 - \varepsilon\mathcal{L}_2 f_0, \pi_0 \rangle = 0$. We focus on specific terms

$$\langle \partial_t f_1, \pi_0 \rangle = 0, \tag{S4.14}$$

then

$$\langle -\mathcal{L}_1 f_1, \pi_0 \rangle = +\partial_{xx} a \frac{\gamma_r q_{\text{on}} + 1}{q_{\text{off}}}, \tag{S4.15}$$

and

$$\langle -\mathcal{L}_2 f_0, \pi_0 \rangle = +\gamma_r \partial_{xx} a \tag{S4.16}$$

such that summing up all contributions and reverting to original dimensions we obtain

$$\partial_t a = \frac{k_B T}{\Gamma_{\text{eff}}^{\gamma/\Gamma=\varepsilon}} \partial_{xx} a \tag{S4.17}$$

with

$$\boxed{\frac{1}{\Gamma_{\text{eff}}^{\gamma/\Gamma=\varepsilon}} = \left(\frac{q_{\text{off}}}{q_{\text{on}} + q_{\text{off}}}\right)\frac{1}{\Gamma} + \left(\frac{q_{\text{on}}}{q_{\text{on}} + q_{\text{off}}}\right)\frac{1}{\Gamma}\left(1 - \frac{\gamma}{\Gamma}\left[1 + \frac{k}{\gamma}\left(\frac{1}{q_{\text{off}}} + \frac{\gamma}{k}\frac{q_{\text{on}}}{q_{\text{off}}}\right)\right]\right)} \tag{S4.18}$$

with is exactly Eq. (21) of the main paper. We note that this is exactly the γ/Γ first order Taylor expansion of the equation obtained without assuming $\gamma/\Gamma \ll 1$, namely of Eq. (12) of the main paper.

4.2.2 Averaging with pre-averaging of tether dynamics (fast tether relaxation dynamics compared to all other dynamics)

Equation set up with pre-averaging and resolution A commonly used framework is to assume that unbound leg dynamics are so fast that essentially when a new bond is created, the leg length may be sampled from its (bare) equilibrium distribution. This may be formally obtained using homogenization as well by

assuming unbound relaxation is very fast compared to binding dynamics, $\gamma/k \ll 1/q_{\rm on/off}$, though we do not report the details here. It is a commonly used framework [58, 59].

The unbound state is described by the variables (x,t) while the bound state is described with (x,l,t). We write the equations for the probability distributions in each state

$$\partial_t p_u = -p_u \int e^{-kl^2/2k_BT} q_{\rm on} dl + \int q_{\rm off} p_b(x,l,t) dl + \frac{k_BT}{\Gamma}\partial_{xx} p_u \tag{S4.19}$$

$$\partial_t p_b = +p_u e^{-kl^2/2k_BT} q_{\rm on} + q_{\rm off} p_b(x,l,t) + \frac{k_BT}{\Gamma+\gamma}\partial_{xx} p_b + (...) \tag{S4.20}$$

where the (...) denote the rest of the bound projected dynamics and Z is some normalization constant that does not depend on l. Notice that here we kept the $\Gamma+\gamma$ in the bound state to highlight that such a term would have to be kept in the case of a great number of springs N, as this would become $\Gamma + N\gamma$ and would therefore have to remain. The equilibrium distribution associated with these dynamics is simply $\pi = \frac{1}{Z}\begin{pmatrix} \frac{q_{\rm off}}{q_{\rm on}} \\ e^{-\beta k l^2} \end{pmatrix}$ and satisfies detailed balance:

$$\pi_u \times q_{\rm on} e^{-\beta k l^2/2} = \frac{1}{Z}\frac{q_{\rm off}}{q_{\rm on}} \times q_{\rm on} e^{-\beta k l^2/2} = \frac{e^{-\beta k l^2/2}}{Z} \times q_{\rm off} = \pi_b \times q_{\rm off}. \tag{S4.21}$$

With this approach (compared to the main paper derivation), the only part of the generator that changes is the lowest order term $\mathcal{L}_0$. In particular one should determine the non-dimensionalization. Importantly here one should notice that $q_{\rm on}$ and $q_{\rm off}$ do not have the same units. The ratio $q_{\rm off}/q_{\rm on} = O(L)$ has units of a lengthscale. We can therefore keep the usual non-dimensionalization for $q_{\rm off}\frac{\Gamma}{k\epsilon^2} = \frac{\tilde{q_{\rm off}}}{\epsilon^2}$ but not for the binding rate, which we take as $q_{\rm on}\frac{\Gamma}{kL\epsilon^2} = \frac{\tilde{q_{\rm on}}}{\epsilon^2}$. We find (dropping the $\tilde{\cdot}$)

$$\mathcal{L}_0 = \begin{pmatrix} -\int q_{\rm on} e^{-l^2/2} dl & +\int q_{\rm on} e^{-l^2/2} dl \\ +q_{\rm off} & -q_{\rm off} - l\partial_l + \partial_{ll}. \end{pmatrix} \tag{S4.22}$$

Resolution for f_0 does not change and we get $f_0 = a(x,t)\begin{pmatrix}1\\1\end{pmatrix}$, with associated equilibrium distribution $\pi_0 = \pi$.

At the next order we get the solution $f_1 = l\partial_x a \frac{1}{1+q_{\rm off}}\begin{pmatrix}0\\1\end{pmatrix}$.

Finally at second order we require the Fredholm alternative $\langle \partial_t f_0 - \mathcal{L}_2 f_0 - \mathcal{L}_1 f_1, \pi_0 \rangle = 0$ yielding

$$\partial_t a = \frac{k_BT}{\Gamma_{\rm eff}^{\rm k/\gamma \gg q}} \partial_{xx} a \tag{S4.23}$$

with

$$\boxed{\frac{1}{\Gamma_{\rm eff}^{\rm k/\gamma \gg q}} = \left(\frac{q_{\rm off}}{q_{\rm on}+q_{\rm off}}\right)\frac{1}{\Gamma} + \left(\frac{q_{\rm on}}{q_{\rm on}+q_{\rm off}}\right)\frac{1}{\Gamma+\gamma+\frac{k}{q_{\rm off}}}.} \tag{S4.24}$$

This is nearly exactly the result obtained without pre-averaging but for the $k\tau_{\rm u}^{\rm relax} = k\left(\frac{\gamma}{k}\frac{q_{\rm on}}{q_{\rm off}}\right)$ contribution corresponding to the time the tether is allowed to relax between 2 binding periods. It is exactly the result reported in Eq. (22) of the main manuscript.

Relation to Ref. [11] In this paragraph we relate our results to the results obtained in Ref. [11]. Eq. (2.48) of Ref. [11] finds an effective long time diffusion, starting from similar equations as Eq. (S4.20),

$$D_{\rm eff}^{\text{Ref. [11]}} = D_0\left(1 + \varepsilon\frac{\nu-2}{\beta_0(1+\beta_0)\lambda}\right) \tag{S4.25}$$

where we will give the meaning of the new notations (ν, ε, β_0, λ) by expressing them with respect to our notations. Here, $\nu = k/k_{\text{tether}} = 1$ in our case because there is no change in recall spring force between the bound (k_{tether}) and unbound states (k). We also have $\beta_0 = \frac{q_{\text{off}}}{q_{\text{on}}}$, here $\varepsilon = \frac{D_0}{q_{\text{on}} L^2}$ and $\lambda = k_B T/kL^2$ such that the effective diffusion writes with our notations

$$D_{\text{eff}}^{\text{Ref. [11]}} = D_0 \left(1 - \frac{k/q_{\text{off}}}{\Gamma} \frac{q_{\text{on}}}{q_{\text{on}} + q_{\text{off}}}\right). \tag{S4.26}$$

Compared to the previous derivation, this result corresponds to an effective friction with pre-averaging of tether dynamics (which is indeed what is done in Ref. [11]) *and* scales with k/q_{off} similarly as the derivation assuming $\gamma/\Gamma = \varepsilon$. In Ref. [11], as the dynamics are already pre-averaged, they are expressed at 0^{th} order in γ/Γ. Therefore the key common point of these derivations (Ref. [11] and Sec. 2.2 here) is to assume similar spatial scales, namely $L_x = L$. This highlights that the assumption $L/L_x = \epsilon$ allows one to "safely" average dynamics without specific assumptions on other physical parameters.

Relation to N legs facing a uniformly sticky membrane In Fig. S6 we show that the pre-averaged result corresponds to the predictions for N legs facing a uniformly sticky surface when the average number of bonds

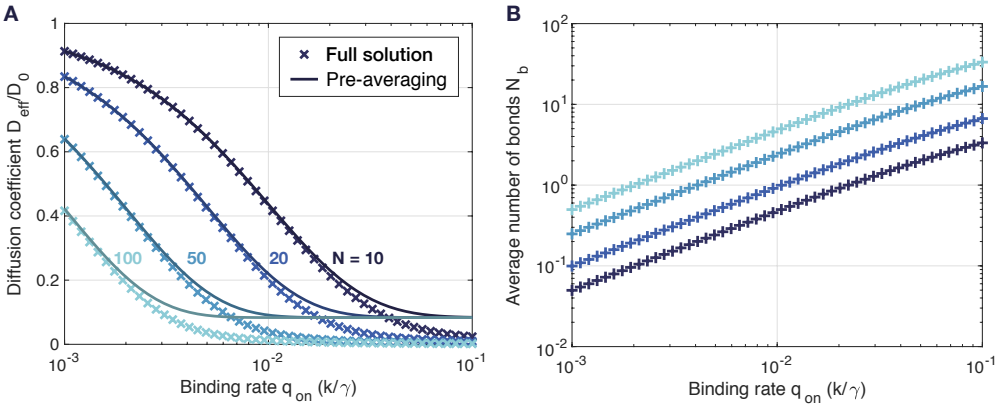

Figure S6: Pre-averaged results correspond to N legs facing a uniformly sticky surface when the average number of bonds legs $N_b \lesssim 1$. (A) D_{eff} as calculated with a numerical resolution of Eq. (15) of the main paper ("Full solution") or with the pre-averaged result of Eq. (22) of the main paper ("Pre-averaging") with respect to the binding rate q_{on}. Other parameters are $\frac{\gamma}{\Gamma} = 1$ and $\frac{q_{\text{off}}\Gamma}{k} = 0.1$; (B) Corresponding average number of bonds N_b.

4.2.3 Averaging with fast binding dynamics compared to relaxation dynamics

To understand how fast binding dynamics affect this system, we use the same non-dimensionalization as in the main text but for $L = L_x$ (thereby allowing relaxation dynamics to be of similar order as the long time mobility of the particle). We obtain the non-dimensional generator

$$\mathcal{L} = \frac{1}{\epsilon^2}\begin{pmatrix} -q_{\text{on}} & q_{\text{on}} \\ q_{\text{off}} & -q_{\text{off}} \end{pmatrix} + \begin{pmatrix} \frac{\Gamma}{\gamma}\left(-l\partial_l + \partial_{ll}\right) + \partial_{xx} & 0 \\ 0 & \frac{\Gamma}{\Gamma+\gamma}\left(l(\partial_x - \partial_l) + (\partial_x - \partial_l)^2\right) \end{pmatrix} = \frac{1}{\varepsilon}\mathcal{L}_0 + \mathcal{L}_1 \tag{S4.27}$$

where we used $\varepsilon = \epsilon^2$.

We then seek a solution as an expansion $f = f_0 + \varepsilon f_1 + \varepsilon^2 f_2 + ...$ At lowest order we need to solve

$$\begin{pmatrix} -q_{\text{on}} & q_{\text{on}} \\ q_{\text{off}} & -q_{\text{off}} \end{pmatrix} f_0 = 0 \tag{S4.28}$$

which simply yields $f_0 = a(x,l,t)\begin{pmatrix}1\\1\end{pmatrix}$ and the associated equilibrium distribution $\pi_0 = \begin{pmatrix}\frac{q_{\rm off}}{q_{\rm on}}\\1\end{pmatrix}$. Notice how here the equilibrium distribution at lowest order does not correspond to the full equilibrium distribution $\pi_0 \neq \pi$. At the following order to find a solution to the problem we require the Fredholm alternative $\langle \partial_t f_0 - \mathcal{L}_1 f_0, \pi_0\rangle = 0$, which gives the equation

$$\begin{aligned}\partial_t a =& p_0 \frac{\Gamma}{\gamma}\left(-l\partial_l + \partial_{ll}\right) + p_0 \partial_{xx} \\ &+ p_1 \frac{\Gamma}{\Gamma+\gamma}\left(l(\partial_x - \partial_l) + (\partial_x - \partial_l)^2\right)\end{aligned} \tag{S4.29}$$

where $p_0 = \frac{q_{\rm off}}{q_{\rm off}+q_{\rm on}} = 1 - p_1$ is the probability to be unbound and p_1 to be bound. This new effective equation can now be explored by means of time and length scale separation by setting a new small scale parameter $\epsilon_2 = \frac{L}{L_x}$. This small scale operator allows us to write

$$\partial_t a = \frac{1}{\epsilon_2^2}\mathcal{L}_{0,2} + \frac{1}{\epsilon_2}\mathcal{L}_{1,2} + \mathcal{L}_{2,2} \tag{S4.30}$$

where $\mathcal{L}_{0,2} = \left(p_0 \frac{\Gamma}{\gamma} + p_1 \frac{\Gamma}{\Gamma+\gamma}\right)\left(-l\partial_l + \partial_{ll}\right)$, $\mathcal{L}_{1,2} = p_1 \frac{\Gamma}{\Gamma+\gamma}\left(l\partial_x - 2\partial_{xl}\right)$ and $\mathcal{L}_{2,2} = \left(p_0 + p_1 \frac{\Gamma}{\Gamma+\gamma}\right)\partial_{xx}$. We seek a solution $a = a_0 + \epsilon_2 a_1 + \epsilon_2^2 a_2 + ...$

At lowest order we need to solve $\mathcal{L}_{0,2} a_0 = 0$ which implies $a_0 = a_0(x,t)$ making use of vanishing flux boundary conditions at infinity. The associated equilibrium distribution is now $\pi_{0,2} = e^{-l^2/2}/Z$.

At the next order we need to solve $\mathcal{L}_{0,2} a_1 = -\mathcal{L}_{1,2} f_0 = -p_1 \frac{\Gamma}{\Gamma+\gamma} l\partial_x a$ such that $a_1 = -\frac{p_1 \frac{\Gamma}{\Gamma+\gamma}}{p_0 \frac{\Gamma}{\gamma} + p_1 \frac{\Gamma}{\Gamma+\gamma}} l\partial_x a = -\frac{l\partial_x a}{1 + \frac{p_0}{p_1}\frac{\gamma}{\Gamma+\gamma}}$. At the following order, to find a solution we require the Fredholm alternative, namely $\langle \partial_t a_0 - \mathcal{L}_{2,2} a_0 - \mathcal{L}_{1,2} a_1, \pi_{0,2}\rangle = 0$. After some standard algebra one finds

$$\partial_t a_0 = \frac{1}{\Gamma^{q\,\rm fast}} \partial_{xx} a \tag{S4.31}$$

where

$$\frac{1}{\Gamma^{q\,\rm fast}} = \frac{p_0}{\Gamma} + \frac{p_1}{\Gamma + \gamma/p_0} \tag{S4.32}$$

which, reverting to dimensional scales, is exactly Eq. (23) of the main paper.

4.3 Arm and/or legs

4.3.1 Arm or leg

In this part we show precisely how having an arm (spring always attached to the surface) or a leg (spring always attached to the particle) affects the dynamics. There are several ways one can consider to obtain the dynamics of the leg or the arm (referred to henceforth as spring). Either assume (1) that the center of mass of the spring is attached to the particle (or the surface), (2) either that the center of mass is located at the free end of the spring (when it is attached to the particle or the surface). Both assumptions do not yield exactly the same dynamics but the differences in the long time effective dynamics are minor.

(1) Arm or leg (spring) attached by their center of mass Consider in general a free spring, where motion is confined to a line but none of the spring ends are attached. The length of the spring l (more accurately here l represents the length imbalance compared to the rest length of the spring $l - l_0$ but we take $l_0 = 0$ for simplicity) obeys the overdamped Langevin equation

$$\frac{dl}{dt} = -\frac{kl}{\gamma} + \sqrt{\frac{2k_B T}{\gamma}}\eta_l. \tag{S4.33}$$

The center of mass c of the spring similarly obeys an overdamped Langevin equation, with diffusion only

$$\frac{dc}{dt} = \sqrt{\frac{2k_BT}{\gamma}}\eta_c \tag{S4.34}$$

and we considered that the diffusion coefficient of the center of mass is similar to that of the spring length. For simplicity we consider here that the center of mass of the spring is located at one of its ends, namely the end that will be permanently attached to a surface in this paragraph.

In addition the particle also diffuses as

$$\frac{dx}{dt} = \sqrt{\frac{2k_BT}{\Gamma}}\eta_x. \tag{S4.35}$$

Arm configuration. If we consider the arm configuration, then the center of mass c is attached to the surface and satisfies the constraint $q(x, l, c) = c - x_{\text{surface}} = 0$. The projected dynamics in that case are trivial and sum up to the ones detailed in the main text and recalled here for consistency:

$$\begin{cases} \frac{dx}{dt} = \sqrt{\frac{2k_BT}{\Gamma}}\eta_x, \\ \frac{dl}{dt} = -\frac{kl}{\gamma} + \sqrt{\frac{2k_BT}{\gamma}}\eta_l, \\ \frac{dc}{dt} = 0. \end{cases} \tag{S4.36}$$

Leg configuration. If we consider the leg configuration, then the center of mass c is attached to the particle and satisfies the constraint $q(x, l, c) = x - c = 0$. This constraint is similar to the one for the bound spring for which the projection formalism is described in Appendix A of the main text. The projected dynamics are therefore

$$\begin{cases} \frac{dx}{dt} = \sqrt{\frac{2k_BT}{\Gamma+\gamma}}\eta_x, \\ \frac{dl}{dt} = -\frac{kl}{\gamma} + \sqrt{\frac{2k_BT}{\gamma}}\eta_l, \\ \frac{dc}{dt} = \frac{dx}{dt}. \end{cases} \tag{S4.37}$$

These dynamics are exactly equivalent to the arm configuration but for the change $\Gamma \to \Gamma + \gamma$, and therefore yield the same resulting effective long time dynamics with a similar change $\Gamma \to \Gamma + \gamma$. One can thus simply consider that Γ is indeed the friction coefficient of the unbound particle, which potentially includes corrections to friction due to legs being attached to the surface.

(2) Arm or leg (spring) with center of mass at the free end We now consider the situation where the center of mass of the spring is located at its free end, and the other end is attached to the particle or the surface.

Leg configuration. Consider in general a spring, attached to one end to the particle (in x) and to the other end to the spring's mass (in $x + l$). Newton's second law on each mass, and taking loosely overdamped dynamics with masses going to 0, yields the system of equations

$$\begin{cases} 0 &= -\Gamma\frac{dx}{dt} + kl + \sqrt{2k_BT\Gamma}\eta_x, \\ 0 &= -\gamma\frac{d(x+l)}{dt} - kl + \sqrt{2k_BT\gamma}\eta_l. \end{cases} \tag{S4.38}$$

The system simplifies for each variable into

$$\begin{cases} \frac{dx}{dt} = +\frac{kl}{\Gamma} + \sqrt{\frac{2k_BT}{\Gamma}}\eta_x, \\ \frac{dl}{dt} = -kl\left(\frac{1}{\Gamma} + \frac{1}{\gamma}\right) - \sqrt{\frac{2k_BT}{\Gamma}}\eta_x + \sqrt{\frac{2k_BT}{\gamma}}\eta_l. \end{cases} \tag{S4.39}$$

This system corresponds to a friction matrix and force field

$$\tilde{\Gamma}^{-1} = \begin{pmatrix} \frac{1}{\Gamma} & -\frac{1}{\Gamma} \\ -\frac{1}{\Gamma} & \frac{1}{\gamma} + \frac{1}{\Gamma} \end{pmatrix} \text{ and } \nabla\mathcal{U} = \begin{pmatrix} 0 \\ kl \end{pmatrix}. \tag{S4.40}$$

When the spring (here the leg) becomes temporarily bound to the surface, the bound equations then simply read (provided appropriate projection, following Appendix A, is made)

$$\begin{cases} \frac{dx}{dt} = +\frac{kl}{\Gamma} + \sqrt{\frac{2k_BT}{\Gamma}}\eta_x, \\ \frac{dl}{dt} = -\frac{dx}{dt} = -\frac{kl}{\Gamma} - \sqrt{\frac{2k_BT}{\Gamma}}\eta_x. \end{cases} \tag{S4.41}$$

In non-dimensional scales, the hierarchy of generators now reads

$$\mathcal{L}_0 = \begin{pmatrix} -q_{\text{on}} + \frac{\Gamma+\gamma}{\Gamma}\left(-l\partial_l + \partial_{ll}\right) & q_{\text{on}} \\ q_{\text{off}} & q_{\text{off}} + \left(-l\partial_l + \partial_{ll}\right) \end{pmatrix}, \tag{S4.42}$$

$$\mathcal{L}_1 = \begin{pmatrix} (l\partial_x - 2\partial_{lx}) & 0 \\ 0 & (l\partial_x - 2\partial_{lx}) \end{pmatrix}, \text{ and } \mathcal{L}_2 = \begin{pmatrix} \partial_{xx} & 0 \\ 0 & \partial_{xx} \end{pmatrix}. \tag{S4.43}$$

Using a coarse-graining method as usual, we obtain simply the usual harmonic sum $\Gamma_{\text{eff}}^{-1} = p_0\Gamma_0^{-1} + p_1\Gamma_1^{-1}$ where the friction coefficients write

$$\begin{cases} \Gamma_0 = & \Gamma + \gamma + k\left(\frac{\gamma}{k}\frac{q_{\text{on}}}{q_{\text{off}}+k/\Gamma}\right) \\ \Gamma_1 = & \Gamma + \gamma + k\left(\frac{1}{q_{\text{off}}} + \frac{\gamma}{k}\frac{q_{\text{on}}+k/\Gamma}{q_{\text{off}}}\right) \text{ (model (2)).} \end{cases} \tag{S4.44}$$

Compared to the coefficients obtained if the spring is attached to the particle by its center of mass (model (1)), namely

$$\begin{cases} \Gamma_0 = & \Gamma + \gamma \\ \Gamma_1 = & \Gamma + \gamma + k\left(\frac{1}{q_{\text{off}}} + \frac{\gamma}{k}\frac{q_{\text{on}}+q_{\text{off}}}{q_{\text{off}}}\right), \text{ (model (1)),} \end{cases} \tag{S4.45}$$

the results are quite similar independent of the attaching model. Qualitatively, in the non-center of mass case (model (2)), we obtain additional feedback friction terms due to the spring, as $k\tau_{\text{eff}}$ where τ_{eff} is a typical time over which the spring relaxes, scaling naturally as γ/k multiplied by a ratio of characteristic times $\frac{\tau_{\cdots}}{\tau_{\cdots}}$. This ratio corresponds to the fact that the spring may only relax in the other state, and hence different ratios appear according to the different modeling options and bound states. Be that as it may, such contributions are generally minor. In fact, one can verify (not shown here) that the numerical values of $\Gamma_{\text{eff}}/\Gamma$ according to model (1) or (2) show very little difference over full $\mathbb{R}^3$ space described by the parameters.

We now explore potential differences when the number of legs is increased. For 2 legs, the dynamics in the unbound state are

$$\begin{cases} \frac{dx}{dt} = +\frac{k(l_1+l_2)}{\Gamma} + \sqrt{\frac{2k_BT}{\Gamma}}\eta_x, \\ \frac{dl_1}{dt} = -\frac{dx}{dt} - \frac{kl_1}{\gamma} + \sqrt{\frac{2k_BT}{\gamma}}\eta_1 \\ \frac{dl_2}{dt} = -\frac{dx}{dt} - \frac{kl_2}{\gamma} + \sqrt{\frac{2k_BT}{\gamma}}\eta_2 \end{cases} \tag{S4.46}$$

and when leg 1 is bound to the surface simply

$$\begin{cases} \frac{dx}{dt} = -\frac{dl_1}{dt} = +\frac{k(l_1+l_2)}{\Gamma} + \sqrt{\frac{2k_BT}{\Gamma}}\eta_x, \\ \frac{dl_2}{dt} = -\frac{dx}{dt} - \frac{kl_2}{\gamma} + \sqrt{\frac{2k_BT}{\gamma}}\eta_2 \end{cases} \tag{S4.47}$$

and when both legs are bound

$$\left\{ \frac{dx}{dt} = -\frac{dl_1}{dt} = -\frac{dl_2}{dt} = +\frac{k(l_1+l_2)}{\Gamma} + \sqrt{\frac{2k_BT}{\Gamma}}\eta_x. \right. \tag{S4.48}$$

Dynamics are then easily extended to N legs using the free spring end model applied to each leg. Coarse-graining and asymptotics (around the average number of bonds) then easily lead to

$$\Gamma_{\text{eff}} \simeq \Gamma_{N_b} = \Gamma + N\gamma + N_b\left[\gamma + k\left(\frac{1}{q_{\text{off}}} + \frac{\gamma}{k}\frac{q_{\text{on}}}{q_{\text{off}}}\right)\right] \text{ (model (2)).} \tag{S4.49}$$

Eq. (S4.49) is exactly the result obtained by attaching legs by their center of mass (model (1)), provided the suitable change $\Gamma \to \Gamma + N\gamma$ is done for N legs. There is thus no difference between the different models in the leg configuration when a large number of legs are involved.

Arm configuration. The arm configuration with mass at the free end (model (2)) is trivially equivalent to that attached by the center of mass as

$$\begin{cases} \frac{dx}{dt} = \sqrt{\frac{2k_BT}{\Gamma}}\eta_x, \\ \frac{dl}{dt} = -\frac{kl}{\gamma} + \sqrt{\frac{2k_BT}{\gamma}}\eta_l. \end{cases} \tag{S4.50}$$

There is thus no difference between the different models in the arm configuration.

4.3.2 Arm and leg

Equations set up We consider random attachement and detachement of two springs to one another, in the leg and arm geometry – see Fig. S7-A.

When the springs are unbound the dynamic equations are

$$\begin{cases} \frac{dl_1}{dt} &= -\frac{k}{\gamma}l_1 + \sqrt{\frac{2k_BT}{\gamma}}\eta_1(t) \\ \frac{dl_2}{dt} &= -\frac{k}{\gamma}l_2 + \sqrt{\frac{2k_BT}{\gamma}}\eta_2(t) \\ \frac{dx}{dt} &= \sqrt{\frac{2k_BT}{\Gamma}}\eta_x(t) \end{cases} \tag{S4.51}$$

where l_1 is the length of the top spring, l_2 the length of the bottom spring, and for simplicity here we took $l_0 = 0$.

In the bound state we need to project the dynamics. When the springs bind, we consider that a rigid bond is formed between the springs' sticky ends that keeps the distance constant – see Fig. S7. The dynamic constraint is then

$$q(x, l_1, l_2) = x + l_1 - l_2 + l_{\text{bond}} = 0 \tag{S4.52}$$

where l_{bond} is the length of the bond and remains constant until the springs detach and reattach to form another bond length. If we imagine that the bottom spring is part of a periodic array of springs, such that at any time, only one bottom spring is accessible to the top spring, l_{bond} is typically of order L – see Fig. S7 – and thus a reasonable physical assumption.

The constraint matrix is then $C = (1, 1, -1)$ and the projection matrix

$$P = 1 - \frac{1}{3}\begin{pmatrix} 1 & 1 & -1 \\ 1 & 1 & -1 \\ -1 & -1 & 1 \end{pmatrix} = \frac{1}{3}\begin{pmatrix} 2 & -1 & 1 \\ -1 & 2 & 1 \\ 1 & 1 & 2 \end{pmatrix} \tag{S4.53}$$

such that the Moore-Penrose pseudo inverse of the projected friction is

$$\Gamma_P^\dagger = \frac{1}{\gamma + 2\Gamma}\begin{pmatrix} 2 & -1 & 1 \\ -1 & \frac{\gamma+\Gamma}{\gamma} & \frac{\Gamma}{\gamma} \\ 1 & \frac{\Gamma}{\gamma} & \frac{\gamma+\Gamma}{\gamma} \end{pmatrix} \tag{S4.54}$$

with a square root

$$\sigma_P = \frac{1}{\gamma + 2\Gamma}\begin{pmatrix} 2\sqrt{\Gamma} & \sqrt{\gamma} & -\sqrt{\gamma} \\ \sqrt{\Gamma} & \sqrt{\gamma}/2 + \frac{\gamma+2\Gamma}{\sqrt{4\gamma}} & -\sqrt{\gamma}/2 + \frac{\gamma+2\Gamma}{\sqrt{4\gamma}} \\ -\sqrt{\Gamma} & -\sqrt{\gamma}/2 + \frac{\gamma+2\Gamma}{\sqrt{4\gamma}} & \sqrt{\gamma}/2 + \frac{\gamma+2\Gamma}{\sqrt{4\gamma}} \end{pmatrix}. \tag{S4.55}$$

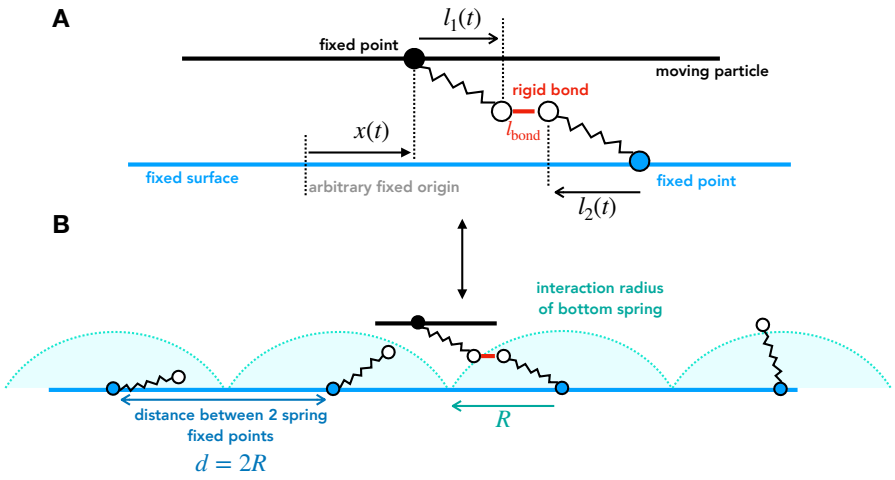

Figure S7: Geometry of binding with a particle having an arm and a leg. (A) The spring attached to the moving particle may bind to the bottom spring by forming a rigid bond that "fills in the distance" between the separated springs. Such a model is equivalent to (B) where the bond is formed with the "closest" available bond. Here if springs on the surface are evenly spaced with a typical spacing $d = 2R$ we consider that the top spring's sticky end binds to a surface spring whose fixed point is closest, and always closer than R. Switching events between one spring and then another are long if the distance between two surface springs is large and are ignored. The equivalence between A and B could be shown more systematically, but is beyond the scope of this manuscript.

The dynamics in the bound state are therefore

$$\begin{cases} \frac{dx}{dt} &= -\frac{k}{2\Gamma+\gamma}(l_1-l_2) + \sqrt{\frac{8k_BT\Gamma}{(2\Gamma+\gamma)^2}}\eta_x + \sqrt{\frac{2k_BT\gamma}{(2\Gamma+\gamma)^2}}(\eta_1-\eta_2) \\ \frac{dl_1}{dt} &= \frac{1}{2}\frac{dx}{dt} - \frac{k}{2\gamma}(l_1+l_2) + \sqrt{\frac{2k_BT}{4\gamma}}(\eta_1+\eta_2) \\ \frac{dl_2}{dt} &= -\frac{1}{2}\frac{dx}{dt} - \frac{k}{2\gamma}(l_1+l_2) + \sqrt{\frac{2k_BT}{4\gamma}}(\eta_1+\eta_2) \end{cases} \tag{S4.56}$$

Generator The generator is then

$$\begin{aligned} \mathcal{L} = &\begin{pmatrix} -q_{\text{on}} & q_{\text{on}} \\ q_{\text{off}} & -q_{\text{off}} \end{pmatrix} + \begin{pmatrix} -\frac{k}{\gamma}l_1\partial_{l_1} + \frac{k_BT}{\gamma}\partial_{l_1l_1} - \frac{k}{\gamma}l_2\partial_{l_2} + \frac{k_BT}{\gamma}\partial_{l_2l_2} + \frac{k_BT}{\Gamma}\partial_{xx} & 0 \\ 0 & 0 \end{pmatrix} \\ &+ \begin{pmatrix} 0 & 0 \\ 0 & -\frac{k}{2\Gamma+\gamma}(l_1-l_2)(\partial_x - \frac{1}{2}\partial_{l_2} + \frac{1}{2}\partial_{l_1}) - \frac{k}{2\gamma}(l_1+l_2)(\partial_{l_2}+\partial_{l_1}) \end{pmatrix} \\ &+ \begin{pmatrix} 0 & 0 \\ 0 & +\frac{2k_BT}{2\Gamma+\gamma}(\partial_x - \frac{1}{2}\partial_{l_2} + \frac{1}{2}\partial_{l_1})^2 + \frac{k_BT}{2\gamma}(\partial_{l_2}+\partial_{l_1})^2 \end{pmatrix} \end{aligned} \tag{S4.57}$$

With this generator one can check that $\mathcal{L}^\star\pi = 0$ with the natural equilibrium distribution

$$\pi = \frac{1}{Z}\begin{pmatrix} q_{\text{off}}/q_{\text{on}} \\ 1 \end{pmatrix} e^{-kl_1^2/2k_BT} e^{-kl_2^2/2k_BT} \tag{S4.58}$$

where Z is a normalization constant.

Homogenization Taking the usual scalings we get the following non-dimensional, expanded generator

$$\begin{aligned}\mathcal{L} =&\frac{1}{\epsilon^2}\Bigg[\begin{pmatrix}-q_{\text{on}} & q_{\text{on}}\\ q_{\text{off}} & -q_{\text{off}}\end{pmatrix}+\frac{\Gamma}{\gamma}\begin{pmatrix}-l_1\partial_{l_1}+\partial_{l_1l_1}-l_2\partial_{l_2}+\partial_{l_2l_2} & 0\\ 0 & 0\end{pmatrix}\\ &+\begin{pmatrix}0 & 0\\ 0 & -\frac{\Gamma}{2(2\Gamma+\gamma)}(l_1-l_2)(\partial_{l_1}-\partial_{l_2})-\frac{\Gamma}{2\gamma}(l_1+l_2)(\partial_{l_2}+\partial_{l_1})+\frac{\Gamma}{2(2\Gamma+\gamma)}(\partial_{l_2}-\partial_{l_1})^2+\frac{\Gamma}{2\gamma}(\partial_{l_2}+\partial_{l_1})^2\end{pmatrix}\Bigg]\\ &+\frac{1}{\epsilon}\begin{pmatrix}0 & 0\\ 0 & -\frac{\Gamma}{2\Gamma+\gamma}(l_1-l_2)\partial_x+\partial_x(\partial_{l_1}-\partial_{l_2})\frac{2\Gamma}{\gamma+2\Gamma}\end{pmatrix}\\ &+1\begin{pmatrix}\partial_{xx} & 0\\ 0 & \frac{2\Gamma}{\gamma+2\Gamma}\partial_{xx}\end{pmatrix}=\frac{1}{\epsilon^2}\mathcal{L}_0+\frac{1}{\epsilon}\mathcal{L}_1+\mathcal{L}_2\end{aligned} \tag{S4.59}$$

We now seek an expanded solution f of $\partial_t f=\mathcal{L}f$ as $f=f_0+\epsilon f_1+\epsilon^2 f_2+...$

At lowest order, $\mathcal{L}_0 f_0=0$ gives $f_0=a(x,t)\begin{pmatrix}1\\1\end{pmatrix}$, and the associated equilibrium distribution $\pi_0=\pi$. At first order we need to solve

$$\mathcal{L}_0 f_1=-\mathcal{L}_1 f_0=+\begin{pmatrix}0\\1\end{pmatrix}\frac{\Gamma}{\gamma+2\Gamma}(l_1-l_2)\partial_x a \tag{S4.60}$$

which has a unique solution

$$f_1=-\begin{pmatrix}\frac{\gamma q_{\text{on}}}{\Gamma+\gamma q_{\text{on}}}\\1\end{pmatrix}\frac{(l_1-l_2)\partial_x a}{1+\frac{\Gamma q_{\text{off}}}{\Gamma+\gamma q_{\text{on}}}\frac{\gamma+2\Gamma}{\Gamma}}. \tag{S4.61}$$

At 2nd order we need to satisfy the Fredholm alternative $\langle\partial_t f_0-\mathcal{L}_2 f_0-\mathcal{L}_1 f_1,\pi_0\rangle=0$. We split up the terms to highlight calculation steps (discarding Z terms to simplify notations, as they would cancel out eventually)

$$\begin{aligned}\langle\mathcal{L}_1 f_1,\pi_0\rangle=&-\langle\left(-(l_1-l_2)^2\frac{\Gamma}{\gamma+2\Gamma}+2\frac{2\Gamma}{\gamma+2\Gamma}\right)e^{-l_1^2/2}e^{-l_2^2/2}\rangle\frac{\partial_{xx}a}{1+\frac{\Gamma q_{\text{off}}}{\Gamma+\gamma q_{\text{on}}}\frac{\gamma+2\Gamma}{\Gamma}}\\ =&-\left(-2\frac{\Gamma}{\gamma+2\Gamma}+2\frac{2\Gamma}{\gamma+2\Gamma}\right)\frac{\partial_{xx}a}{1+\frac{\Gamma q_{\text{off}}}{\Gamma+\gamma q_{\text{on}}}\frac{\gamma+2\Gamma}{\Gamma}}\\ =&-\frac{2\Gamma}{\gamma+2\Gamma}\frac{\partial_{xx}a}{1+\frac{\Gamma q_{\text{off}}}{\Gamma+\gamma q_{\text{on}}}\frac{\gamma+2\Gamma}{\Gamma}}\end{aligned} \tag{S4.62}$$

and

$$\langle\mathcal{L}_2 f_0,\pi_0\rangle=\left(\frac{q_{\text{off}}}{q_{\text{on}}}+\frac{2\Gamma}{\gamma+2\Gamma}\right)\partial_{xx}a. \tag{S4.63}$$

Gathering terms as $\langle\partial_t f_0,\pi_0\rangle=\langle\mathcal{L}_2 f_0,\pi\rangle+\langle\mathcal{L}_1 f_1,\pi_0\rangle$ we get

$$\left(1+\frac{q_{\text{off}}}{q_{\text{on}}}\right)\partial_t a=\left(\frac{q_{\text{off}}}{q_{\text{on}}}+\frac{2\Gamma}{\gamma+2\Gamma}\frac{\frac{\Gamma q_{\text{off}}}{\Gamma+\gamma q_{\text{on}}}\frac{\gamma+2\Gamma}{\Gamma}}{1+\frac{\Gamma q_{\text{off}}}{\Gamma+\gamma q_{\text{on}}}\frac{\gamma+2\Gamma}{\Gamma}}\right)\partial_{xx}a. \tag{S4.64}$$

Now shifting back to dimensional scales and reorganizing terms slightly we obtain

$$\partial_t a=\left(\frac{q_{\text{off}}}{q_{\text{on}}+q_{\text{off}}}\frac{k_BT}{\Gamma}+\frac{q_{\text{on}}}{q_{\text{on}}+q_{\text{off}}}\frac{k_BT}{\Gamma+\frac{1}{2}\left(\frac{k}{q_{\text{off}}}+\frac{q_{\text{on}}}{q_{\text{off}}}\gamma+\gamma\right)}\right)\partial_{xx}a. \tag{S4.65}$$

Using the notations of the main papaer $p_0 = q_{\rm off}/(q_{\rm on}+q_{\rm off})$ the probability to be unbound, $p_1 = 1-p_0$ the probability to have 1 bond and $\gamma_{\rm eff} = \gamma + \frac{k}{q_{\rm off}} + \gamma\frac{q_{\rm on}}{q_{\rm off}}$ we obtain

$$\boxed{\frac{1}{\Gamma_{\rm eff}^{\rm leg+arm}} = \frac{p_0}{\Gamma} + \frac{p_1}{\Gamma + \frac{1}{2}\gamma_{\rm eff}}} \tag{S4.66}$$

that is exactly Eq. (24) in the main paper.

4.3.3 Several arms for 1 leg

Equations set up We consider random attachment and detachment of two springs to one another, in the leg and arm geometry, but now when there are possibly M arms to attach to.

When the springs are unbound the dynamic equations are

$$\begin{cases} \frac{dl}{dt} &= -\frac{k}{\gamma}l + \sqrt{\frac{2k_BT}{\gamma}}\eta(t) \\ \frac{dl_i}{dt} &= -\frac{k}{\gamma}l_i + \sqrt{\frac{2k_BT}{\gamma}}\eta_i(t) \text{ for } i = 1\dots M \\ \frac{dx}{dt} &= \sqrt{\frac{2k_BT}{\Gamma}}\eta_x(t) \end{cases} \tag{S4.67}$$

where l is the length of the top spring, l_i are the lengths of all the bottom springs, and for simplicity here we took $l_0 = 0$.

In the bound state we need to project the dynamics. The dynamic constraint with the bound bottom spring indexed by b is then

$$q(x, l, l_b) = x + l - l_b + l_{\rm bond} = 0 \tag{S4.68}$$

where $l_{\rm bond}$ is the length of the bond, similarly as in the previous section. The constraint process leaves the unbound spring equations completely unaffected and we find after the projection step

$$\begin{cases} \frac{dx}{dt} &= -\frac{k}{2\Gamma+\gamma}(l_1 - l_2) + \sqrt{\frac{8k_BT\Gamma}{(2\Gamma+\gamma)^2}}\eta_x + \sqrt{\frac{2k_BT\gamma}{(2\Gamma+\gamma)^2}}(\eta - \eta_b) \\ \frac{dl}{dt} &= \frac{1}{2}\frac{dx}{dt} - \frac{k}{2\gamma}(l + l_b) + \sqrt{\frac{2k_BT}{4\gamma}}(\eta + \eta_b) \\ \frac{dl_b}{dt} &= -\frac{1}{2}\frac{dx}{dt} - \frac{k}{2\gamma}(l + l_b) + \sqrt{\frac{2k_BT}{4\gamma}}(\eta + \eta_b) \\ \frac{dl_i}{dt} &= -\frac{k}{\gamma}l_i + \sqrt{\frac{2k_BT}{\gamma}}\eta_i(t) \text{ for } i = 1..M \text{ and } i \neq b \end{cases} \tag{S4.69}$$

Generator The generator is similarly

$$\mathcal{L} = \mathcal{Q} + \mathcal{U} = \begin{pmatrix} -Mq_{\rm on} & q_{\rm on} & q_{\rm on} & .. & q_{\rm on} \\ q_{\rm off} & -q_{\rm off} & 0 & ... & 0 \\ q_{\rm off} & 0 & -q_{\rm off} & ... & 0 \\ ... & & & & \\ q_{\rm off} & 0 & 0 & ... & -q_{\rm off} \end{pmatrix} + \mathcal{U} \tag{S4.70}$$

and $\mathcal{U}$ is a diagonal matrix. The first term of $\mathcal{U}$ corresponds to fully unbound dynamics

$$\mathcal{U}_{00} = -\frac{k}{\gamma}l\partial_l + \frac{k_BT}{\gamma}\partial_{ll} + \sum_i\left(-\frac{k}{\gamma}l_i\partial_{l_i} + \frac{k_BT}{\gamma}\partial_{l_il_i}\right) + \frac{k_BT}{\Gamma}\partial_{xx} \tag{S4.71}$$

and further terms correspond each to a bond with the b^{th} arm

$$\begin{aligned} \mathcal{U}_{bb} = &-\frac{k}{2\Gamma+\gamma}(l - l_b)(\partial_x - \frac{1}{2}\partial_{l_b} + \frac{1}{2}\partial_l) - \frac{k}{2\gamma}(l + l_b)(\partial_{l_b} + \partial_l) \\ &+ \frac{2k_BT}{2\Gamma+\gamma}(\partial_x - \frac{1}{2}\partial_{l_b} + \frac{1}{2}\partial_l)^2 + \frac{k_BT}{2\gamma}(\partial_{l_b} + \partial_l)^2 + \sum_{i\neq b}\left(-\frac{k}{\gamma}l_i\partial_{l_i} + \frac{k_BT}{\gamma}\partial_{l_il_i}\right) \end{aligned} \tag{S4.72}$$

With this generator one can check that $\mathcal{L}^\star \pi = 0$ with the natural equilibrium distribution

$$\pi = \frac{1}{Z} \begin{pmatrix} 1 \\ q_{\text{on}}/q_{\text{off}} \\ q_{\text{on}}/q_{\text{off}} \\ ... \end{pmatrix} e^{-kl^2/2k_BT} e^{-\sum_i kl_i^2/2k_BT} \tag{S4.73}$$

where Z is a normalization constant.

Homogenization Taking the usual scalings we get the non-dimensional generator $\mathcal{L} = \frac{1}{\epsilon^2}\mathcal{L}_0 + \frac{1}{\epsilon}\mathcal{L}_1 + \mathcal{L}_2$, where $\mathcal{L}_0 = \mathcal{Q} + \mathcal{U}_0$ where $\mathcal{U}_0$ is diagonal with

$$(\mathcal{U}_0)_{00} = \frac{\Gamma}{\gamma}\left(-l\partial_l + \partial_{ll} + \sum_i (-l_i\partial_{l_i} + \partial_{l_i l_i})\right) \tag{S4.74}$$

$$\begin{aligned}(\mathcal{U}_0)_{bb} = &-\frac{\Gamma}{2(2\Gamma+\gamma)}(l-l_b)(\partial_l - \partial_{l_b}) - \frac{\Gamma}{2\gamma}(l+l_b)(\partial_{l_b} + \partial_l) + \frac{\Gamma}{2(2\Gamma+\gamma)}(\partial_{l_b} - \partial_l)^2 + \frac{\Gamma}{2\gamma}(\partial_{l_b} + \partial_l)^2 \\ &\frac{\Gamma}{\gamma}\sum_{i\neq b}(-l_i\partial_{l_i} + \partial_{l_i l_i})\end{aligned} \tag{S4.75}$$

and $\mathcal{L}_1$ is such that $(\mathcal{L}_1)_{00} = 0$ and

$$(\mathcal{L}_1)_{bb} = -\frac{\Gamma}{2\Gamma+\gamma}(l-l_b)\partial_x + \partial_x(\partial_l - \partial_{l_b})\frac{2\Gamma}{\gamma+2\Gamma} \tag{S4.76}$$

and finally

$$\mathcal{L}_2 = \begin{pmatrix} \partial_{xx} & 0 & 0 & ... \\ 0 & \frac{2\Gamma}{\gamma+2\Gamma}\partial_{xx} & 0 & ... \\ 0 & 0 & \frac{2\Gamma}{\gamma+2\Gamma}\partial_{xx} & ... \end{pmatrix} \tag{S4.77}$$

We now seek an expanded solution f of $\partial_t f = \mathcal{L} f$ as $f = f_0 + \epsilon f_1 + \epsilon^2 f_2 + ...$

At lowest order the resolution gives $f_0 = a(x,t)\begin{pmatrix} 1 \\ 1 \\ 1 \\ ... \end{pmatrix}$, and the associated equilibrium distribution $\pi_0 = \pi$.

At first order we need to solve f_1 and it is useful to seek a genuinely symmetric solution

$$\mathcal{L}_0 f_1 = + \begin{pmatrix} 0 \\ (l-l_1) \\ (l-l_2) \\ ... \end{pmatrix} \frac{\Gamma}{\gamma+2\Gamma}\partial_x a, \text{seeking } f_1 = \begin{pmatrix} u_0 l + u_0' l_1 + u_0' l_2 + .. \\ b_1 l + b_1' l_1 + u_1' l_2 + ... \\ b_1 l + u_1' l_1 + b_1' l_2 + ... \\ ... \end{pmatrix} \partial_x a \tag{S4.78}$$

where u_0, u_0', b_1, b_1' and u_1' are constants. Notice that here u and b refer respectively to unbound and bound contributions, with x and x' corresponding respectively to leg or arm contributions, and the indices

correspond to the number of bonds of the state. The constants obey the system of equations

$$\begin{aligned}
-Mq_{\rm on}u_0 + q_{\rm on}Mb_1 - u_0\frac{\Gamma}{\gamma} &= 0\\
-Mq_{\rm on}u_0' + q_{\rm on}b_1' + (M-1)q_{\rm on}u_1' - u_0'\frac{\Gamma}{\gamma} &= 0\\
q_{\rm off}u_0 - q_{\rm off}b_1 - \frac{\Gamma}{2(2\Gamma+\gamma)}(b_1-b_1') - \frac{b_1+b_1'}{2}\frac{\Gamma}{\gamma} &= \frac{\Gamma}{2\Gamma+\gamma}\\
q_{\rm off}u_0' - q_{\rm off}b_1' + \frac{\Gamma}{2(2\Gamma+\gamma)}(b_1-b_1') - \frac{b_1+b_1'}{2}\frac{\Gamma}{\gamma} &= -\frac{\Gamma}{2\Gamma+\gamma}\\
-q_{\rm off}u_1' + q_{\rm off}u_0' - u_1'\frac{\Gamma}{\gamma} &= 0
\end{aligned} \tag{S4.79}$$

that has a unique solution. For now we do not report the coefficients here for simplicity.

At 2nd order we need to satisfy the Fredholm alternative $\langle \partial_t f_0 - \mathcal{L}_2 f_0 - \mathcal{L}_1 f_1, \pi_0\rangle = 0$. We split up the terms to highlight calculation steps (discarding Z terms to simplify notations, as they would cancel out eventually)

$$\begin{aligned}
\langle \mathcal{L}_1 f_1, \pi_0\rangle =& \sum_i \frac{q_{\rm on}}{q_{\rm off}}\frac{\Gamma}{\gamma+2\Gamma}\langle(-(l-l_i)(b_1 l - b_1' l_i) + 2(b_1-b_1'))\, e^{-l^2/2}e^{-l_i^2/2}\rangle \partial_{xx}a\\
=& M\frac{2\Gamma}{\gamma+2\Gamma}\frac{(b_1-b_1')}{2}\partial_{xx}a
\end{aligned} \tag{S4.80}$$

and

$$\langle \mathcal{L}_2 f_0, \pi_0\rangle = \left(1 + \frac{2\Gamma}{\gamma+2\Gamma}\frac{Mq_{\rm on}}{q_{\rm off}}\right)\partial_{xx}a. \tag{S4.81}$$

Gathering terms as $\langle \partial_t f_0, \pi_0\rangle = \langle \mathcal{L}_2 f_0, \pi\rangle + \langle \mathcal{L}_1 f_1, \pi_0\rangle$ we get

$$\left(1 + M\frac{q_{\rm on}}{q_{\rm off}}\right)\partial_t a = \left(1 + \frac{Mq_{\rm on}}{q_{\rm off}}\frac{2\Gamma}{\gamma+2\Gamma}(1 + \frac{(b_1-b_1')}{2})\right)\partial_{xx}a. \tag{S4.82}$$

Reorganizing terms slightly we arrive at (in dimensional scales)

$$\partial_t a = k_B T\left(\frac{p_{0,M}}{\Gamma} + \frac{p_{1,M}}{\Gamma_{1,M}}\right)\partial_{xx}a. \tag{S4.83}$$

with $p_{0,M} = \frac{q_{\rm off}}{q_{\rm off}+Mq_{\rm on}}$ and $p_{1,M} = 1 - p_{0,M}$ and

$$\Gamma_{1,M} = \frac{\Gamma + \gamma/2}{1 - (b_1 - b_1')/2}. \tag{S4.84}$$

We can further expand $\Gamma_{1,M}$ by using the expressions for b_1 and b_1'. We find

$$\Gamma_{1,M} = \Gamma + \frac{\left(\gamma + \frac{k}{q_{\rm off}}\right)\left(\gamma + \frac{k}{q_{\rm off}} + \gamma\frac{Mq_{\rm on}}{q_{\rm off}}\right)}{\left(\gamma + \frac{k}{q_{\rm off}}\right) + \left(\gamma + \frac{k}{q_{\rm off}} + \gamma\frac{(M-1)q_{\rm on}}{q_{\rm off}}\right)} \tag{S4.85}$$

that is exactly Eq. (25) in the main paper. Notice that, since arm and leg are interchangeable, a similar effect would be observed for a particle with M legs allowed to bind to 1 arm.

Notice that when M is large, we obtain that the above expression simplifies to

$$\Gamma_{1,M} = \Gamma + \gamma_{\rm eff,1,M} \text{ with } \frac{1}{\gamma_{\rm eff,1,M}} = \frac{1}{\gamma_{\rm eff,M,1}} + \frac{1}{\gamma_{\rm eff,1,1}}, \tag{S4.86}$$

with $\gamma_{\rm eff,M,1} = k\left(\frac{1}{q_{\rm off}} + \frac{\gamma}{k}\frac{(M-1)q_{\rm on}+q_{\rm off}}{q_{\rm off}}\right)$ the effective friction due to the leg $\gamma_{\rm eff,1,1} = k\left(\frac{1}{q_{\rm off}} + \frac{\gamma}{k}\right)$ due to arms.

4.3.4 N legs facing M potential arms

2 legs facing 2 arms To understand the dynamics at play in the case of N legs facing M potential arms we first investigate the more specialized 2 for 2 scenario. We number legs as 1 and 2 and arms as 3 and 4. We write the generator for this system directly in the non-dimensional scales. It is a bit lengthy as there are now 7 possible states. We arrange the states as state #1 is the unbound state, states $\#2-5$ correspond to 1 bond states, and states $\#6-7$ to 2 bond states. We write $\mathcal{L}=\mathcal{Q}+\mathcal{U}$. The transition rate matrix for the generator is simply

$$\mathcal{Q}=\frac{1}{\epsilon^2}\begin{pmatrix} -4q_{\text{on}} & q_{\text{on}} & q_{\text{on}} & q_{\text{on}} & q_{\text{on}} & . & . \\ q_{\text{off}} & -q_{\text{off}}-q_{\text{on}} & . & . & . & q_{\text{on}} & . \\ q_{\text{off}} & . & -q_{\text{off}}-q_{\text{on}} & . & . & . & .q_{\text{on}} \\ q_{\text{off}} & . & . & -q_{\text{off}}-q_{\text{on}} & . & .q_{\text{on}} & . \\ q_{\text{off}} & . & . & . & -q_{\text{off}}-q_{\text{on}} & . & .q_{\text{on}} \\ . & q_{\text{off}} & . & q_{\text{off}} & . & -2q_{\text{off}} & . \\ . & . & q_{\text{off}} & . & q_{\text{off}} & . & -2q_{\text{off}} \end{pmatrix} \tag{S4.87}$$

Then we write the diagonal (only non zero) components of $\mathcal{U}$. For the unbound state we have

$$\mathcal{U}_{11}=\frac{1}{\epsilon^2}\frac{\Gamma}{\gamma}\sum_{i=1}^{4}D_{l_i}+\partial_{xx} \tag{S4.88}$$

where $D_{l_i}=-l_i\partial_{l_i}+\partial_{l_il_i}$ is the unbound relaxation operator. Then in the 2..5 states where just one tether is bound we have (for example for the 2 state where tethers say 1 and 3 are bound)

$$\begin{aligned}\mathcal{U}_{22}=&\frac{1}{\epsilon^2}\left(-\frac{\Gamma}{2(2\Gamma+\gamma)}(l_1-l_3)(\partial_{l_1}-\partial_{l_3})-\frac{\Gamma}{2\gamma}(l_1+l_3)(\partial_{l_3}+\partial_{l_1})+\frac{\Gamma}{2(2\Gamma+\gamma)}(\partial_{l_3}-\partial_{l_1})^2+\frac{\Gamma}{2\gamma}(\partial_{l_3}+\partial_{l_1})^2\right)\\&+\frac{1}{\epsilon^2}\frac{\Gamma}{\gamma}\left(D_{l_2}+D_{l_4}\right)+\frac{1}{\epsilon}\frac{\Gamma}{2\Gamma+\gamma}\left(-(l_1-l_3)\partial_x+2\partial_x(\partial_{l_1}-\partial_{l_3})\right)+1\left(\frac{2\Gamma}{2\Gamma+\gamma}\partial_{xx}\right)\end{aligned} \tag{S4.89}$$

and similarly for the other 1 bond states. Finally for the 6 and 7 states, 2 bonds are formed. In these state we have, for example for state #6 that contains the bonds $1-3$ and $2-4$

$$\begin{aligned}\mathcal{U}_{66}=&-\frac{\Gamma}{2\Gamma+2\gamma}(l_1-l_3+l_2-l_4)(\frac{1}{\epsilon}\partial_x-\frac{1}{\epsilon^2}\frac{1}{2}\partial_{l_3}+\frac{1}{\epsilon^2}\frac{1}{2}\partial_{l_1}-\frac{1}{\epsilon^2}\frac{1}{2}\partial_{l_4}+\frac{1}{\epsilon^2}\frac{1}{2}\partial_{l_2})\\&-\frac{1}{\epsilon^2}\frac{\Gamma}{2\gamma}(l_1+l_3)(\partial_{l_3}+\partial_{l_1})-\frac{1}{\epsilon^2}\frac{\Gamma}{2\gamma}(l_2+l_4)(\partial_{l_4}+\partial_{l_2})\\&+\frac{\Gamma}{2(2\Gamma+2\gamma)}\left(2\partial_x+\frac{1}{\epsilon}\left(\partial_{l_1}+\partial_{l_2}-\partial_{l_3}-\partial_{l_4}\right)\right)^2+\frac{\Gamma}{2\gamma}\frac{1}{\epsilon^2}\left[\left(\partial_{l_1}+\partial_{l_3}\right)^2+\left(\partial_{l_2}+\partial_{l_4}\right)^2\right]\end{aligned} \tag{S4.90}$$

and reordering this last expression as a function of the scales in ϵ

$$\begin{aligned}\mathcal{U}_{66}=&\frac{1}{\epsilon^2}\left(-\frac{\Gamma(l_1-l_3+l_2-l_4)}{2(2\Gamma+2\gamma)}(\partial_{l_1}-\partial_{l_3}+\partial_{l_2}-\partial_{l_4})-\frac{(l_1+l_3)\Gamma}{2\gamma}(\partial_{l_3}+\partial_{l_1})-\frac{(l_2+l_4)\Gamma}{2\gamma}(\partial_{l_2}+\partial_{l_4})\right)\\&+\frac{1}{\epsilon^2}\left(\frac{\Gamma}{2(2\Gamma+2\gamma)}\left(\partial_{l_1}+\partial_{l_2}-\partial_{l_3}-\partial_{l_4}\right)^2+\frac{\Gamma}{2\gamma}\left[\left(\partial_{l_1}+\partial_{l_3}\right)^2+\left(\partial_{l_2}+\partial_{l_4}\right)^2\right]\right)\\&+\frac{1}{\epsilon}\left(\frac{2\Gamma}{(2\Gamma+2\gamma)}\partial_x\left(\partial_{l_1}+\partial_{l_2}-\partial_{l_3}-\partial_{l_4}\right)-\frac{\Gamma(l_1-l_3+l_2-l_4)}{2\Gamma+2\gamma}\partial_x\right)\\&+1\left(\frac{2\Gamma}{2\Gamma+2\gamma}\partial_{xx}\right)\end{aligned} \tag{S4.91}$$

Here the equilibrium distribution is

$$\pi = \frac{1}{\sqrt{2\pi}\left(2+4\frac{q_{\rm off}}{q_{\rm on}}+\frac{q_{\rm off}^2}{q_{\rm on}^2}\right)}\left(q_{\rm off}^2/q_{\rm on}^2,\quad q_{\rm off}/q_{\rm on},\quad q_{\rm off}/q_{\rm on},\quad q_{\rm off}/q_{\rm on},\quad q_{\rm off}/q_{\rm on},\quad 1,\quad 1\right)^T. \tag{S4.92}$$

We seek a solution to the expanded generator $\mathcal{L} = \frac{1}{\epsilon^2}\mathcal{L}_0 + \frac{1}{\epsilon}\mathcal{L}_1 + \mathcal{L}_2$ as $f = f_0 + \epsilon f_1 + \epsilon^2 f_2 ....$ No steps change in the resolution compared to previous calculations but for finding the solution at order 1. Here we seek a solution

$$\mathcal{L}_0 f_1 = -\mathcal{L}_1 f_0 = \begin{pmatrix} 0 \\ \frac{1}{2\Gamma+\gamma}(l_1-l_3) \\ \frac{1}{2\Gamma+\gamma}(l_1-l_4) \\ \frac{1}{2\Gamma+\gamma}(l_2-l_4) \\ \frac{1}{2\Gamma+\gamma}(l_2-l_3) \\ \frac{1}{2\Gamma+2\gamma}(l_1-l_3+l_2-l_4) \\ \frac{1}{2\Gamma+2\gamma}(l_1-l_4+l_2-l_3) \end{pmatrix} \Gamma\partial_x a \tag{S4.93}$$

The solution is expected to preserve the symmetries of the problem and therefore we may seek

$$f_1 = \begin{pmatrix} u_0 l_1 + u_0 l_2 + u_0' l_3 + u_0' l_4 \\ b_1 l_1 + u_1 l_2 + b_1' l_3 + u_1' l_4 \\ ... \\ b_2 l_1 + b_2 l_2 + b_2' l_3 + b_2' l_4 \\ ... \end{pmatrix} \partial_x a \tag{S4.94}$$

where b_n, b_n', u_n, u_n' are constants that refer to bound and unbound configurations of the leg or the arms. They solve a linear system of equations that possesses a single solution that we will report below.

The Fredholm alternative at the next order requires $\langle \partial_t f_0 - \mathcal{L}_2 f_0 - \mathcal{L}_1 f_1, \pi\rangle$. We obtain, splitting the relevant contributions

$$\langle \mathcal{L}_1 f_1, \pi\rangle = 0 + \frac{(b_1-b_1')\Gamma}{2\Gamma+\gamma}p_1 + \frac{2(b_2-b_2')\Gamma}{2\Gamma+2\gamma}p_2 \tag{S4.95}$$

and assembling all terms allows to get an effective long time diffusion equation $\partial_t a = \frac{\Gamma}{\Gamma_{\rm eff}^{2,2}}\partial_{xx} a$ where

$$\frac{1}{\Gamma_{\rm eff}^{2,2}} = \frac{1}{\Gamma}p_0 + \frac{1}{\frac{\Gamma+\gamma/2}{\left(1-\frac{b_1-b_1'}{2}\right)}}p_1 + \frac{1}{\frac{\Gamma+2\gamma/2}{\left(1-2\frac{b_2-b_2'}{2}\right)}}p_2 \tag{S4.96}$$

which is similarly as in all cases a weighted harmonic sum of friction coefficients, with p_n the probability to have n bonds.

The system of equations that the constants satisfy is

$$\begin{aligned}
&-4q_{\rm on}u_0 - u_0 + 2q_{\rm on}b_1 + 2q_{\rm on}u_1 = 0\\
&-4q_{\rm on}u'_0 - u'_0 + 2q_{\rm on}b'_1 + 2q_{\rm on}u'_1 = 0\\
&q_{\rm off}u_0 - q_{\rm off}b_1 - q_{\rm on}b_1 + q_{\rm on}b_2 - \frac{\gamma}{2(2\Gamma+\gamma)}(b_1 - b'_1) - \frac{b_1+b'_1}{2} = \frac{\gamma}{2\Gamma+\gamma}\\
&q_{\rm off}u'_0 - q_{\rm off}b'_1 - q_{\rm on}b'_1 + q_{\rm on}b'_2 + \frac{\gamma}{2(2\Gamma+\gamma)}(b_1 - b'_1) - \frac{b_1+b'_1}{2} = -\frac{\gamma}{2\Gamma+\gamma}\\
&q_{\rm off}u_0 - q_{\rm off}u_1 - q_{\rm on}u_1 + q_{\rm on}b_2 - u_1 = 0\\
&q_{\rm off}u'_0 - q_{\rm off}u'_1 - q_{\rm on}u'_1 + q_{\rm on}b'_2 - u'_1 = 0\\
&q_{\rm off}b_1 + q_{\rm off}u_1 - 2q_{\rm off}b_2 - \frac{2\gamma}{2(2\Gamma+2\gamma)}(b_2 - b'_2) - \frac{b_2+b'_2}{2} = \frac{\gamma}{2\Gamma+2\gamma}\\
&q_{\rm off}b'_1 + q_{\rm off}u'_1 - 2q_{\rm off}b'_2 + \frac{2\gamma}{2(2\Gamma+2\gamma)}(b_2 - b'_2) - \frac{b_2+b'_2}{2} = -\frac{\gamma}{2\Gamma+2\gamma}
\end{aligned} \tag{S4.97}$$

Since the bottom and top tethers don't exactly have the same positions it's not possible to simplify further, typically $b_n \neq -b'_n$. This really shows the structure of the equations.

N legs facing M arms The above system of equations allows to generalize the derivation for n bonds in some N legs for M arms structure. For each possible number of bonds say n, the tethers are either unbound (u_n, u'_n) or bound (b_n, b'_n) and can exchange with their counterparts.

When there are n bonds, focusing on a connected pair, one can still bind more pairs, and there are $(M-n)(N-n)$ possible ways to do so. In any case the connected pair will remain connected during that transformation. When there are n bonds, one can unbind n pairs. $n-1$ possibilities lead to the given pair still being bound.

For an unconnected leg (resp. arm), there are only $M-n$ possibilities (resp. $(N-n)$) to form a bond that will connect the unconnected one.

We obtain the general system of equations as

$$\begin{aligned}
&nq_{\rm off}u_{n-1} - (nq_{\rm off} + (N-n)(M-n)q_{\rm on})u_n + q_{\rm on}(M-n)b_{n+1} + q_{\rm on}(N-n-1)(M-n)u_{n+1} - u_n\frac{\Gamma}{\gamma} = 0\\
&nq_{\rm off}u'_{n-1} - (nq_{\rm off} + (N-n)(M-n)q_{\rm on})u'_n + q_{\rm on}(N-n)b'_{n+1} + q_{\rm on}(M-n-1)(N-n)u'_{n+1} - u'_n\frac{\Gamma}{\gamma} = 0\\
&q_{\rm off}u_{n-1} + (n-1)q_{\rm off}b_{n-1} - (nq_{\rm off} + (N-n)(M-n)q_{\rm on})b_n + q_{\rm on}(N-n)(M-n)b_{n+1}...\\
&\qquad -\frac{n\Gamma}{2(2\Gamma+n\gamma)}(b_n - b'_n) - \frac{b_n+b'_n}{2}\frac{\Gamma}{\gamma} = -\frac{\Gamma}{2\Gamma+n\gamma}\\
&q_{\rm off}u'_{n-1} + (n-1)q_{\rm off}b'_{n-1} - (nq_{\rm off} + (N-n)(M-n)q_{\rm on})b'_n + q_{\rm on}(N-n)(M-n)b'_{n+1}...\\
&\qquad +\frac{n\Gamma}{2(2\Gamma+n\gamma)}(b_n - b'_n) - \frac{b_n+b'_n}{2}\frac{\Gamma}{\gamma} = \frac{\Gamma}{2\Gamma+n\gamma}\\
&\qquad\qquad \frac{\Gamma+n\gamma/2}{1-n(b_n-b'_n)/2} = \Gamma_n
\end{aligned} \tag{S4.98}$$

Looking for the average number of bonds contribution, we may assume similarly that for $n = N_b$ we have

$u_n \simeq u_{n-1} \simeq u_n = \bar{u}$, and similarly for other quantities. We thus obtain the closed system of equations

$$\begin{aligned}
-(M-N_b)q_{\rm on}\bar{u} + q_{\rm on}(M-N_b)\bar{b} - \bar{u}\frac{\Gamma}{\gamma} &= 0 \\
-(N-N_b)q_{\rm on}\bar{u}' + q_{\rm on}(N-N_b)\bar{b}' - \bar{u}'\frac{\Gamma}{\gamma} &= 0 \\
q_{\rm off}\bar{u} - q_{\rm off}\bar{b} - \frac{N_b\Gamma}{2(2\Gamma+N_b\gamma)}(\bar{b}-\bar{b}') - \frac{\bar{b}+\bar{b}'}{2}\frac{\Gamma}{\gamma} &= \frac{\Gamma}{2\Gamma+N_b\gamma} \\
q_{\rm off}\bar{u}' - q_{\rm off}\bar{b}' + \frac{N_b\Gamma}{2(2\Gamma+N_b\gamma)}(\bar{b}-\bar{b}') - \frac{\bar{b}+\bar{b}'}{2}\frac{\Gamma}{\gamma} &= -\frac{\Gamma}{2\Gamma+N_b\gamma} \\
\frac{\Gamma+N_b\gamma/2}{1-N_b(\bar{b}-\bar{b}')/2} &= \Gamma_{N_b}
\end{aligned} \tag{S4.99}$$

This finally yields

$$\Gamma_{N_b} = \Gamma + N_b\gamma_{\rm eff,N,M}, \text{ with } \frac{1}{\gamma_{\rm eff,N,M}} = \frac{1}{\gamma_{\rm eff}^{\rm leg}} + \frac{1}{\gamma_{\rm eff}^{\rm arm}}, \tag{S4.100}$$

with the effective friction due to legs as $\gamma_{\rm eff}^{\rm leg} = \gamma + k\left(\frac{1}{q_{\rm off}} + \frac{\gamma}{k}\frac{(M-N_b)q_{\rm on}}{q_{\rm off}}\right)$ and that due to arms $\gamma_{\rm eff}^{\rm arm} =$ $\gamma + k\left(\frac{1}{q_{\rm off}} + \frac{\gamma}{k}\frac{(N}{}\right.$ ıe leg) is $\tau_{\rm on} = 1/(M-N_b)$ ɔle arms.

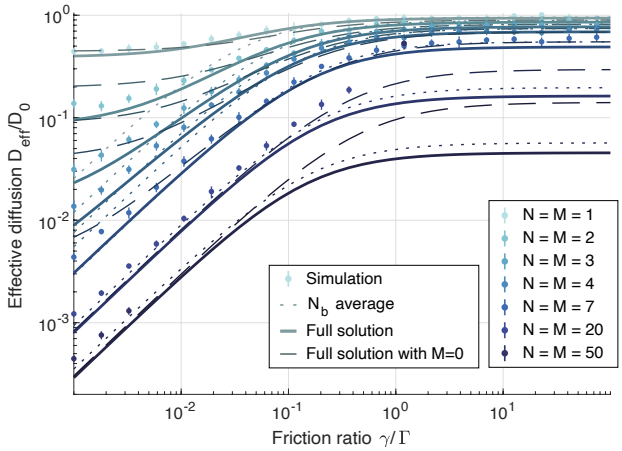

Figure S8: Effective diffusion for systems with an equal number of arms and legs all interacting with one another ($N = M$) from stochastic simulations. We overlay the predictions using Eq. (S4.101) (N_b average) and fully solving for the system of equations Eq. (S4.98) (Full solution). For reference we also show the result of the full system in the case of N legs with $M = 0$ arms, from solving Eq. (S1.20). Here the values of other parameters are $\frac{q_{\rm on}\Gamma}{k} = 1.0$ and $\frac{q_{\rm off}\Gamma}{k} = 0.8$

Here we can explore limiting regimes. If there are as many legs as there are arms we have $M = N$, then the effective friction simplifies to

$$\Gamma_{N_b} = \Gamma + \frac{N_b}{2}\left[\gamma + k\left(\frac{1}{q_{\rm off}} + \frac{\gamma}{k}\frac{(N-N_b)q_{\rm on}}{q_{\rm off}}\right)\right], \tag{S4.101}$$

where we see that the additional friction is divided by 2, as expected from the leg and arm case. One notable difference is that here we see that the characteristic binding time $\tau_{\rm on} = 1/(N-N_b)q_{\rm on}$, due to the increased number of possibilities due to multiple arms and legs. According to the large N limit investigated, $(N-N_b)q_{\rm on}$ does not necessarily diverge. In particular for very sticky systems $(N-N_b) \simeq 0$ and therefore this part does not contribute significantly to the dynamics.

If there are a large number of arms, say $M \gg N_b$, then we find $\gamma_{\mathrm{eff,M,N}} \to \gamma_{\mathrm{eff}}^{\mathrm{arm}}$ is dominated by the arm contributions to the effective friction.

These effective results capture well stochastic simulation results, as shown in Fig. S8.

References

[1] J. S. Oh, Y. Wang, D. J. Pine, and G.-R. Yi, "High-density peo-b-dna brushes on polymer particles for colloidal superstructures," *Chemistry of Materials*, vol. 27, no. 24, pp. 8337–8344, 2015.

[2] S. Hiki and K. Kataoka, "A facile synthesis of azido-terminated heterobifunctional poly (ethylene glycol) s for "click" conjugation," *Bioconjugate chemistry*, vol. 18, no. 6, pp. 2191–2196, 2007.

[3] Q. Xu, L. Feng, R. Sha, N. Seeman, and P. Chaikin, "Subdiffusion of a sticky particle on a surface," *Physical review letters*, vol. 106, no. 22, p. 228102, 2011.

[4] Y. Wang, Y. Wang, X. Zheng, É. Ducrot, J. S. Yodh, M. Weck, and D. J. Pine, "Crystallization of dna-coated colloids," *Nature communications*, vol. 6, no. 1, pp. 1–8, 2015.

[5] A. Rohatgi, "WebPlotDigitizer: Version 4.5," 2021.

[6] F. Cui, S. Marbach, J. Zheng, M. Holmes-Cerfon, and D. J. Pine, "Comprehensive view of nanoscale interactions between dna-coated colloids," *to appear*, 2021.

[7] S. T. Milner, T. A. Witten, and M. E. Cates, "Theory of the grafted polymer brush," *Macromolecules*, vol. 21, no. 8, pp. 2610–2619, 1988.

[8] P. Varilly, S. Angioletti-Uberti, B. M. Mognetti, and D. Frenkel, "A general theory of dna-mediated and other valence-limited colloidal interactions," *The Journal of chemical physics*, vol. 137, no. 9, p. 094108, 2012.

[9] C. P. Goodrich, M. P. Brenner, and K. Ribbeck, "Enhanced diffusion by binding to the crosslinks of a polymer gel," *Nature communications*, vol. 9, no. 1, pp. 1–8, 2018.

[10] C. Fröhner and F. Noé, "Reversible interacting-particle reaction dynamics," *The Journal of Physical Chemistry B*, vol. 122, no. 49, pp. 11240–11250, 2018.

[11] B. Fogelson and J. P. Keener, "Transport facilitated by rapid binding to elastic tethers," *SIAM Journal on Applied Mathematics*, vol. 79, no. 4, pp. 1405–1422, 2019.

[12] S. Marbach, "Intrinsic fractional noise in nanopores: The effect of reservoirs," *The Journal of Chemical Physics*, vol. 154, no. 17, p. 171101, 2021.

[13] C. Sun, C. Migliorini, and L. L. Munn, "Red blood cells initiate leukocyte rolling in postcapillary expansions: a lattice boltzmann analysis," *Biophysical journal*, vol. 85, no. 1, pp. 208–222, 2003.

[14] G. Pavliotis and A. Stuart, *Multiscale methods: averaging and homogenization*. Springer Science & Business Media, 2008.

[15] M. Zoli, "End-to-end distance and contour length distribution functions of dna helices," *The Journal of chemical physics*, vol. 148, no. 21, p. 214902, 2018.

[16] J. X. Zhang, J. Z. Fang, W. Duan, L. R. Wu, A. W. Zhang, N. Dalchau, B. Yordanov, R. Petersen, A. Phillips, and D. Y. Zhang, "Predicting dna hybridization kinetics from sequence," *Nature chemistry*, vol. 10, no. 1, pp. 91–98, 2018.

[17] S. Xu, J. Zhan, B. Man, S. Jiang, W. Yue, S. Gao, C. Guo, H. Liu, Z. Li, J. Wang, *et al.*, "Real-time reliable determination of binding kinetics of dna hybridization using a multi-channel graphene biosensor," *Nature communications*, vol. 8, no. 1, pp. 1–10, 2017.

[18] S. Y. Park, A. K. Lytton-Jean, B. Lee, S. Weigand, G. C. Schatz, and C. A. Mirkin, "Dna-programmable nanoparticle crystallization," *Nature*, vol. 451, no. 7178, pp. 553–556, 2008.

[19] S. J. Hurst, A. K. Lytton-Jean, and C. A. Mirkin, "Maximizing dna loading on a range of gold nanoparticle sizes," *Analytical chemistry*, vol. 78, no. 24, pp. 8313–8318, 2006.

[20] H. Ting-Beall, D. Needham, and R. Hochmuth, "Volume and osmotic properties of human neutrophils.," *Blood*, vol. 81, no. 10, pp. 2774–2780, 1993.

[21] S. Chen and T. A. Springer, "Selectin receptor–ligand bonds: Formation limited by shear rate and dissociation governed by the bell model," *Proceedings of the National Academy of Sciences*, vol. 98, no. 3, pp. 950–955, 2001.

[22] J.-Y. Shao, H. P. Ting-Beall, and R. M. Hochmuth, "Static and dynamic lengths of neutrophil microvilli," *Proceedings of the National Academy of Sciences*, vol. 95, no. 12, pp. 6797–6802, 1998.

[23] J. Fritz, A. G. Katopodis, F. Kolbinger, and D. Anselmetti, "Force-mediated kinetics of single p-selectin/ligand complexes observed by atomic force microscopy," *Proceedings of the National Academy of Sciences*, vol. 95, no. 21, pp. 12283–12288, 1998.

[24] U. S. Schwarz and R. Alon, "L-selectin-mediated leukocyte tethering in shear flow is controlled by multiple contacts and cytoskeletal anchorage facilitating fast rebinding events," *Proceedings of the National Academy of Sciences*, vol. 101, no. 18, pp. 6940–6945, 2004.

[25] R. Alon, D. A. Hammer, and T. A. Springer, "Lifetime of the p-selectin-carbohydrate bond and its response to tensile force in hydrodynamic flow," *Nature*, vol. 374, no. 6522, pp. 539–542, 1995.

[26] R. Alon, S. Chen, K. D. Puri, E. B. Finger, and T. A. Springer, "The kinetics of l-selectin tethers and the mechanics of selectin-mediated rolling," *The Journal of cell biology*, vol. 138, no. 5, pp. 1169–1180, 1997.

[27] C. Korn and U. Schwarz, "Dynamic states of cells adhering in shear flow: from slipping to rolling," *Physical review E*, vol. 77, no. 4, p. 041904, 2008.

[28] P. Mehta, R. D. Cummings, and R. P. McEver, "Affinity and kinetic analysis of p-selectin binding to p-selectin glycoprotein ligand-1," *Journal of Biological Chemistry*, vol. 273, no. 49, pp. 32506–32513, 1998.

[29] O. Dwir, A. Solomon, S. Mangan, G. S. Kansas, U. S. Schwarz, and R. Alon, "Avidity enhancement of l-selectin bonds by flow: shear-promoted rotation of leukocytes turn labile bonds into functional tethers," *The Journal of cell biology*, vol. 163, no. 3, pp. 649–659, 2003.

[30] S. Bakshi, A. Siryaporn, M. Goulian, and J. C. Weisshaar, "Superresolution imaging of ribosomes and rna polymerase in live escherichia coli cells," *Molecular microbiology*, vol. 85, no. 1, pp. 21–38, 2012.

[31] E. Miller, T. Garcia, S. Hultgren, and A. F. Oberhauser, "The mechanical properties of e. coli type 1 pili measured by atomic force microscopy techniques," *Biophysical journal*, vol. 91, no. 10, pp. 3848–3856, 2006.

[32] O. Yakovenko, V. Tchesnokova, E. V. Sokurenko, and W. E. Thomas, "Inactive conformation enhances binding function in physiological conditions," *Proceedings of the National Academy of Sciences*, vol. 112, no. 32, pp. 9884–9889, 2015.

[33] M. M. Sauer, R. P. Jakob, T. Luber, F. Canonica, G. Navarra, B. Ernst, C. Unverzagt, T. Maier, and R. Glockshuber, "Binding of the bacterial adhesin fimh to its natural, multivalent high-mannose type glycan targets," *Journal of the American Chemical Society*, vol. 141, no. 2, pp. 936–944, 2018.

[34] M. M. Sauer, R. P. Jakob, J. Eras, S. Baday, D. Eriş, G. Navarra, S. Berneche, B. Ernst, T. Maier, and R. Glockshuber, "Catch-bond mechanism of the bacterial adhesin fimh," *Nature communications*, vol. 7, no. 1, pp. 1–13, 2016.

[35] F. C. Neidhardt, J. L. Ingraham, and M. Schaechter, *Physiology of the bacterial cell; a molecular approach*. No. 589.901 N397, Sinauer associates, 1990.

[36] C. B. Korn, S. Klumpp, R. Lipowsky, and U. S. Schwarz, "Stochastic simulations of cargo transport by processive molecular motors," *The Journal of chemical physics*, vol. 131, no. 24, p. 12B624, 2009.

[37] F. Gibbons, J.-F. Chauwin, M. Despósito, and J. V. José, "A dynamical model of kinesin-microtubule motility assays," *Biophysical journal*, vol. 80, no. 6, pp. 2515–2526, 2001.

[38] T. Duke and S. Leibler, "Motor protein mechanics: a stochastic model with minimal mechanochemical coupling," *Biophysical journal*, vol. 71, no. 3, pp. 1235–1247, 1996.

[39] R. D. Vale, T. Funatsu, D. W. Pierce, L. Romberg, Y. Harada, and T. Yanagida, "Direct observation of single kinesin molecules moving along microtubules," *Nature*, vol. 380, no. 6573, pp. 451–453, 1996.

[40] C. Leduc, O. Campàs, K. B. Zeldovich, A. Roux, P. Jolimaitre, L. Bourel-Bonnet, B. Goud, J.-F. Joanny, P. Bassereau, and J. Prost, "Cooperative extraction of membrane nanotubes by molecular motors," *Proceedings of the National Academy of Sciences*, vol. 101, no. 49, pp. 17096–17101, 2004.

[41] J. Wu, A. H. Corbett, and K. M. Berland, "The intracellular mobility of nuclear import receptors and nls cargoes," *Biophysical journal*, vol. 96, no. 9, pp. 3840–3849, 2009.

[42] I. V. Aramburu and E. A. Lemke, "Floppy but not sloppy: Interaction mechanism of fg-nucleoporins and nuclear transport receptors," in *Seminars in cell & developmental biology*, vol. 68, pp. 34–41, Elsevier, 2017.

[43] R. Y. Lim, N.-P. Huang, J. Köser, J. Deng, K. A. Lau, K. Schwarz-Herion, B. Fahrenkrog, and U. Aebi, "Flexible phenylalanine-glycine nucleoporins as entropic barriers to nucleocytoplasmic transport," *Proceedings of the National Academy of Sciences*, vol. 103, no. 25, pp. 9512–9517, 2006.

[44] L.-C. Tu, G. Fu, A. Zilman, and S. M. Musser, "Large cargo transport by nuclear pores: implications for the spatial organization of fg-nucleoporins," *The EMBO journal*, vol. 32, no. 24, pp. 3220–3230, 2013.

[45] A. Harris, G. Cardone, D. C. Winkler, J. B. Heymann, M. Brecher, J. M. White, and A. C. Steven, "Influenza virus pleiomorphy characterized by cryoelectron tomography," *Proceedings of the National Academy of Sciences*, vol. 103, no. 50, pp. 19123–19127, 2006.

[46] V. Reiter-Scherer, J. L. Cuellar-Camacho, S. Bhatia, R. Haag, A. Herrmann, D. Lauster, and J. P. Rabe, "Force spectroscopy shows dynamic binding of influenza hemagglutinin and neuraminidase to sialic acid," *Biophysical journal*, vol. 116, no. 6, pp. 1037–1048, 2019.

[47] C. Sieben, C. Kappel, R. Zhu, A. Wozniak, C. Rankl, P. Hinterdorfer, H. Grubmüller, and A. Herrmann, "Influenza virus binds its host cell using multiple dynamic interactions," *Proceedings of the National Academy of Sciences*, vol. 109, no. 34, pp. 13626–13631, 2012.

[48] N. K. Sauter, M. D. Bednarski, B. A. Wurzburg, J. E. Hanson, G. M. Whitesides, J. J. Skehel, and D. C. Wiley, "Hemagglutinins from two influenza virus variants bind to sialic acid derivatives with millimolar dissociation constants: a 500-mhz proton nuclear magnetic resonance study," *Biochemistry*, vol. 28, no. 21, pp. 8388–8396, 1989.

[49] M. Müller, D. Lauster, H. H. Wildenauer, A. Herrmann, and S. Block, "Mobility-based quantification of multivalent virus-receptor interactions: New insights into influenza a virus binding mode," *Nano letters*, vol. 19, no. 3, pp. 1875–1882, 2019.

[50] T. Sakai, S. I. Nishimura, T. Naito, and M. Saito, "Influenza a virus hemagglutinin and neuraminidase act as novel motile machinery," *Scientific reports*, vol. 7, no. 1, pp. 1–11, 2017.

[51] M. Laue, A. Kauter, T. Hoffmann, L. Möller, J. Michel, and A. Nitsche, "Morphometry of sars-cov and sars-cov-2 particles in ultrathin plastic sections of infected vero cell cultures," *Scientific reports*, vol. 11, no. 1, pp. 1–11, 2021.

[52] J. Yang, S. J. Petitjean, M. Koehler, Q. Zhang, A. C. Dumitru, W. Chen, S. Derclaye, S. P. Vincent, P. Soumillion, and D. Alsteens, "Molecular interaction and inhibition of sars-cov-2 binding to the ace2 receptor," *Nature communications*, vol. 11, no. 1, pp. 1–10, 2020.

[53] W. Cao, C. Dong, S. Kim, D. Hou, W. Tai, L. Du, W. Im, and X. F. Zhang, "Biomechanical characterization of sars-cov-2 spike rbd and human ace2 protein-protein interaction," *Biophysical journal*, vol. 120, no. 6, pp. 1011–1019, 2021.

[54] M. Ponga, "Quantifying the adhesive strength between the sars-cov-2 s-proteins and human receptor and its effect in therapeutics," *Scientific reports*, vol. 10, no. 1, pp. 1–7, 2020.

[55] A. C. Walls, Y.-J. Park, M. A. Tortorici, A. Wall, A. T. McGuire, and D. Veesler, "Structure, function, and antigenicity of the sars-cov-2 spike glycoprotein," *Cell*, vol. 181, no. 2, pp. 281–292, 2020.

[56] S. Marbach and M. Holmes-Cerfon, "Can mass change the diffusion coefficient of dna-coated colloids?," *arXiv preprint arXiv:2112.05266*, 2021.

[57] J. P. Lee-Thorp and M. Holmes-Cerfon, "Modeling the relative dynamics of dna-coated colloids," *Soft matter*, vol. 14, no. 40, pp. 8147–8159, 2018.

[58] B. Fogelson and J. P. Keener, "Enhanced nucleocytoplasmic transport due to competition for elastic binding sites," *Biophysical journal*, vol. 115, no. 1, pp. 108–116, 2018.

[59] P. K. Jana and B. M. Mognetti, "Translational and rotational dynamics of colloidal particles interacting through reacting linkers," *Physical Review E*, vol. 100, no. 6, p. 060601, 2019.